ELSEVIER

Journal of Fluids and Structures 26 (2010) 849–899

JOURNAL OF FLUIDS AND STRUCTURES

www.elsevier.com/locate/jfs

Two circular cylinders in cross-flow: A review

D. Sumner*

Department of Mechanical Engineering, University of Saskatchewan, 57 Campus Drive, Saskatoon, Saskatchewan, Canada S7N 5A9

Received 21 June 2010; accepted 15 July 2010

Abstract

Pairs of circular cylinders immersed in a steady cross-flow are encountered in many engineering applications. The cylinders may be arranged in tandem, side-by-side, or staggered configurations. Wake and proximity interference effects, which are determined primarily by the longitudinal and transverse spacing between the cylinders, and also by the Reynolds number, have a strong influence on the flow patterns, aerodynamic forces, vortex shedding, and other parameters. This paper reviews the current understanding of the flow around two "infinite" circular cylinders of equal diameter immersed in a steady cross-flow, with a focus on the near-wake flow patterns, Reynolds number effects, intermediate wake structure and behaviour, and the general trends in the measurements of the aerodynamic force coefficients and Strouhal numbers. A primary focus is on the key experimental and numerical studies that have appeared since the last major review of this subject more than 20 years ago.

Keywords: Bluff body; Circular cylinder; Cylinder groups; Wake interference; Vortex shedding

1. Introduction

Because of its common occurrence in many forms and in different applications, fluid flow around a circular cylinder has been well studied and is one of the classical problems of fluid mechanics. There are several comprehensive reviews of the flow around a single, isolated circular cylinder in the literature, including articles by Morkovin (1964), Gerrard (1978), Coutanceau and Defaye (1991) and Williamson (1996), and monographs by Sumer and Fredsøe (1997) and Zdravkovich (1997, 2003). Cylinder-like structures can be found both alone and in groups in the designs for heat exchangers, cooling systems for nuclear power plants, offshore structures, buildings, chimneys, power lines, struts, grids, screens, and cables, in both air- and water-flow. In many of these engineering applications, Kármán vortex shedding is responsible for problems with flow-induced vibration and noise. A complete understanding of the fluid dynamics for the flow around a circular cylinder includes such fundamental subjects as the boundary layer, separation, the free shear layer, the wake, and the dynamics of vortices.

Less well studied and understood are the changes to the flow around a single circular cylinder which may occur when two or more circular cylinders are placed in close proximity to one another. The flow fields of multiple-cylinder configurations involve complex interactions between the shear layers, vortices, wakes, and Kármán vortex streets. The most basic multiple-cylinder configurations in cross-flow are shown in Fig. 1, where the two circular cylinders have the

*Tel.: +1 306 966 5537; fax: +1 306 966 5427.
E-mail address: david.sumner@usask.ca

0889-9746/$ - see front matter © 2010 Elsevier Ltd. All rights reserved.
doi:10.1016/j.jfluidstructs.2010.07.001

Nomenclature

AR	aspect (slenderness) ratio
C_D	mean drag force coefficient
C_D'	fluctuating drag force coefficient
C_L	mean lift force coefficient
C_L'	fluctuating lift force coefficient
C_P	mean pressure coefficient
C_P'	fluctuating pressure coefficient
C_{PB}	mean base pressure coefficient
D	cylinder diameter (m)
f	vortex shedding frequency (Hz)
G	Griffin number
G	gap width (m)
H	cylinder height, span, or length (m)
L	centre-to-centre longitudinal spacing (pitch) (m)
L/D	longitudinal pitch ratio
$(L/D)_c$	critical longitudinal pitch ratio
l_f	vortex formation length
Nu	Nusselt number
P	centre-to-centre spacing (pitch) (m)
P/D	pitch ratio
Re	Reynolds number
Sh	Sherwood number
St	Strouhal number
T	centre-to-centre transverse spacing (pitch) (m)
T/D	transverse pitch ratio
U	freestream velocity (m/s)
x	streamwise coordinate (m)
y	cross-stream coordinate (m)
z	vertical coordinate (m)
α	incidence angle (deg.)
μ	dynamic viscosity (Pa s)
ρ	density (kg/m^3)
φ	phase

same diameter, D. For the case of "infinite" cylinders, i.e., each cylinder's aspect ratio (or slenderness ratio), AR = H/D (where H is the height, length, or span of the cylinder), is sufficiently high that the flow around the cylinder can be considered nominally two-dimensional, the three most important variables governing the fluid flow behaviour are (i) the spacing between the cylinders, (ii) the orientation of the cylinders in the x–y plane relative to the oncoming flow, and (iii) the Reynolds number, Re. In most studies, the Reynolds number has been defined using the uniform approach (or freestream) velocity, U, and the cylinder diameter, i.e., $\mathrm{Re} = \rho UD/\mu$ where ρ is the fluid density and μ is the dynamic viscosity. For the case of "finite" cylinders mounted normal to a ground plane, additional variables governing the fluid flow behaviour include (iv) the cylinder aspect ratio and (v) the properties of the boundary layer on the ground plane.

The two idealized arrangements of the cylinders which have received the most study are the tandem and side-by-side configurations, shown in Fig. 1(a, b), where the geometry is described by the centre-to-centre longitudinal and transverse spacings, or pitches, L and T, respectively. In each case, the spacing between the cylinders is usually expressed in non-dimensional form, as the longitudinal or transverse pitch ratio, L/D or T/D. For the transverse and side-by-side configurations (Fig. 1(a, b)), some authors have used the gap width, G, instead of the longitudinal and transverse spacings.

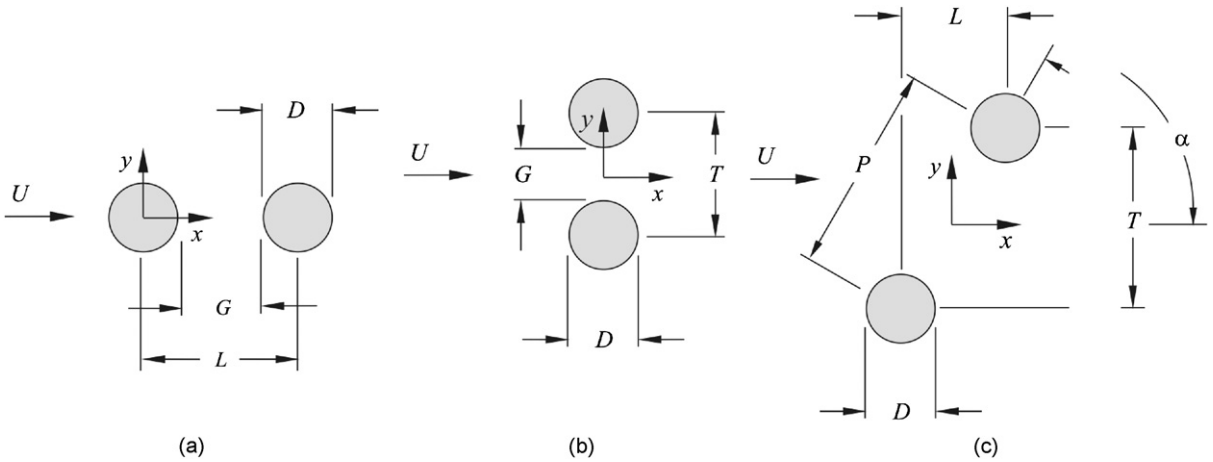

Fig. 1. Two circular cylinders of equal diameter in cross-flow: (a) tandem configuration; (b) side-by-side configuration; and (c) staggered configuration.

The most general arrangement of two cylinders is the staggered configuration, which is likely the arrangement most encountered in practice, since in very few cases will an oncoming flow be perfectly aligned with the cylinders, or precisely perpendicular to them. The geometry of the staggered pair of cylinders, shown in Fig. 1(c), is set by the centre-to-centre pitch, P, between the cylinders and the angle of incidence; as in the case of the tandem and side-by-side configurations, the spacing is typically expressed as a dimensionless centre-to-centre pitch ratio, P/D. Alternatively, it may be defined in a similar manner to the tandem and side-by-side configurations, by the longitudinal and transverse spacings, L and T, as shown in Fig. 1(c). Perhaps because of the added variable (α) used to define the geometry, however, the staggered configuration has received somewhat less research attention despite its predominance in engineering applications.

The fluid dynamics of multiple cylinder configurations immersed in steady cross-flow have been examined by many researchers (one of the earliest experimental studies, on two circular cylinders in tandem and side-by-side configurations, was performed by Biermann and Herrnstein (1934), who were interested in the interference effects of airplane struts), and more than 130 such studies were collected and reviewed for this paper (many of the experimental studies are summarized in Tables 1–3). The behaviour of groups of cylinders in cross-flow has been reviewed by Zdravkovich (1977, 1987, 1993, 2003), Nishimura (1986), and Chen (1987), with the last major review article published more than 20 years ago by Ohya et al. (1989). However, within the last 10–20 years, there have been many new contributions to the understanding of the flow around multiple cylinders, and this has motivated the present review of the literature.

To limit the scope of the material on the flow around multiple cylinders, the primary focus of this review is on configurations of two infinite circular cylinders of equal diameter immersed in steady cross-flow. Researchers have also studied the flow around two cylinders of different diameters (e.g., Suzuki et al. (1971), Hiwada et al. (1979), Igarashi (1982), Bokaian and Geoola (1984), Baxendale et al. (1985), Lam et al. (1993), Ko et al. (1996), Alam and Zhou (2008)), two cylinders located close to a plane wall (e.g., Bhattacharyya and Dhinakaran (2008)), two cylinders partially buried in a channel bed (e.g., Cokgor and Avci (2001)), and two cylinders immersed in oscillatory flow (e.g., Cokgor and Avci (2003), Chern et al. (2010)), for example, but these more specialized studies are not reviewed here. An extensive body of literature, motivated by industrial problems, also exists on the flow-induced vibrations (e.g., Zdravkovich (1985), Chen (1987), Mahir and Rockwell (1996a, 1996b), Ting et al. (1998), Zhou et al. (2001), Price et al. (2007), Papaioannou et al. (2008), Lee et al. (2009), Prasanth and Mittal (2009a, 2009b)) and acoustic resonance (e.g., Mohany and Ziada (2005, 2009), Hanson et al. (2009)) associated with groups of cylinders in cross-flow; however, to further limit the scope of the review, this subject is not considered here.

2. Approaches to understanding the fluid behaviour

A number of approaches have been used in an attempt to classify the fluid behaviour of multiple circular cylinders in steady cross-flow, based on a combination of theory, measurement and observation of the flow.

For two-cylinder configurations in steady mean cross-flow, the simplest of the approaches is the more theoretical treatment by Zdravkovich (1987), who classified the fluid behaviour into two basic types of interference, based on the location of the downstream cylinder with respect to the upstream one. The two types of interference, and the conditions under which they occur, are shown in Fig. 2: (i) wake interference, when one of the cylinders is partially or completely submerged in the wake of the other, and (ii) proximity interference, when the two cylinders are located close to one another, but neither is submerged in the wake of the other. An example of wake interference would be the widening of the two separated free shear layers from one cylinder located immediately upstream of a second cylinder, in a tandem configuration (Fig. 1(a)), such that vortex formation from the first cylinder is suppressed. Proximity interference, on the other hand, is often difficult to predict, since often there is no obvious or visible displacement of a wake, for example, but it typically has an effect on the vortex shedding behaviour. An example of proximity interference for a two-cylinder arrangement is a specific frequency or phase synchronization between two Kármán vortex streets, typically seen for the side-by-side configuration of two cylinders (Fig. 1(b)). Other locations of the downstream cylinder correspond to a ''no-interference'' region, although this may be a misnomer, since for the side-by-side configuration, ''interference'' in the form of anti-phase synchronization of the vortex shedding processes (e.g., Williamson (1985), Sumner et al. (1999b)) may be found. For the staggered configuration (Fig. 1(c)), Gu and Sun (1999) extended Zdravkovich's (1987) classification to three different types, namely wake interference, shear layer interference, and neighbourhood interference. Both these classification schemes, by Zdravkovich (1987) and Gu and Sun (1999), however, fail in some respects to recognize the complex behaviour displayed in experiments and the wide range of flow patterns observed.

A second approach has been through the interpretation of experimental (and numerical) data; specifically, vortex shedding frequencies, static pressure measurements on the cylinder surfaces, and mean lift and drag forces. These measurements are acquired for different arrangements of the cylinders, as the pitch ratio(s), incidence angle and

Table 1
Selected experimental studies of two tandem circular cylinders in cross-flow. CTA = constant temperature anemometry; FV = flow visualization; LIF = laser-induced fluorescence; PIV = particle image velocimetry.

Researchers	Re	L/D	AR	Blockage ratio (%)	Turbulence intensity (%)	Test facility	Technique	Measurements
Alam et al. (2003b)	6.5×10^4	1.1–9	8	8	0.19	Wind tunnel	FV, pressure, force	St, C_P, C_P', C_D, C_D', C_L'
Arie et al. (1983)	1.57×10^5	2–10	11	9	0.3	Wind tunnel	Pressure	St, C_P, C_P', C_D', C_L'
Biermann and Herrnstein (1934)	6.1×10^4–1.5×10^5	1–9	48–120	1.2–3	Not given	Wind tunnel	Force	Interference drag
Hiwada et al. (1982)	1.5×10^4–8×10^4	1–6	8, 20	7, 13	0.2	Wind tunnel	FV, CTA, pressure, temperature	St, C_D, C_D', Sh, Nu
Hori (1959)	200–1.2×10^4	1.2–3	120	1	0.03	Wind tunnel	CTA, pressure	St, C_P, C_{PB}, velocity profiles
Huhe-Aode et al. (1985)	100, 300, 1×10^3	1.5–10	30	2	Not given	Towing tank	FV, CTA	St
Igarashi (1981)	8.7×10^3–5.2×10^4	1–5	4	6	0.6	Wind tunnel	FV, CTA, pressure	St, C_P, C_P', C_D
Igarashi (1984)	1.15×10^4–1.03×10^5	1–1.5	3	13	0.6	Wind tunnel	FV, CTA, pressure	St, C_P, C_P', C_D
Ishigai et al. (1972, 1973)	1.5×10^3–1.5×10^4	1–5	11	9	Not given	Wind tunnel	FV, CTA, pressure	St, C_P
Jendrzejcyk and Chen (1986)	1.5×10^4–1.5×10^5	1.4–10	12	9	1–11	Water tunnel	Force	St, C_D', C_L'
Kiya et al. (1992)	2×10^4–3.7×10^4	2.5–4	11	10	0.1–10	Wind tunnel	CTA, pressure	–
Kostic and Oka (1972)	1.3×10^4–4×10^4	1.6–9	5	20	2.8	Wind tunnel	Pressure, temperature	C_P, C_D, Nu
Kwon et al. (1996)	1.7×10^4	1–5	11	2	2.5	Water channel	PIV	Velocity field
Lee and Basu (1997)	2.4×10^4–5.1×10^4	2, 3.2	20	6.3	0.35	Wind tunnel	FV, CTA, pressure	St, C_P
Lee and Panagakos (1997)	2.4×10^4–5.1×10^4	2, 3.2	20	5	0.35	Wind tunnel	FV, CTA, pressure	St, C_P, C_P'
Lin et al. (2002)	1×10^4	1.15–5.1	8.3	10	Not given	Water channel	PIV	Velocity field
Ljungkrona and Sundén (1993)	3.3×10^3–4×10^4	1.25–4	16	6	0.1	Wind tunnel	FV, pressure	St, C_P, C_P'
Ljungkrona et al. (1991)	2×10^4	1.25–5	16	6	0.1–3.2	Wind tunnel	FV, pressure	St, C_P, C_P', C_D
Nishimura et al. (1986)	800–1×10^4	1.2–7.2	5	9	0.6	Water tunnel	FV	Sh
Okajima (1979)	4×10^4–6.2×10^5	1.1–6.3	7	8	0.1	Wind tunnel	FV	St, C_D
Sun et al. (1992)	3.25×10^5, 6.5×10^5	2.2–4	15	5	0.12	Wind tunnel	Pressure	C_P, C_P'
Xu and Zhou (2004)	800–4.2×10^4	1–15	40, 16	2.5, 6.7	Not given	Wind tunnel, water tunnel	CTA, LIF	St
Wu et al. (1994)	1×10^3, 1.7×10^4–4×10^4	3–7	24, 20	4, 5	0.1, 0.15	Water tunnel, wind tunnel	FV, CTA, pressure	St
Zdravkovich and Pridden (1977)	6×10^4	2.5–7	33	2	0.1	Wind tunnel	CTA, pressure	C_P, C_{PB}, C_D
Zhang and Melbourne (1992)	1.11×10^5	2–10	8	5	0.4–11.5	Wind tunnel	Pressure, force	C_P, C_P', C_D, C_D', C_L'
Zhou and Yiu (2006)	7×10^3	1.3–6	40	2.5	0.4	Wind tunnel	CTA	Velocity, temperature

Table 2
Selected experimental studies of two side-by-side circular cylinders in cross-flow. CCA = constant current anemometry; CTA = constant temperature anemometry; FV = flow visualization; LDV = laser Doppler velocimetry; PIV = particle image velocimetry. Blockage ratio based on the maximum total blockage for two cylinders.

Researchers	Re	T/D	AR	Blockage ratio (%)	Turbulence intensity (%)	Test facility	Technique	Measurements
Alam and Zhou (2007a)	4.7×10^4	1.1–1.2	6	8	0.5	Wind tunnel	FV, pressure	C_P, C_L
Alam et al. (2003a)	350, 5.5×10^4	1.1–3.4, 1.1–5	12.5, 6	11, 8	Not given, 0.5	Water channel, wind tunnel	FV, CTA, pressure, force	St, C_P, C_P', C_D, C_L, C_D', C_L'
Bearman and Wadcock (1973)	2.5×10^4	1–6	31	4	0.2	Wind tunnel	FV, CTA, pressure	St, C_P, C_{PB}, C_D, C_L
Biermann and Herrnstein (1934)	6.1×10^4–1.5×10^5	1–5.3	48–120	2–6	Not given	Wind tunnel	Force	Interference C_D
Brun et al. (2004)	1×10^3–1.4×10^4	1.583	10	14	Not given	Water channel	LDV	St, velocity profiles
Hori (1959)	200–1.2×10^4	1.2–3	120	1	0.03	Wind tunnel	CTA, pressure	St, C_P, C_{PB}, velocity profiles
Ishigai et al. (1972)	1.5×10^3–1.5×10^4	1.25–3	11	18	Not given	Wind tunnel	FV, CTA, pressure	St
Jendrzejcyk and Chen (1986)	1.5×10^4–1.5×10^5	1.35, 2.7	12	17	1-11	Wind tunnel	Force	St, C_D', C_L'
Kamemoto (1976)	662	1.5–3	75	3	n/a	Towing tank	FV, CTA	St
	3×10^4	1–3	5	13	Not given	Wind tunnel	CTA	St
Kim and Durbin (1988)	3.3×10^3	1–3	27	3	0.2	Wind tunnel	FV, CTA, pressure	St, C_{PB}, velocity field
Le Gal et al. (1990)	110	1–7.5	50	4	1	Water tunnel	FV	–
Peschard and Le Gal (1996)	90–150	1–6	7	Not given	1	Water tunnel	FV	–
Spivack (1946)	5×10^3–9.3×10^4	1–6	39	5	0.02	Wind tunnel	CTA	St, velocity profiles
Sumner et al. (1999b)	$500–3 \times 10^3$, 1.2×10^3–3×10^3	1–6, 1–3	16, 27	13, 7	0.5, n/a	Water tunnel, towing tank	FV, CTA, PIV	St, velocity field
Sun et al. (1992)	3.3×10^5, 6.5×10^5	2.2	15	10	0.12	Wind tunnel	Pressure	C_P'
Wang et al. (2002b)	120–1.65×10^3	1.13, 1.7, 3	15	13.3	Not given	Water tunnel	FV	–
Williamson (1985)	50–150, 200	1.2–6	140, 13	1, 16	Not given	Wind tunnel, water channel	FV	St
Xu et al. (2003)	150–1×10^3, 300–1.4×10^4	1.2–1.6	15, 47	13, 4.2	Not given, 0.4	Water tunnel, wind tunnel	FV, CTA, PIV	St, velocity field
Zdravkovich and Pridden (1977)	6×10^4	1.25–2	33	4	0.1	Wind tunnel	Force	C_D, C_L
Zhou et al. (2002)	5.8×10^3	1.5–3	47	4.2	0.4	Wind tunnel	CTA, CCA	Velocity field, temperature field
Zhou et al. (2000)	1.8×10^3	1.5–3	79	2.5	0.5	Wind tunnel	CTA, CCA	Velocity profiles, temperature profiles

Table 3
Selected experimental studies of two staggered circular cylinders in cross-flow. CCA = constant current anemometry; CTA = constant temperature anemometry; FV = flow visualization; PIV = particle image velocimetry. Blockage ratio based on the maximum total blockage for two cylinders.

Researchers	Re	Geometry	AR	Blockage ratio (%)	Turbulence intensity (%)	Test facility	Technique	Measurements
Akosile and Sumner (2003)	5×10^4	$P/D = 1.125–1.25$, $\alpha = 0–90°$	18	4	0.6	Wind tunnel	CTA, pressure, force	St, C_{PB}, C_D, C_L
Alam and Sakamoto (2005)	5.5×10^4	$P/D = 1.1–6$, $\alpha = 10–75°$	6	8	0.5	Wind tunnel	Pressure	St
Alam et al. (2005)	5.5×10^4, 350	$P/D = 1.1–6$, $\alpha = 10–75°$	6, 13	8	0.5, not given	Wind tunnel, water channel	FV, pressure, force	C_P, C_P', C_D, C_L, C_D', C_L'
Bokaian and Geoola (1984)	5.9×10^3	$L/D = 1.5–4$, $T/D = 0–6$	18.1	10.7	6.5	Water channel	Force	C_D, C_L
Cooper (1974)	$1 \times 10^4–1.25 \times 10^5$	$L/D = 1.35–50.51$, $T/D = 0–7.43$	24	8	Not given	Wind tunnel	Pressure, force	C_P, C_D, C_L
Gu and Sun (1999)	5.6×10^3, $2.2 \times 10^5–3.3 \times 10^5$	$P/D = 1.5–2$, $\alpha = 0–45°$, $P/D = 1.1–3.5$, $\alpha = 0–90°$	Not given, 6.4	Not given, 8	Not given, 0.2	Wind tunnel, wind tunnel	FV, pressure	–
Gu et al. (1993)	6.5×10^5	$P/D = 1.05–4$, $\alpha = 0–90°$	15	11.4	0.12–10	Wind tunnel	Pressure	C_P, C_D, C_L
Hu and Zhou (2008a, 2008b)	7×10^3, 300	$P/D = 1.2–4$, $\alpha = 0–90°$	48, 30	4, 3	0.4, not given	Wind tunnel, water tunnel	FV, CTA, CCA, PIV	St, velocity field, temperature field
Ishigai et al. (1972, 1973)	$1.5 \times 10^3–1.5 \times 10^4$	$L/D = 0.68–4$, $T/D = 0.5–3$	11	9	Not given	Wind tunnel	FV, CTA, pressure	St, C_P
Kiya et al. (1980)	$2 \times 10^4–3.7 \times 10^4$	$P/D = 0–5.5$, $\alpha = 0–90°$	11	19	0.8	Wind tunnel	CTA	St
Moriya and Sakamoto (1985)	6.53×10^4	$L/D = 2–6$, $T/D = 0–1.5$	10	20	0.4	Wind tunnel	FV, pressure, force	St, C_P, C_P', C_D, C_L, C_D', C_L'
Ozono et al. (2001)	$2.5 \times 10^3–7.5 \times 10^3$, 3×10^4	$L/D = 1–4$, $T/D = 0–2$	23.3, 14.6	7.5, 8.8	1, 2	Water channel, wind tunnel	FV, CTA, pressure	St, C_{PB}
Price (1976)	$1.7 \times 10^4–8 \times 10^4$	$L/D = 6–18$, $T/D = 0–2.42$	37, 42	5–12	1–11	Wind tunnel	FV, pressure, force	C_P, C_D, C_L
Price and Païdoussis (1984)	$1.7 \times 10^4–8.6 \times 10^4$	$L/D = 1.5–5$, $T/D = 0.75–2$	24	6	0.5	Wind tunnel	Force	C_D, C_L
Sun et al. (1992)	$3.25 \times 10^5–6.5 \times 10^5$	$P/D = 2.2$, $\alpha = 12.5°$	15	10	0.12–10	Wind tunnel	Pressure	C_P, C_P'
Sumner (2004)	5×10^4	$P/D = 1.125–1.25$, $\alpha = 0–90°$	18	4	0.6	Wind tunnel	CTA, pressure, force	St, C_{PB}, C_D, C_L, G
Sumner et al. (2000)	$850–1.35 \times 10^3$, 1.9×10^3	$P/D = 1–5$, $\alpha = 0–90°$, $P/D = 1–4$, $\alpha = 0–90°$	16, 27	13, 7	0.5, n/a	Water tunnel, towing tank	FV, PIV	St, velocity field
Sumner et al. (2005)	$3.2 \times 10^4–7.4 \times 10^4$	$P/D = 1.125–4$, $\alpha = 0–90°$	18, 24	3.5, 5.6	0.6	Wind tunnel	CTA, force	St, C_D, C_L
Sumner and Richards (2003)	$3.2 \times 10^4–7 \times 10^4$	$P/D = 2–2.5$, $\alpha = 0–90°$	24	5.6	0.6	Wind tunnel	CTA, force	St, C_D, C_L
Sumner and Schenstead (2006)	$3.2 \times 10^4–7.4 \times 10^4$	$P/D = 1.125–4$, $\alpha = 0–90°$	18, 24	3.5, 5.6	0.6	Wind tunnel	CTA, pressure, force	St, C_{PB}, C_D, C_L, G
Suzuki et al. (1971)	1.3×10^3, $1 \times 10^5–6.3 \times 10^5$	$P/D = 2$, $\alpha = 0–15°$, $P/D = 1.1–3.9$, $\alpha = 0–15°$	Not given, 6–18	Not given, 12–24	Not given	Water tunnel, wind tunnel	FV, pressure	C_P, C_D
Ting et al. (1998)	$4 \times 10^4–2 \times 10^5$	$L/D = 1.5–5$, $T/D = 0.1–1.05$	5.3–12.8	10.6–25	0.8	Wind tunnel	Pressure, force	C_D, C_L
Wardlaw and Cooper (1973)	$1.2 \times 10^4–1.4 \times 10^5$	$P/D = 1.2–35$, $\alpha = 0–75°$	45	3	Not given	Wind tunnel	Force	C_D, C_L
Zdravkovich and Pridden (1977)	6×10^4	$L/D = 0–5$, $T/D = 0–3$	33	5	0.1	Wind tunnel	Pressure, force	C_P, C_D, C_L
Zhou et al. (2009)	$1.5 \times 10^3–2 \times 10^4$	$P/D = 1.2–4$, $\alpha = 0–90°$	48	4	0.4	Wind tunnel	CTA	St

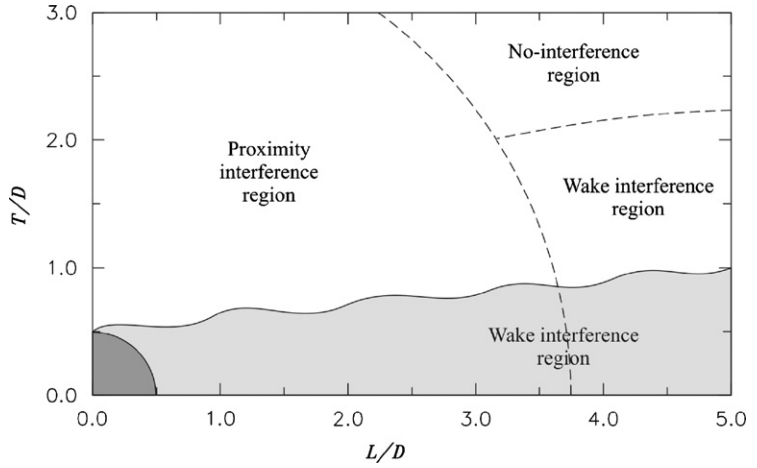

Fig. 2. Wake interference and proximity interference boundaries (referenced to the location of the downstream cylinder relative to the upstream cylinder, Fig. 1(c)) for two staggered circular cylinders of equal diameter immersed in steady cross-flow, based on Zdravkovich (1987).

Reynolds number are varied, and the changes to the flow field and other features are then inferred from the behaviour of the experimental data. As examples: (i) vortex shedding frequency data have been used to infer the existence of two Kármán vortex shedding processes for staggered-cylinder configurations, by Kiya et al. (1980); (ii) static pressure coefficient data have been offered as evidence of a stable pair of eddies within the gap between two tandem cylinders, and continuous reattachment of the two shear layers, by Igarashi (1981, 1984), Hiwada et al. (1982) and Ljungkrona (1992); and (iii) peak mean lift force measurements for two staggered circular cylinders, and rapid changes in the mean lift force for small adjustments to the geometry, have been attributed to the strong influence of the high speed flow deflected through the gap between cylinders, as described by Zdravkovich and Pridden (1977). Such an approach is useful from an engineering design point of view, and has led to recommendations for avoiding the occurrence of flow-induced vibration, for instance. However, determining the fluid behaviour from measured quantities is prone to misinterpretation, particularly when done without the benefit of accompanying flow visualization (the studies of Zdravkovich and Pridden (1977), Kiya et al. (1980), and Eastop and Turner (1982) are selected as examples of the measurement-only approach, but they are by no means the only ones), or from time-averaged data acquired in flows which are fundamentally periodic (such as the single cylinder and multiple cylinders).

A third approach to understanding the fluid dynamics of multiple cylinders in cross-flow, and arguably the most useful, is to identify from flow visualization (and other means) the various flow patterns which arise for different choices of the geometry. The understanding of the fluid dynamics of tandem cylinders in cross-flow has greatly benefited from this approach, as demonstrated, for example, by Igarashi (1981, 1984). His studies identified up to eight different flow patterns from a *combination* of flow visualization and measured data for various combinations of L/D and Re. The side-by-side configuration has also been addressed in a similar manner, by Williamson (1985) and Kumada et al. (1984). Sumner et al. (2000) pursued the flow-pattern identification approach for the staggered configuration and identified up to nine flow patterns.

A fourth, more recent approach has been to study the flow around two cylinders using numerical simulations (e.g., Meneghini et al. (2001)). All of the traditional computational fluid dynamics methods have been employed, including direct numerical simulation, large-eddy simulation (e.g., Chen et al. (2003), Palau-Salvador et al. (2008), Kitagawa and Ohta (2008)), Reynolds-averaged Navier–Stokes methods, using finite-difference, finite-element (e.g., Edamoto and Kawahara (1998)), and finite-volume (e.g., Li et al. (2003)) schemes, and also the vortex-in-cell (e.g., Ng and Ko (1995), Akbari and Price (2005)) and lattice-Boltzman (e.g., Agrawal et al. (2006)) methods. Owing to the complexity of the flow around groups of cylinders, the numerical approach has been less popular and successful than the experimental approach. Many of the simulations in the literature are two-dimensional and are restricted to low Reynolds numbers ($Re < 300$).

3. Tandem configuration

When two circular cylinders are arranged in-line and parallel to the mean flow in a tandem (or in-line) configuration (Fig. 1(a)), the downstream cylinder is shielded from the oncoming flow by the cylinder immediately upstream.

The wake of the upstream cylinder modifies the incoming flow conditions (specifically, the incident vorticity field (Lin et al., 2002)) for the downstream cylinder, while this second cylinder interferes with the wake dynamics and vortex formation region of the upstream cylinder. This mutual interference means that the upstream cylinder may behave as a turbulence generator, the downstream cylinder may behave as a drag-reduction device or "wake stabilizer" (Lee and Basu, 1997), and the two cylinders may behave as if a single bluff body or as two independent bodies depending on the spacing between their centres.

The tandem configuration falls within the wake interference region (Fig. 2) of Zdravkovich (1987). The fluid behaviour is a function of the Reynolds number (more so than for the other basic two-cylinder groups) and the centre-to-centre longitudinal pitch ratio, L/D (some studies have used the gap ratio, $G/D = L/D-1$). At small pitch ratios Kármán vortex shedding from the upstream cylinder is suppressed. At intermediate pitch ratios, complex flow patterns occur in the gap between the two cylinders. Of prime importance at larger pitch ratios is the critical pitch ratio, $(L/D)_c$, at which Kármán vortex shedding first begins to occur from the upstream cylinder, and the sensitivity of this critical pitch ratio to the Reynolds number (e.g., Ljungkrona et al. (1991), Ljungkrona and Sundén (1993), Xu and Zhou (2004)) and the freestream turbulence intensity (e.g., Ljungkrona et al., 1991). For instance, an increase in freestream turbulence intensity is associated with a reduction in $(L/D)_c$ (Ljungkrona et al., 1991). Elevated turbulence intensity also has pronounced effects on the fluid forces, vortex shedding frequencies, and flow regimes (e.g., Jendrzejcyk and Chen (1986), Ljungkrona et al. (1991), Zhang and Melbourne (1992), Gu et al. (1993)).

Many experimental studies of tandem cylinders in steady cross-flow have been undertaken, from low Reynolds numbers (e.g., Huhe-Aode et al. (1985) at $Re = 100$) to the critical and post-critical regimes (e.g., Sun et al. (1992) at $Re = 6.5 \times 10^5$), and for rows of two cylinders (the majority of studies, in fact those of particular interest in this review), three cylinders (e.g., Aiba and Yamazaki (1976), Aiba et al. (1980b), Igarashi and Suzuki (1984)), four cylinders (e.g., Aiba et al. (1980a, 1981), Igarashi (1986)) and five cylinders (e.g., Hetz et al. (1991)), spaced from one diameter (i.e., $L/D = 1$, where the cylinders are in contact) to more than twenty diameters apart in some cases. Some selected experimental investigations of two-cylinder tandem configurations are summarized in Table 1.

Other studies of two tandem circular cylinders have focused on heat transfer (e.g., Kostic and Oka (1972), Aiba and Yamazaki (1976), Aiba et al. (1980a, 1980b, 1981), Hiwada et al. (1982), Zhou and Yiu (2006)) and mass transfer (e.g., Nishimura et al. (1986)) effects. There have also been many numerical studies of the flow around two circular cylinders in tandem, primarily at low Reynolds numbers (e.g., Mittal et al. (1997) for $Re = 100$ and 1000; Farrant et al. (2000) for $Re = 200$; Meneghini et al. (2001) for $Re = 100$ and 200; Sharman et al. (2005) for $Re = 100$; Carmo and Meneghini (2006) for $Re = 160$–320; Papaioannou et al. (2006) for $Re = 100$–1000; Carmo et al. (2010a) for $Re = 50$–500; Carmo et al. (2010b) for $Re = 200$–350; Singha and Sinhamahapatra (2010) for Re 40–150), although some higher Reynolds number simulations also exist (e.g., Kitagawa and Ohta (2008) for $Re = 2.2 \times 10^4$).

Related studies in the literature that are not reviewed in this paper include the flow around two tandem square prisms (e.g., Edamoto and Kawahara (1998), Liu and Chen (2002), Alam and Zhou (2007b), Yen et al. (2008)), flow around two tandem elliptic cylinders (e.g., Ota et al. (1986), Ota and Nishiyama (1986), Nishiyama et al. (1988)), the flow around impulsively started cylinders in tandem (e.g., Sumner et al. (1999a)), and the flow around two surface-mounted finite-height cylinders in tandem (e.g., Sarode et al. (1981), Luo et al. (1996), Palau-Salvador et al. (2008)).

3.1. Flow patterns

The flow around two tandem circular cylinders is sensitive to both Re and L/D. The pioneering studies of the tandem configuration by Igarashi (1981, 1984) identified eight different flow patterns for two tandem circular cylinders of equal diameter in steady cross-flow, as shown in Fig. 3; Igarashi's map of the flow patterns, in Re–L/D space, is also shown in Fig. 3. This classification of the flow patterns has been widely referenced in other studies in the literature.

Following Zdravkovich's (1987) approach, the flow patterns in Fig. 3 can be subdivided into three basic types of wake interference behaviour: (i) single bluff-body behaviour, also referred to as the "extended-body regime" by Xu and Zhou (2004) and Zhou and Yiu (2006), at small L/D, where the two cylinders are sufficiently close to act as if a single structure; (ii) shear layer reattachment behaviour, also referred to as the "reattachment regime" by Xu and Zhou (2004) and Zhou and Yiu (2006), at intermediate L/D, where the separated free shear layers from the upstream cylinder reattach onto the surface of the downstream cylinder and vortices may form in the gap between the cylinder; and (iii) Kármán vortex shedding from each cylinder, also referred as the "co-shedding regime" by Xu and Zhou (2004) and Zhou and Yiu (2006), at larger L/D.

A similar classification scheme was used by Carmo et al. (2010a, 2010b), based on numerical simulations of two tandem circular cylinders at low Reynolds numbers, with three main flow patterns: (i) SG (symmetric in the gap) observed at $L/D = 1.5$; (ii) AG (alternating in the gap) observed at $L/D = 1.8$ and 2.3; and (iii) WG (wake in the gap) observed at $L/D = 5$.

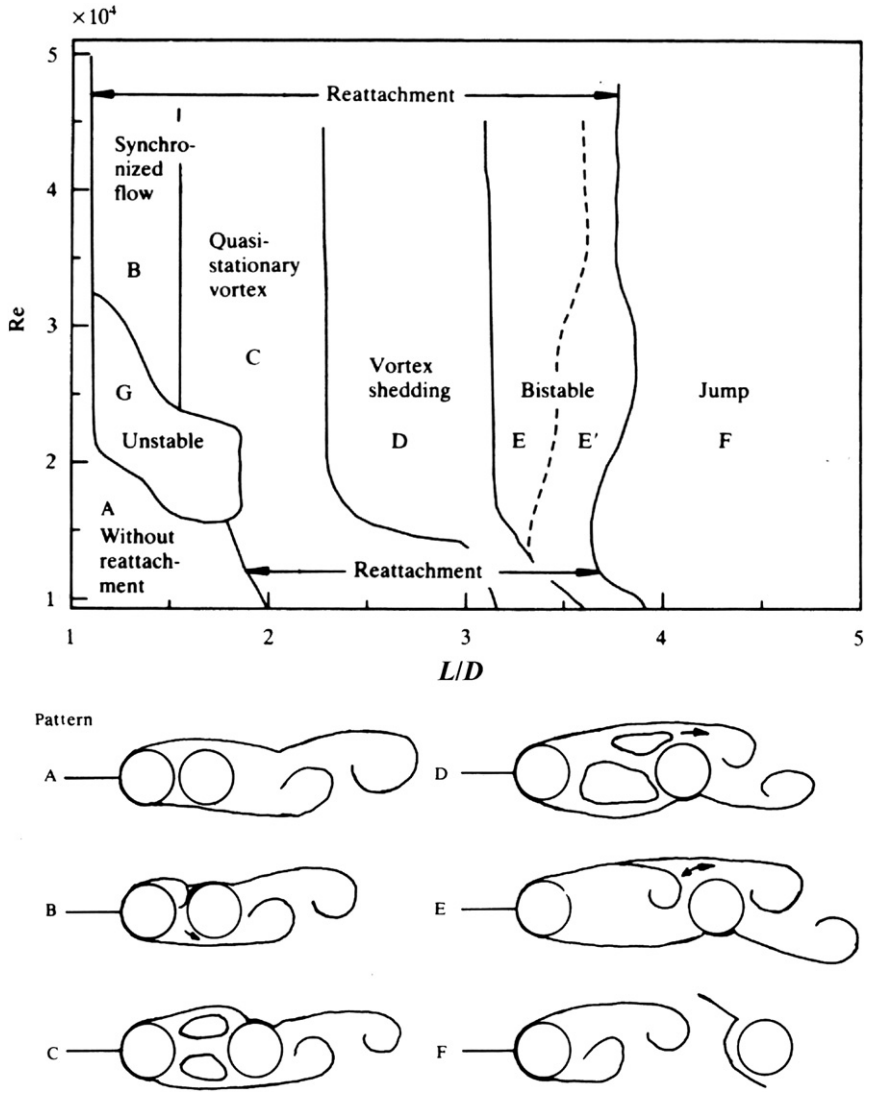

Fig. 3. Classification of flow patterns for two tandem circular cylinders in cross-flow, from Igarashi (1981), as a function of the longitudinal centre-to-centre pitch ratio and Reynolds number.

(Figure taken from Ljungkrona et al. (1991)).

The reattachment regime can be subdivided into two basic flow regimes based on the behaviour of the Strouhal number (Xu and Zhou, 2004) and the wake flow structure and vortex dynamics (Zhou and Yiu, 2006). The four resulting flow regimes for the tandem configuration, based on these more recent studies, are shown in Fig. 4. Here, the reattachment regime extends from $L/D = 2$–5 (although these boundaries are functions of Re) but has two subdivisions: for $L/D = 2$–3, shear layer reattachment occurs more often on the rear surfaces (“after-body”) of the downstream cylinder, while for $L/D = 3$–5 it occurs more often on the leading surfaces (“fore-body”) of the downstream cylinder (Zhou and Yiu, 2006).

The variety of fluid behaviours for the tandem configuration is illustrated in the selected flow visualization images in Fig. 5. Further details on the flow regimes are now provided in the following subsections.

3.1.1. *Single bluff body behaviour (“extended-body” regime)*

For small pitch ratios (approx. $1 < L/D < 1.2$–1.8 (Zdravkovich, 1987) or $1 < L/D < 2$ (Zhou and Yiu, 2006), depending on the Re range) the two cylinders behave as a single bluff body or “extended-body” (Pattern An of Igarashi

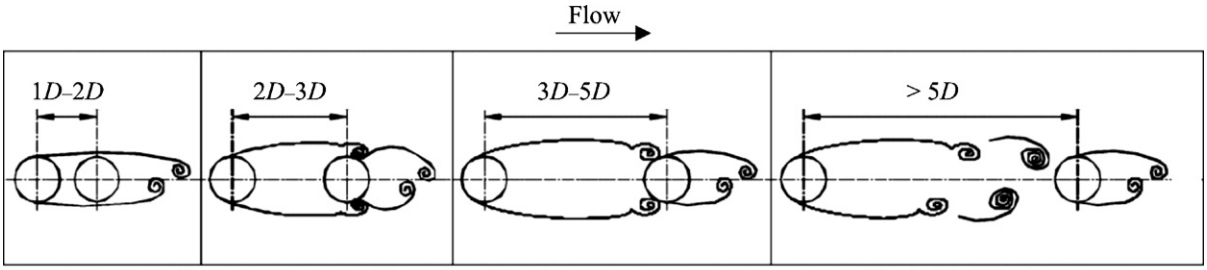

"Extended-body" Regime
$L/D = 1–2$

"Reattachment" Regime
$L/D = 2–5$ with
Sub-division $L/D = 2–3$
Sub-division $L/D = 3–5$

"Co-shedding" Regime
$L/D > 5$

Fig. 4. Simplified classification scheme of the flow patterns for two tandem circular cylinders in cross-flow, from Xu and Zhou (2004) and Zhou and Yiu (2006).

(Figure taken from Zhou and Yiu (2006)).

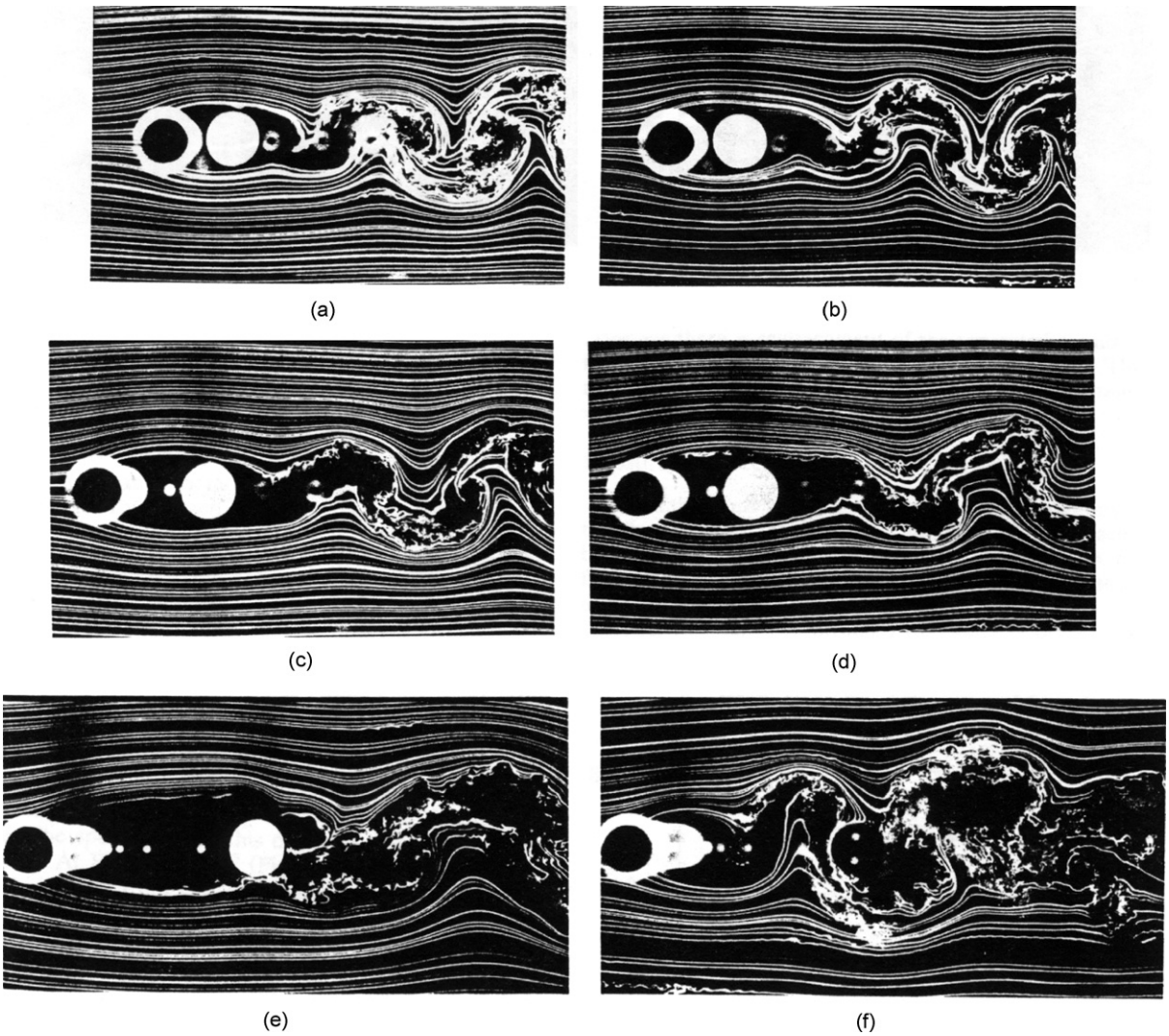

Fig. 5. Flow past two tandem circular cylinders, flow from left to right (figures taken from Ljungkrona and Sundén (1993)). Extended-body regime: (a) $L/D = 1.25$, $Re = 1 \times 10^4$; (b) $L/D = 1.25$, $Re = 1.2 \times 10^4$. Reattachment regime: (c) $L/D = 2$, $Re = 1 \times 10^4$, (d) $L/D = 2$, $Re = 1.2 \times 10^4$; (e) $L/D = 4$, $Re = 1 \times 10^4$. Co-shedding regime: (f) $L/D = 4$, $Re = 1.2 \times 10^4$.

(1981) in Fig. 3); some flow visualization images from the literature are shown in Fig. 5(a, b). The downstream cylinder sits inside the vortex formation region of the upstream cylinder (Ishigai et al., 1972) and the separated shear layers from the upstream cylinder are forced to enclose or wrap around the downstream cylinder, without any reattachment onto its surface, before rolling up alternately into Kármán vortices behind the downstream cylinder. The downstream cylinder, in some respects, can be considered to behave in a manner similar to a short splitter plate (Zhou and Yiu, 2006). The shear layers from the upstream cylinder become considerably elongated compared to the case of a single cylinder. The gap between the cylinders is thought to contain mostly stagnant fluid (Zdravkovich, 1985) although there may be some oscillatory cavity-flow-type behaviour (Hetz et al., 1991). Kármán vortex shedding from the cylinder pair occurs at a Strouhal number higher than a single cylinder. Vortex roll-up behind the downstream cylinder has been seen to occur closer to the cylinder when compared to the single-cylinder case (Meneghini et al., 2001). The wake is narrower and the Kármán vortices are more elongated compared to the case of the single cylinder (Lin et al., 2002) (Fig. 6).

3.1.2. *Shear layer reattachment behaviour (''reattachment'' regime)*

For intermediate pitch ratios (approx. $1.2–1.8 < L/D < 3.4–3.8$ (Zdravkovich, 1987) or $2 < L/D < 5$ (Zhou and Yiu, 2006), depending on the range of Re) the cylinders are placed sufficiently far apart that the shear layers from the upstream cylinder can no longer enclose the downstream cylinder, but instead reattach onto the downstream cylinder. From Igarashi's (1981) classification of the flow patterns (Fig. 3), and from the examples shown in Fig. 5(c, d, e), Figs. 7 and 8, a wide variety of fluid behaviour can be observed in this ''reattachment regime'' (Patterns G, B, C, D, E, and E′ in Fig. 3). This behaviour principally involves the reattachment of the shear layers from the upstream cylinder and the formation and shedding of eddies in the gap region between the two cylinders. The gap eddies can vary substantially and intermittently in terms of their strength, asymmetry, and general behaviour (Lin et al., 2002).

The shear layer and gap flow dynamics have been extensively investigated by Igarashi (1981, 1984), Hiwada et al. (1982), Zdravkovich (1985, 1987), Hetz et al. (1991), Lee and Panagakos (1997), Lee and Basu (1997), Lin et al. (2002), and others. These studies have used various measurement techniques, including conventional flow visualization (Figs. 5(c, d, e) and 7) and particle image velocimetry (PIV) (Figs. 6 and 8) to examine the flow field, and surface oil flow visualization (Alam et al., 2003b), surface-mounted hot-film sensor arrays (e.g., Lee and Basu (1997), Lee and Panagakos (1997)) and fluctuating surface pressure distributions (e.g., Alam et al. (2003b)) to determine the reattachment and separation points. Despite the large number of studies, however, a complete picture of what happens in the gap remains somewhat elusive, likely due to the Reynolds number sensitivity of the shear layers (Lin et al., 2002) and the vortex formation length (Ljungkrona et al., 1991; Ljungkrona and Sundén, 1993).

At smaller pitch ratios ($1.1 < L/D < 1.6$ from Igarashi (1981)) within the reattachment regime, the shear layers from the upstream cylinder may alternately reattach onto the front face of the downstream cylinder, this reattachment process being synchronized with Kármán vortex shedding from the downstream cylinder (Pattern B of Igarashi (1981) in Fig. 3). An alternating reattachment behaviour was also observed by Alam et al. (2003b) for $L/D < 2$. at $\mathrm{Re} = 6.5 \times 10^4$.

At intermediate pitch ratios ($1.6 < L/D < 2.3–2.4$ from Igarashi (1981)) within the reattachment regime, shear layer reattachment may be nearly continuous and a pair of quasi-stationary eddies forms in the gap (Pattern C of Igarashi (1981) in Fig. 3). Steady reattachment of the shear layers on the downstream cylinder was also reported by Alam et al. (2003b) at $\mathrm{Re} = 6.5 \times 10^4$. Coinciding with the appearance of the eddies, a ''jet-like flow'' is established on the gap centreline directed upstream (Lin et al., 2002). In contrast, the numerical simulations of Kitagawa and Ohta (2008), for $L/D = 2$ and $\mathrm{Re} = 2.2 \times 10^4$, showed alternate reattachment of the shear layers onto the downstream cylinder (behaviour similar to Pattern B).

Zhou and Yiu (2006), in their subdivision of the reattachment regime (Fig. 4), noted that for $L/D = 2–3$ shear layer reattachment occurs more often on the downstream side of the second cylinder. This interferes with boundary layer development and separation on the downstream cylinder, and the Kármán vortices formed behind the downstream cylinder are relatively weak and small. In contrast, for $L/D = 3–5$, reattachment occurs more often on the second cylinder's upstream side. With less influence on the downstream cylinder's boundary layer development, the resulting Kármán vortices are stronger (Zhou and Yiu, 2006). The change in the reattachment point positions can also be discerned in the velocity field data, for various pitch ratios, in Fig. 8.

At higher pitch ratios ($2.5 < L/D < 3.1–3.5$ from Igarashi (1981)) within the reattachment regime, the shear layers enclosing the gap may exhibit more oscillatory behaviour (Ljungkrona et al., 1991) and intermittent shedding of the gap vortices (Pattern D of Igarashi (1981) in Fig. 3) may occur (Zdravkovich, 1985), interfering with vortex shedding from the downstream cylinder (Zdravkovich, 1987). Examples of the gap vortices and intermittent shedding are shown in Fig. 7. The numerical simulations of Kitagawa and Ohta (2008), for $L/D = 3$ and $\mathrm{Re} = 2.2 \times 10^4$, showed two main modes of fluid behaviour, one where the shear layers from the upstream cylinder symmetrically reattached onto the downstream cylinder, and another (the more dominant mode) in which a small vortex forms just upstream of the

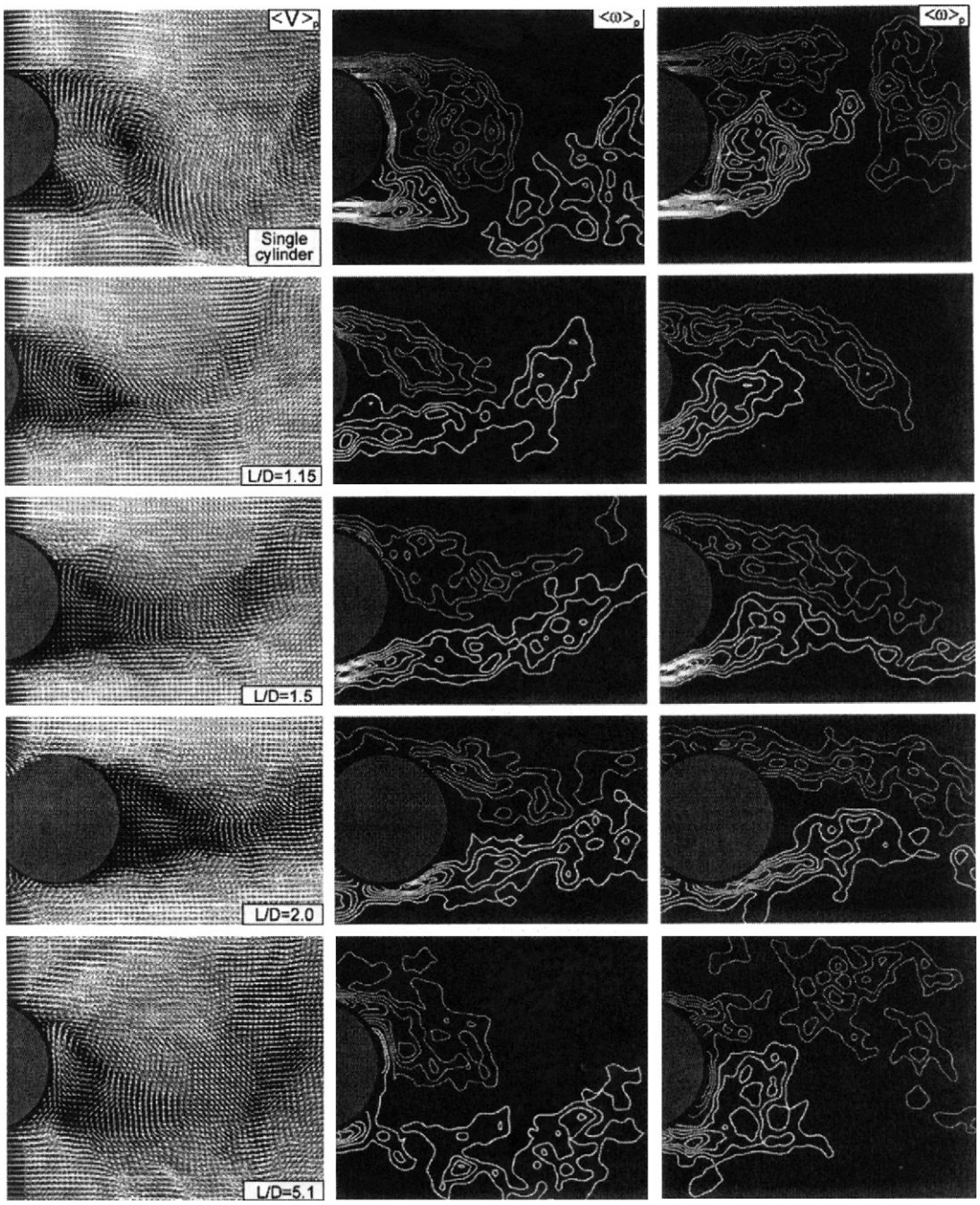

Fig. 6. Vortex shedding behind the downstream cylinder for different longitudinal pitch ratios (phase-averaged velocity and vorticity fields from PIV measurements), $Re = 1 \times 10^4$, flow from left to right.

(Figures taken from Lin et al. (2002)).

downstream cylinder and becomes entrained into the Kármán vortex shedding process. Periodic (as opposed to intermittent) shedding of the gap vortices has also been indicated (Igarashi 1981, 1984; Hetz et al., 1991).

Throughout this flow regime, Kármán vortex shedding occurs only from the downstream cylinder. At smaller pitch ratios, the vortices appear different than those from an isolated circular cylinder (Fig. 6) and the vortex formation and shedding mechanism is distinct (Lin et al., 2002).

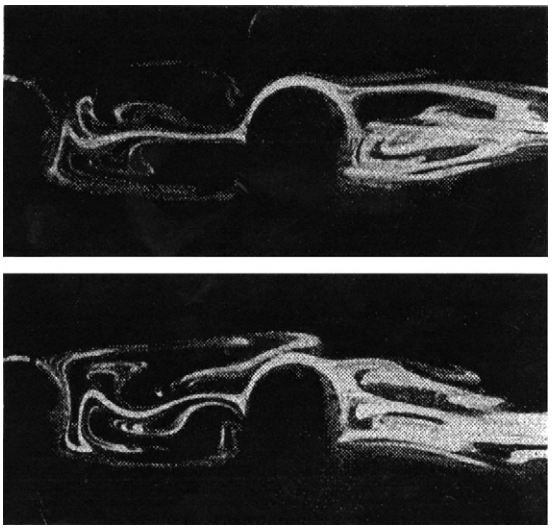

Fig. 7. Gap flow patterns for two tandem circular cylinders at intermediate pitch ratios ($L/D = 3$) at $Re = 100$, representative of the extended-body regime, flow from left to right.
(Figures taken from Huhe-Aode et al. (1985)).

Igarashi (1981) also identified some transitional flow patterns, identifying Pattern G as an "unstable" flow pattern where the extended-body regime changes over to the reattachment regime. Similar transitional behaviour was identified by Xu and Zhou (2004) from Strouhal number measurements, who also found this flow pattern to be bistable.

3.1.3. Vortex shedding from both cylinders ("co-shedding" regime)

At higher pitch ratios (approx. $L/D > 3.4$–3.8 (Zdravkovich, 1987) or $L/D > 5$ (Zhou and Yiu, 2006), depending on the range of Re) the downstream cylinder is sufficiently far away that Kármán vortex shedding can now occur from the upstream cylinder as well as the downstream one. The downstream cylinder is now located outside the vortex formation region of the upstream cylinder (Ishigai et al., 1972) and experiences the periodic impingement of shed Kármán vortices from the upstream cylinder. A flow visualization example is shown in Fig. 5(f). In this "co-shedding" flow regime, both cylinders undergo vortex shedding at the same frequency, and "vortex shedding from the downstream cylinder is triggered by the arrival of vortices generated by the upstream cylinder" (Alam and Zhou, 2007b). In the numerical simulations of Meneghini et al. (2001), vortex impingement results in an "amalgamation process", as vortices shed from the upstream cylinder merge with those forming from the downstream cylinder. The incident vortices are "severely distorted as they are swept about the [downstream] cylinder" (Lin et al., 2002) and the Kármán vortices form very close to the base of the downstream cylinder (Fig. 6), in contrast to the reattachment regime and the single-cylinder case. The resulting Kármán vortices shed from the downstream cylinder are larger but weaker compared to those in the extended-body and reattachment regimes (Zhou and Yiu, 2006). The shed vortices comprising the vortex street weaken and dissipate more quickly due partially to the vortex impingement process (Zhou and Yiu, 2006).

The critical pitch ratio, $(L/D)_c$, at which Kármán vortex shedding occurs from the upstream cylinder, varies from 3.5 to 5 depending on the Reynolds number (Xu and Zhou, 2004). The switchover from shear layer reattachment to Kármán vortex shedding from the upstream cylinder is sudden, and the third type of behaviour has been called the "jumped" flow pattern because of the abrupt changeover. In the flow visualization examples from the literature in Fig. 5(e, f), for $L/D = 4$, due to the Reynolds-number sensitivity of the critical pitch ratio, vortex shedding is seen to occur from both cylinders only for the highest Reynolds number (Fig. 5(f)).

The transition to and from the co-shedding regime is known to be bistable, with intermittent appearance of the two flow patterns (Patterns E and E′ from Igarashi (1981) in Fig. 3) on either side of the critical pitch ratio (Igarashi, 1981; Kiya et al., 1992; Xu and Zhou, 2004). Hysteretic behaviour can also be observed depending on whether L/D or Re is being increased or decreased (Zdravkovich, 1987); this behaviour has also been observed for two tandem square prisms (Liu and Chen, 2002). For $L/D < 6$–8, there may be synchronization between the vortex shedding processes and vortex streets of the upstream and downstream cylinders, and the possible formation of a "binary vortex street" behind the

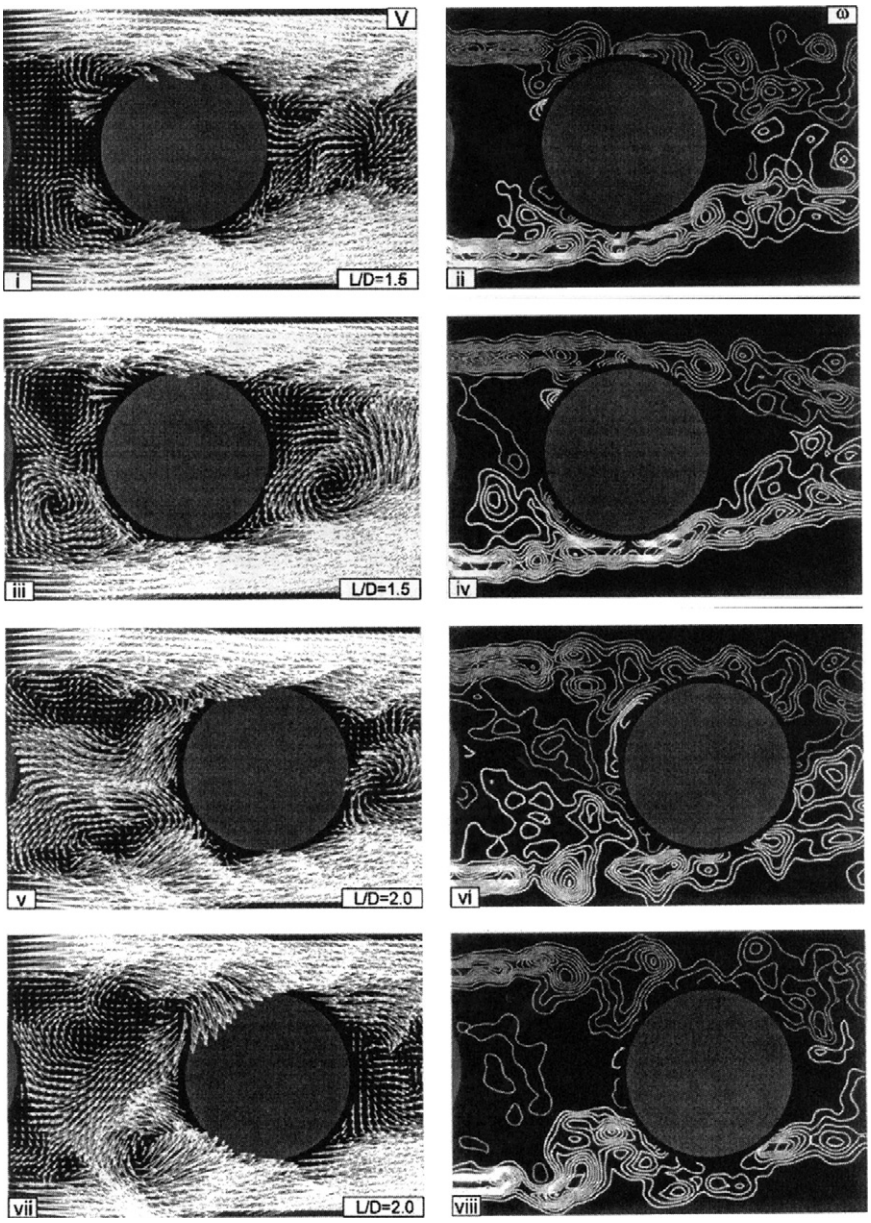

Fig. 8. Gap flow behaviour at intermediate pitch ratios (instantaneous velocity and vorticity fields from PIV measurements), $Re = 1 \times 10^4$, flow from left to right.

(Figures taken from Lin et al. (2002)).

downstream cylinder (Zdravkovich, 1987). Vortex formation from the two cylinders is independent for $L/D > 6$–8 (Ohya et al., 1989).

3.2. Reynolds number effects

As the flow pattern boundaries of Igarashi (1981) indicate (Fig. 3), the flow around two tandem circular cylinders is particularly sensitive to the Reynolds number. Extensive Strouhal number data by Xu and Zhou (2004) for Re = 800–4.2×10^4 further illustrate the Reynolds number sensitivity beyond the flow pattern boundaries established earlier by

Igarashi (1981); this is shown in Fig. 9(a). Experiments at supercritical and transcritical Reynolds numbers were performed by Okajima (1979) and Sun et al. (1992).

At lower Reynolds numbers, the Reynolds number sensitivity of the flow patterns has been investigated numerically by Carmo et al. (2010a, 2010b). Their flow pattern boundaries are shown in Fig. 9(b) for the SG (symmetric in the gap), AG (alternating in the gap), and WG (wake in the gap) flow pattern classification. The flow pattern boundaries show several ranges of L/D and Re where the flow is bistable, alternating between two-dimensional and three-dimensional wakes or between different flow patterns.

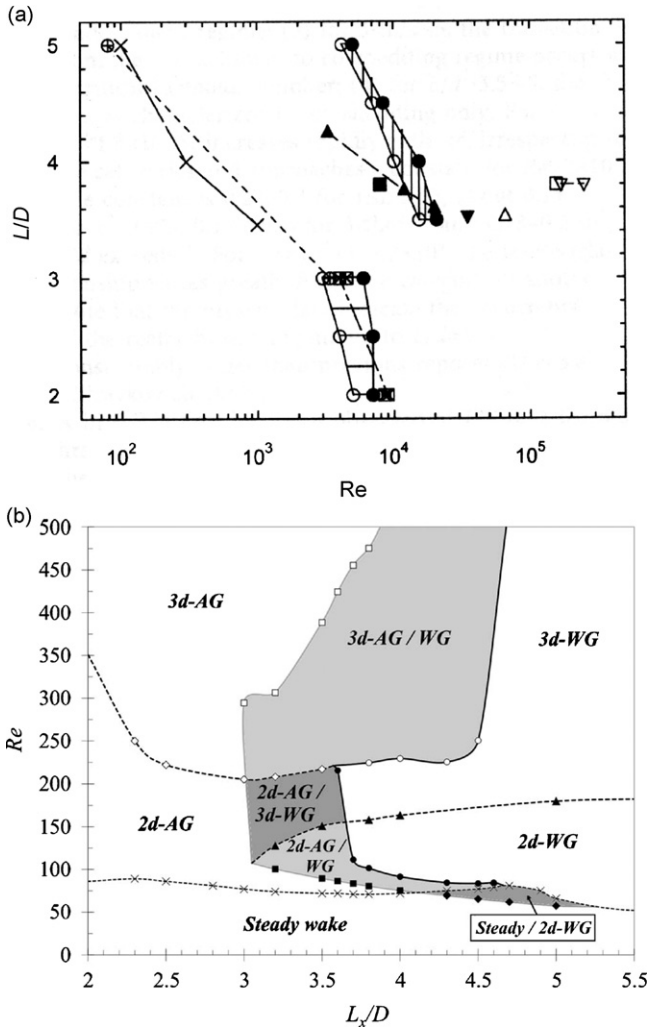

Fig. 9. Reynolds number sensitivity for two tandem circular cylinders in cross-flow: (a) from experimental Strouhal number data (figure taken from Xu and Zhou (2004)); (b) vortex shedding regimes from the numerical simulations of Carmo et al. (2010a). (a) ○, lower Re for transition between flow regimes; ●, upper Re for transition between flow regimes; ■, Ishigai et al. (1972); ▽, Okajima (1979); ▼, Igarashi (1981); □, Arie et al. (1983); ×, Huhe-Aode et al. (1985); △, Moriya and Sakamoto (1986); ▲, Ljungkrona et al. (1991); horizontal hatched area, transition from extended-body to reattachment regime; vertical hatched area, transition from reattachment to co-shedding regime. (b) ◇, mode T3 critical Reynolds numbers;▲, mode A critical Reynolds numbers; ♦, two-dimensional transition from shedding regime WG to steady flow; ■, two-dimensional vortex shedding transition from WG to AG; □, three-dimensional vortex shedding transition from WG to AG; ●, two-dimensional vortex shedding transition from AG to WG; ○, three-dimensional vortex shedding transition from AG to WG; dashed lines for data obtained from stability calculations; solid lines for data from direct numerical simulations.

(Figure taken Carmo et al. (2010a)).

The critical pitch ratio, $(L/D)_c$, is particularly sensitive to the Reynolds number, and from the various studies in the literature varies from $(L/D)_c = 3$–5. It is noted that the critical pitch ratio behaviour closely follows the Reynolds-number sensitivity of the vortex formation length (Fig. 10) (Ljungkrona et al., 1991; Ljungkrona and Sundén, 1993). Also contributing to the Reynolds number effects is the behaviour of the shear layers from the upstream cylinder, and the development of shear layer instability (Kelvin–Helmholtz) vortices (Lin et al., 2002). Within the reattachment regime the small-scale shear-layer instability vortices "buffet the surface of the downstream cylinder" (Lin et al., 2002).

From Figs. 3, 9 and 10, the trend in the experimental data is towards a larger critical pitch ratio at low Reynolds numbers. The experimental study with the lowest reported values of Reynolds number, Huhe-Aode et al. (1985), reported $(L/D)_c = 4.5$–5 for Re = 100, $(L/D)_c = 3.5$–4 for Re = 300, and $(L/D)_c = 3$–3.5 for Re = 1000. In contrast, however, many numerical studies at low Reynolds number have reported much lower values of the critical pitch ratio, e.g., $(L/D)_c = 3$ at Re = 100 (Li et al., 1991), $(L/D)_c = 3.7$–4 at Re = 100 (Sharman et al., 2005), $(L/D)_c = 3$ at Re = 200 (Meneghini et al., 2001).

3.3. Wake structure and vortex dynamics

The wake structure and vortex dynamics of the tandem cylinder group have been studied experimentally by Lin et al. (2002) at $Re = 1 \times 10^4$ (using PIV) and Zhou and Yiu (2006) at Re = 7000 (using hot-wire anemometry). A comparison of the Kármán vortex formation and shedding processes in the near wake of the downstream cylinder, for various L/D, is shown in Fig. 6. It can be seen that the vortex formation process is substantially different from the case of the single cylinder.

A comparison of the shed vortices and their strengths, for various L/D, from Zhou and Yiu (2006), is shown in Fig. 11. In the extended-body and co-shedding regimes, the shed Kármán vortices weaken more rapidly compared to the reattachment regime; however, the wake growth is slower in the reattachment regime compared to the other two flow regimes (Zhou and Yiu, 2006).

The three-dimensional structure of the flow field was examined experimentally by Wu et al. (1994), with a focus on the formation of secondary streamwise vortex structures and the spanwise coherence or correlation of the velocity field. Within the reattachment regime, the streamwise vortex structures are absent behind the upstream cylinder, and the spanwise correlation in the wake of the downstream cylinder is higher than what is found in the wake of a single circular cylinder. In contrast, within the co-shedding regime, the spanwise coherence behind the downstream cylinder is lowered due to the effects of vortex impingement, elevated turbulence intensity, and streamwise vortex structures in the approaching flow. Their results were generally consistent with the spanwise correlation length data of Arie et al. (1983) obtained from surface pressure measurements. Several numerical studies have also focused on the three-dimensional

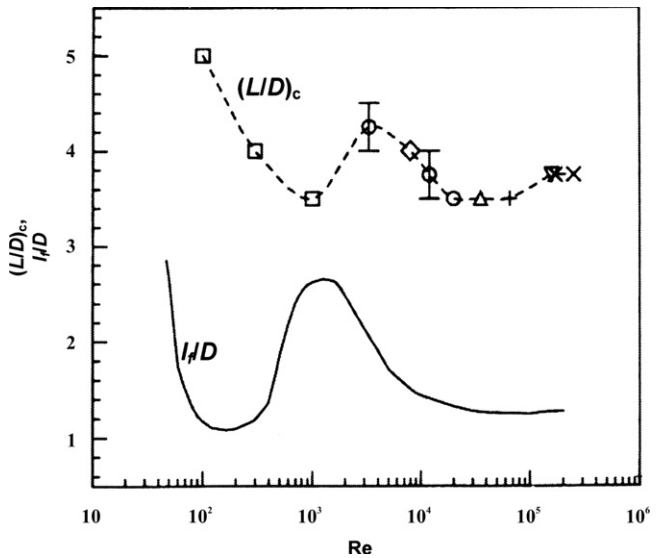

Fig. 10. The Reynolds-number sensitivity of the vortex formation length (for a single circular cylinder) and the critical pitch ratio (for two tandem circular cylinders), where l_f = vortex formation length.

(Figure taken from Ljungkrona and Sundén (1993)).

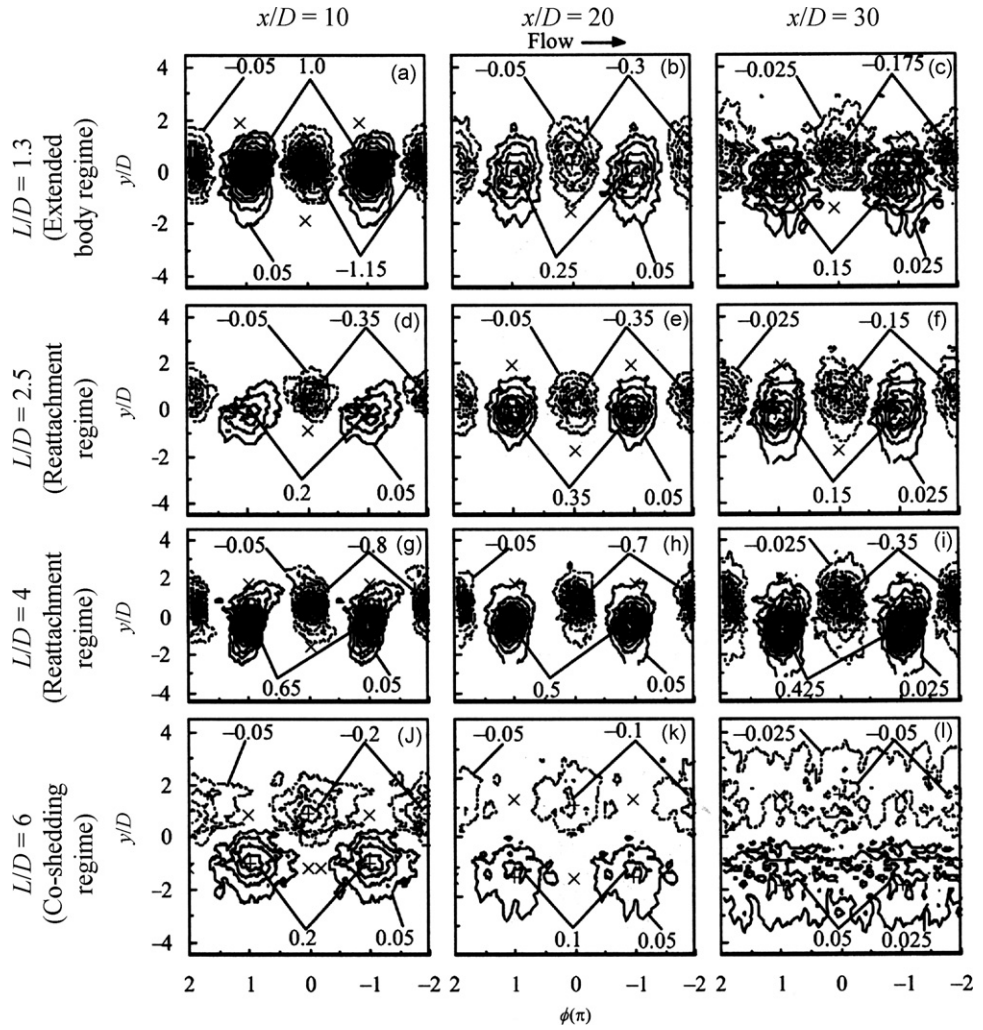

Fig.11. Phase-averaged vorticity contours in the wake of two tandem circular cylinders, Re = 7000, for different longitudinal pitch ratios and streamwise distances from the downstream cylinder, for phase, φ.

(Figures taken from Zhou and Yiu (2006)).

structure, in particular its appearance and development at lower Reynolds numbers (Carmo and Meneghini, 2006; Deng et al., 2006; Papaioannou et al., 2006; Carmo et al., 2010a, 2010b).

3.4. Measurements

Many studies in the literature have reported on the complex behaviour of the measured data, including the surface mean and fluctuating pressure coefficients (e.g., Arie et al. (1983), Ljungkrona et al. (1991), Alam et al. (2003b)), mean and fluctuating drag and lift force coefficients, and the Strouhal number. The reader is referred to Table 1 for a list of selected studies and the measured data they report. Some additional comments on the force coefficients and Strouhal number are presented in the following sub-sections.

3.4.1. Force coefficients

The complexity of the mean drag force coefficients for the upstream and downstream cylinders is shown in Fig. 12. For the upstream cylinder, C_D is typically lower than the single-cylinder value (the splitter-plate effect of the downstream cylinder) within the extended-body and reattachment regimes. There is a slow decrease in C_D with

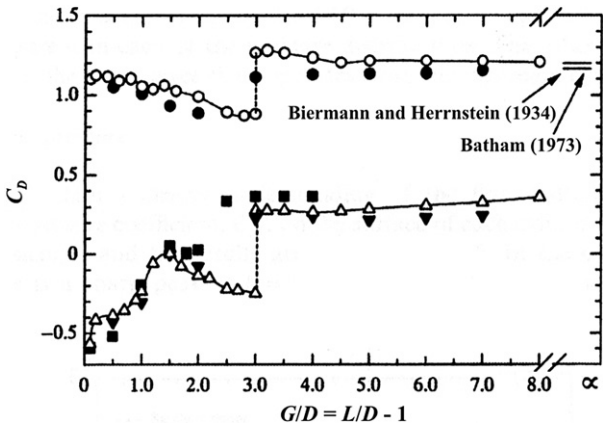

Fig. 12. Mean drag force coefficient data for two tandem circular cylinders in cross-flow as a function of gap ratio: ○, Alam et al. (2003b), upstream cylinder, $Re = 6.5 \times 10^4$; △, Alam et al. (2003b), downstream cylinder, $Re = 6.5 \times 10^4$; ●, Biermann and Herrnstein (1934), upstream cylinder; ▼, Biermann and Herrnstein (1934), downstream cylinder; ■, Zdravkovich and Pridden (1977), downstream cylinder; solid line refers to single circular cylinder (Batham, 1973).

(Figure taken from Alam et al. (2003b)).

increasing L/D until the end of the reattachment regime. After the critical L/D, where the flow suddenly transitions to the co-shedding regime, the mean C_D jumps to a higher value of C_D close to the value for a single cylinder.

In the extended-body and reattachment regimes, the mean drag coefficient for the downstream cylinder is negative (and may reach zero drag at a given value of L/D, depending on the Reynolds number and study), indicating this cylinder experiences a thrust force. A discontinuous jump from a small negative drag coefficient to a larger positive mean drag coefficient occurs as the flow "jumps" from the reattachment regime to the co-shedding regime. At increasingly large pitch ratios, the C_D values for the cylinders will eventually approach the single-cylinder value. Since the mean drag coefficient for the downstream cylinder is for the most part negative for $L/D < (L/D)_c$, and positive for $L/D > (L/D)_c$, the critical pitch ratio has also been termed the "drag inversion" spacing (Carmo et al., 2010a, 2010b).

The complexity of the fluctuating lift and drag force coefficients is shown in Fig. 13. It is noted that the downstream cylinder in the co-shedding regime experiences large unsteady forces (Mittal et al., 1997).

3.4.2. Strouhal number

The most extensive set of Strouhal number data for two tandem circular cylinders is that of Xu and Zhou (2004), for a wide range of Reynolds numbers ($Re = 800$–4.2×10^4) and pitch ratios ($L/D = 1$–15). The relationship between Strouhal number and pitch ratio is shown in Fig. 14. The complexity of the Strouhal number behaviour with both L/D and Re is illustrated in Fig. 15. In general, only a single value of Strouhal number is measured for two tandem cylinders at all pitch ratios.

When the cylinders behave as a single bluff body at small L/D, the Strouhal number is initially higher than the single-cylinder value but decreases rapidly with increasing L/D. The higher shedding frequency for the extended-body regime is a reflection of the shorter vortex formation length when the cylinders are situated very close together (Zdravkovich, 1977). At the boundary between the extended-body and reattachment regimes (e.g., Pattern G of Igarashi (1981) shown in Fig. 3), two dominant frequencies (Strouhal numbers) may be found (Igarashi, 1981, 1984; Ljungkrona et al., 1991). A slower decrease in St occurs during the reattachment regime as L/D is increased, and the Strouhal number becomes lower than the value for a single cylinder. The lower shedding frequency reflects a "stabilization" of the flow field by the presence of the downstream cylinder in a fashion similar to a splitter plate. Within the extended-body and reattachment regimes, the vortex shedding peaks in the power spectra tend to be smaller and more broad-banded (Kiya et al., 1980).

A discontinuous jump in St occurs at the critical L/D, as the Strouhal number suddenly increases from a low value to a high value. The existence of bistable flow patterns at the boundary between the reattachment and co-shedding regimes (e.g., Patterns E and E′ of Igarashi (1981) shown in Fig. 3) means that over a small range of pitch ratio two dominant frequencies are found. Within the co-shedding regime, the same St value is measured behind both cylinders, and the value of St slowly increases and approaches the single-cylinder value as L/D increases. Complex behaviour in the Strouhal number data with Reynolds number (including the appearance of an additional Strouhal number) is seen at very high pitch ratios ($L/D = 6$–80), as summarized in the review by Ohya et al. (1989).

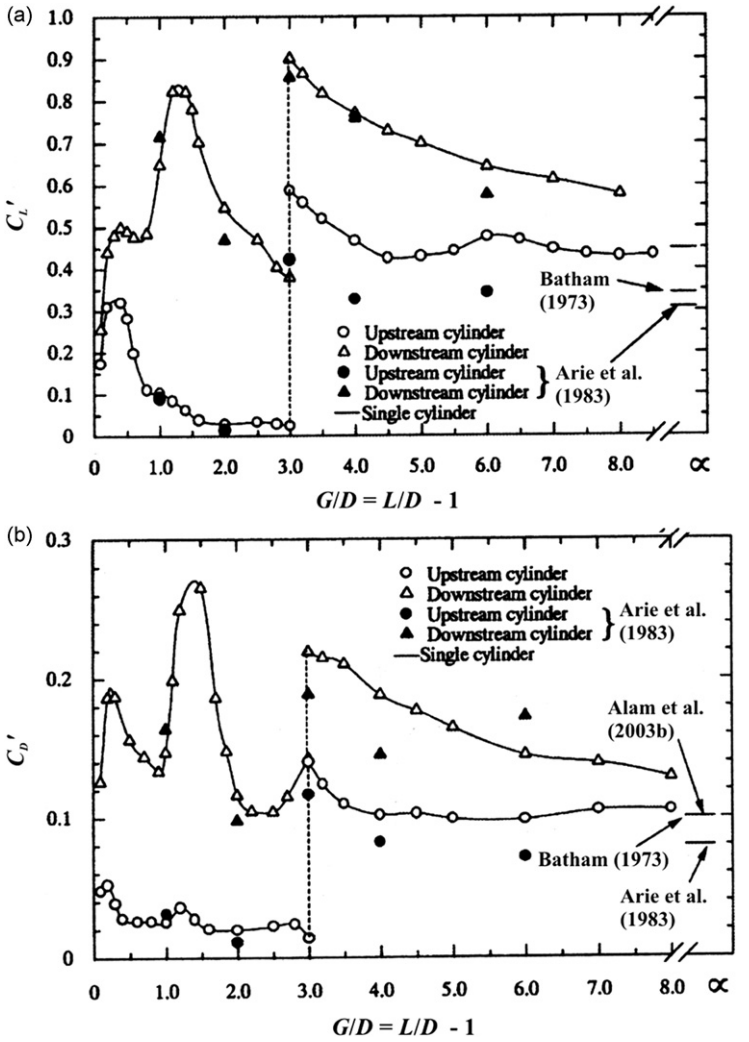

Fig. 13. Fluctuating force coefficients for two tandem circular cylinders in cross-flow as a function of gap ratio, $Re = 6.5 \times 10^4$: (a) fluctuating lift force coefficient and (b) fluctuating drag force coefficient.

(Figure taken from Alam et al. (2003b)).

4. Side-by-side configuration

When two circular cylinders are arranged transverse to the mean flow in a side-by-side (or transverse) configuration (Fig. 1(b)), the wakes of the two cylinders interact with one another on either side of the gap between the two cylinders. If the cylinders are in very close proximity, they may behave as if a single bluff body with the added effect of "base bleed" (Bearman, 1967; Wood, 1967). If the cylinders are spaced sufficiently far apart, they may behave as two independent bluff bodies, although synchronization between the adjacent vortex streets may occur. Complex wake and vortex-street interactions occur when the cylinders are spaced between these two extremes, in particular an asymmetric, or biased, flow pattern that may be bistable in nature.

The side-by-side configuration falls within the proximity interference region of Zdravkovich (1987) shown in Fig. 2. The fluid behaviour is primarily a function of the centre-to-centre transverse pitch ratio, T/D (some studies have used the gap width ratio, $G/D = T/D-1$). There are also some Reynolds number effects, but these effects are less prominent than for the tandem configuration.

Many experimental studies of side-by-side cylinders in steady cross-flow have been undertaken, from low Reynolds numbers (e.g., Williamson (1985) at $Re = 50$) to the post-critical regime (e.g., Sun et al. (1992) at $Re = 6.5 \times 10^5$), for

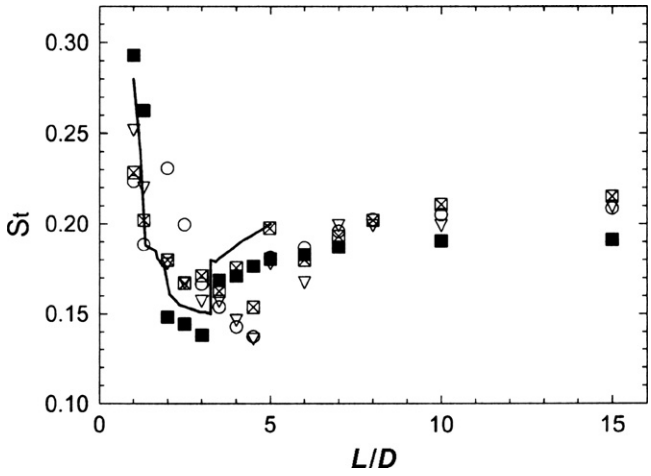

Fig. 14. Strouhal number data for two tandem circular cylinders in cross-flow as a function of the longitudinal pitch ratio: ▽, $Re = 1.2 \times 10^3$ (Xu and Zhou, 2004); ⊠, $Re = 2.9 \times 10^3$ (Xu and Zhou, 2004); ○, $Re = 7 \times 10^3$ (Xu and Zhou, 2004) ; ■, $Re = 4.2 \times 10^4$ (Xu and Zhou, 2004); solid line, $Re = 2.2 \times 10^4$ (Igarashi, 1981).

(Figure taken from Xu and Zhou (2004)).

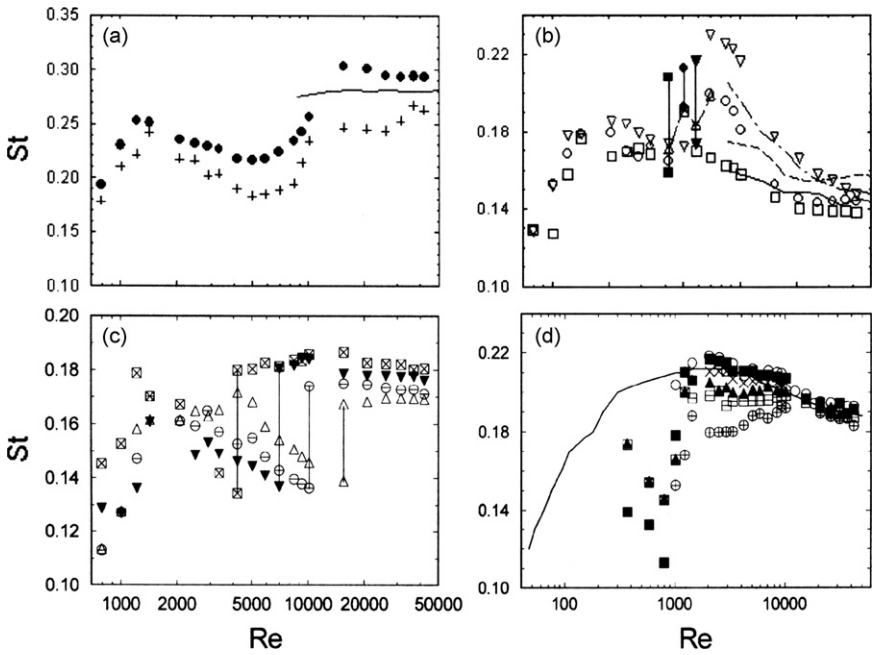

Fig. 15. Strouhal number data for two tandem circular cylinders as a function of the Reynolds number and longitudinal pitch ratio: (a) "extended-body" regime ($L/D = 1$–1.3); (b) lower portion of the "reattachment" regime ($L/D = 2$–3.09); (c) upper portion of the "reattachment" regime ($L/D = 3.5$–5); (d) "co-shedding" regime ($L/D > 5$). ●, $L/D = 1$ (Xu and Zhou, 2004); +, $L/D = 1.3$ (Xu and Zhou, 2004); solid line in (a), $L/D = 1.03$ (Igarashi, 1981); ▽, $L/D = 2$ (Xu and Zhou, 2004); ○ in (b), $L/D = 2.5$ (Xu and Zhou, 2004); □, $L/D = 3$ (Xu and Zhou, 2004); solid line in (b), $L/D = 3.09$ (Igarashi, 1981); dashed line in (b), $L/D = 2.5$ (Igarashi, 1981); unequal-length dashed line in (b), $L/D = 2.06$ (Igarashi, 1981); △, $L/D = 3.5$ (Xu and Zhou, 2004); ⊖, $L/D = 4$; ▼, $L/D = 4.5$ (Xu and Zhou, 2004); ⊠, $L/D = 5$ (Xu and Zhou, 2004); ⊗, $L/D = 6$ (Xu and Zhou, 2004); ⊟, $L/D = 7$ (Xu and Zhou, 2004); ▲, $L/D = 8$ (Xu and Zhou, 2004); ×, $L/D = 10$ (Xu and Zhou, 2004); ■, $L/D = 15$ (Xu and Zhou, 2004); solid line in (d), single circular cylinder (Norberg, 1994); ○ in (d), single circular cylinder (Xu and Zhou, 2004); vertical lines in (b) and (c) highlight the co-existence of two prominent peaks at the same Re.

(Figure taken from Xu and Zhou (2004)).

two cylinders (the majority of studies, those of particular interest in this review), and three cylinders (e.g., Eastop and Turner (1982), Kumada et al. (1984), Williamson (1985), Sumner et al. (1999b), Zhou et al. (2000), Zhang and Zhou (2001), Wang et al. (2002a), Zhou (2003)). A number of experimental investigations of two-cylinder side-by-side configurations are summarized in Table 2.

Larger numbers of cylinders arranged side-by-side in a single column have also been examined (e.g., Ishigai and Nishikawa (1975), Auger and Coutanceau (1978, 1979), Moretti and Cheng (1987), Cheng and Moretti (1988), Zdravkovich and Stonebanks (1990), Le Gal et al. (1996)). These single columns are noted for irregular flow patterns involving the coalescence and deflection of any number of the gap-flow jets, particularly for $T/D<2$. The gap flows may also intermittently switch direction, and different groups of jets may intermittently coalesce. These flows have been termed "metastable" (Zdravkovich and Stonebanks, 1990). These features of the flow are similar to those observed for the two- and three-cylinder arrangements.

There have also been numerical studies of the flow around two circular cylinders in a side-by-side configuration, primarily at low Reynolds numbers (e.g., Chang and Song (1990) for $Re = 100$; Farrant et al. (2000) for $Re = 200$; Meneghini et al. (2001) for $Re = 100$ and 200; Chen et al. (2003) for $Re = 750$).

Related studies in the literature that are not reviewed here include the flow around side-by-side square prisms (e.g., Kolář et al. (1997), Edamoto and Kawahara (1998), Liu and Chen (2002), Alam et al. (2003a), Agrawal et al. (2006), Alam and Zhou (2007a), Kumar et al. (2008), Chatterjee et al. (2010)), rectangular prisms (e.g., Kondo (2004)), flat plates (e.g., Miau et al. (1996)), impulsively started circular cylinders (e.g., Sumner et al. (1997)), and surface-mounted finite-height cylinders (e.g., Park and Lee (2003), Liu and Cui (2006)).

4.1. Flow patterns

There are three main flow patterns for the side-by-side configuration, shown in Fig. 16, namely (i) single-bluff-body behaviour at small pitch ratios (approximately $1<T/D<1.1$–1.2, Fig. 16(a)), (ii) a biased flow pattern at intermediate pitch ratios (approximately 1.1–$1.2<T/D<2$–2.2, Fig. 16(b)), and (iii) parallel vortex streets at high pitch ratios (approximately $T/D>2$–2.5, Fig. 16(b)). These flow patterns are discussed in more detail in the following subsections.

4.1.1. Single-bluff-body behaviour

At smaller pitch ratios, $T/D<1.1$–1.2 (including when the cylinders are in contact with each other, at $T/D=1$) (Fig. 16(a)), the two cylinders behave in a similar fashion to a single bluff-body. A single Kármán vortex street forms in the wake (Sumner et al., 1999b; Wang et al., 2002b). Some flow visualization examples are shown in Fig. 17, which illustrate the range of behaviours for this flow regime.

When there is a small gap between the cylinders, for $1<T/D<1.1$–1.2, the single bluff-body behaviour noted for $T/D=1$ becomes slightly modified. Flow through the gap behaves in a similar fashion to base-bleed (Bearman, 1967; Wood, 1967; Bearman and Wadcock, 1973), whereby higher-momentum fluid, which enters the near-wake through the gap, increases the base pressure, reduces the drag of both cylinders, and increases the streamwise extent of the vortex formation region. The vortex shedding frequency, however, tends to remain close to that observed for $T/D=1$. Furthermore, a single vortex street is still observed in the combined wake of the two cylinders, and shedding occurs only from the outside shear layers (Fig. 17). Vortex formation and shedding cannot occur from the inner shear layers due to the "near-wall effect", i.e. the cylinders are very close together and the gap between them is very small (Xu et al., 2003).

Within the base-bleed flow patterns at small pitch ratios, different "modes" of behaviour may be observed in the instantaneous flow fields (Sumner et al., 1999b). In some cases, a symmetrical near-wake is formed, where the gap flow is parallel to the flow axis (Sumner et al., 1999b; Wang et al., 2002b) and symmetrical vortex shedding occurs from the outer shear layers (Wang et al., 2002b) (Fig. 17(e, f)). More commonly, an asymmetrical near-wake region is formed where the weak gap

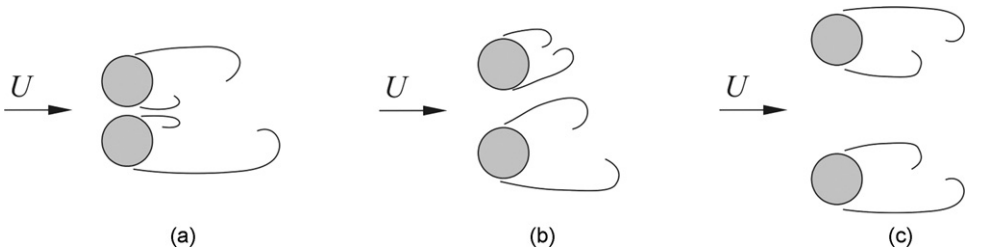

Fig. 16. Flow patterns for two side-by-side circular cylinders in cross-flow (given T/D boundaries are approximate): (a) single-bluff-body behaviour for $1<T/D<1.1$–1.2; (b) biased flow pattern for 1.1–$1.2<T/D<2$–2.2; and (c) parallel vortex streets for $T/D>2$–2.2.

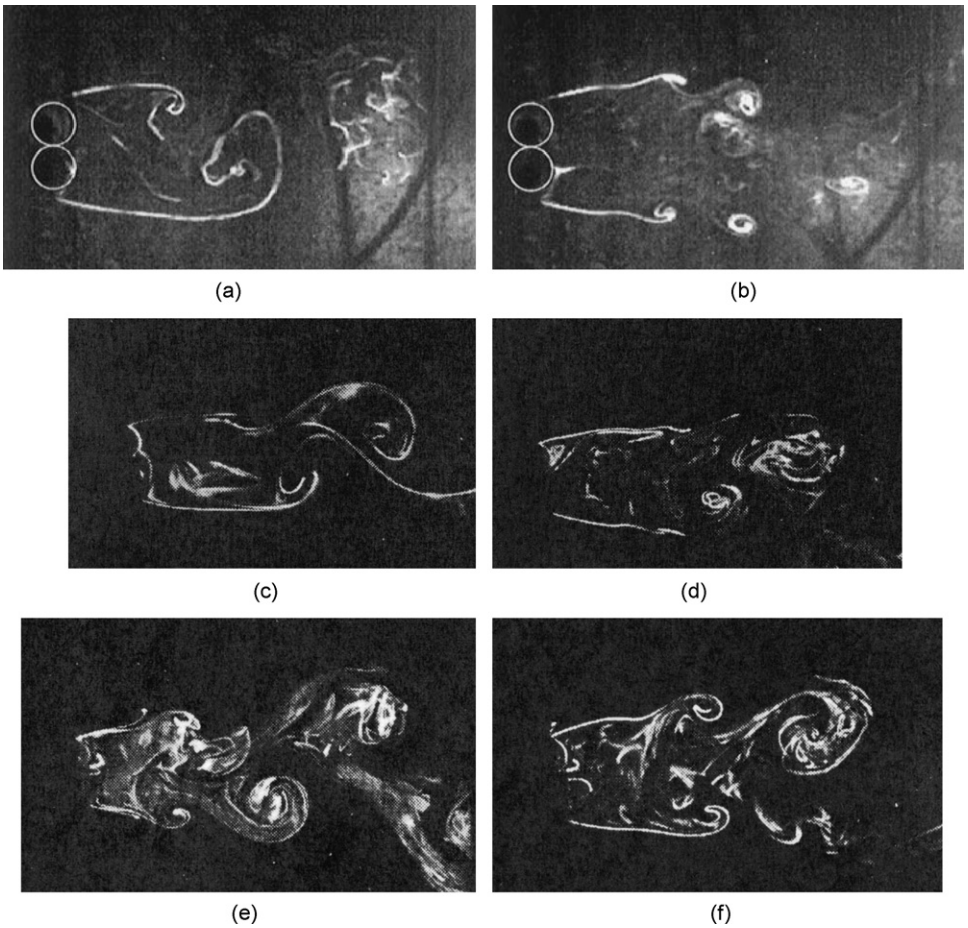

Fig. 17. Flow past two side-by-side circular cylinders at small pitch ratios, showing examples of single-bluff-body behaviour, flow from left to right: (a) $T/D = 1$, $\mathrm{Re} = 1320$, antisymmetric vortex shedding (figure taken from Sumner et al. (1999b)); (b) $T/D = 1$, $\mathrm{Re} = 820$, irregular vortex shedding (figure taken from Sumner et al. (1999b)); (c) $T/D = 1.13$, $\mathrm{Re} = 150$, antisymmetric vortex shedding, base-bleed gap flow directed upwards (figure taken from Wang et al. (2002b)); (d) $T/D = 1.13$, $\mathrm{Re} = 450$, antisymmetric vortex shedding, base-bleed gap flow directed downwards (figure taken from Wang et al. (2002b); (e) $T/D = 1.13$, $\mathrm{Re} = 250$, symmetric vortex shedding. (figure taken from Wang et al. (2002b)); and (f) $T/D = 1.13$, $\mathrm{Re} = 300$, symmetric vortex shedding.

(Figure taken from Wang et al. (2002b)).

flow is deflected or highly biased towards one of the cylinders (Fig. 17(c, d)), but a single vortex street still forms further downstream (Sumner et al., 1999b; Wang et al., 2002b; Alam et al., 2003a). At $T/D = 1.1$, the highly biased gap flow sweeps around one of the cylinders over a significant distance and a separation bubble may form on the cylinder towards which the gap flow is deflected; this separation bubble no longer forms for $T/D \geq 1.2$ (Alam and Zhou, 2007a). In the interim pitch ratios, discontinuous changes in the near-wake flow structure may be observed, involving switching of the gap flow direction and formation and bursting of the separation bubbles; four modes of near-wake behaviour were observed by Alam and Zhou (2007a) at $T/D = 1.13$, for instance. In other cases, no significant gap flow is observed or irregular vortex formation may occur (Sumner et al., 1999b) (Fig. 17(b)). This variation in the instantaneous behaviour of the base-bleed flow is also seen for two staggered circular cylinders at high incidence angles (close to the side-by-side configuration) (Sumner et al., 2000).

4.1.2. Biased flow pattern

At intermediate values of T/D the two side-by-side circular cylinders have long been known to exhibit an asymmetrical or biased flow pattern (Spivack, 1946; Hori, 1959; Ishigai et al., 1972; Bearman and Wadcock, 1973; Williamson, 1985; Kim and Durbin, 1988; Sumner et al., 1999b; Wang et al., 2002b; Zhou et al., 2002; Alam et al., 2003a; Xu et al., 2003). The range of pitch ratios where the biased flow pattern is observed extends from approximately

$T/D = 1.1$–1.2 to $T/D = 2$–2.2 depending on the experimental conditions and the Reynolds number. The asymmetrical flow pattern is characterized by a gap flow biased towards one of the two cylinders. The cylinder towards which the flow is biased has a narrow near-wake, higher-frequency vortex shedding, and a higher drag coefficient, while the other cylinder has a wider near-wake, lower-frequency vortex shedding, and a lower drag coefficient. Some flow visualization examples are shown in Fig. 18. The biased flow pattern is not caused by the "Coanda effect" since similar patterns are observed for side-by-side square prisms and flat plates (e.g., Miau et al. (1996)).

The deflection of the biased gap flow varies with T/D. The trend is toward a smaller degree of deflection with increasing T/D and is similar to the difference between the high and low vortex shedding frequencies (Sumner et al., 1999b). This can be seen by comparing the various flow visualization figures shown in Fig. 18.

In terms of the vortex dynamics of the combined wake for the biased flow pattern, two main types of basic behaviour were noted by Williamson (1985) for $Re = 200$. In the "first harmonic mode" or "fundamental mode", shown in Figs. 19 and 20, vortices which form on both sides of the biased gap flow are squeezed and enveloped into the stronger vortices from the outer shear layer of the configuration, on the side of the wake to which the gap flow is deflected. This process eventually produces a single vortex street in the combined wake of the cylinders. In the "second harmonic mode," shown in Fig. 21, the combined wake of the two cylinders is marked by pairs of vortices on one side, behind the cylinder with the narrower near-wake region, and single vortices of larger size on the opposite side. In this case, the gap vortices are amalgamated into the side of the wake where the pairs of vortices are seen. This mode was the most commonly observed, particularly for $T/D = 1.6$–1.9; intermittent break-down and resumption of this mode were also observed. A "third harmonic mode" was also reported by Williamson (1985) characterized by a pair of vortices followed by a weaker third vortex.

For these various modes, integer ratios (harmonics) of the fundamental shedding frequency were noticed, i.e., a ratio of 3:1 between the high and low Strouhal numbers (Williamson, 1985). The experiments by Kim and Durbin (1988) at $Re = 3300$ reported a ratio close to, but less than, 3:1.

Later flow visualization experiments by Wang et al. (2002b), for $Re = 120$–1650 at $T/D = 1.7$, showed a vortex amalgamation process (Fig. 22) that seems to be consistent with Williamson's (1985) first harmonic mode (Fig. 20). In this case, the two Kármán vortices in the narrow wake re-orient and pair themselves to entrain the gap vortex from the wider

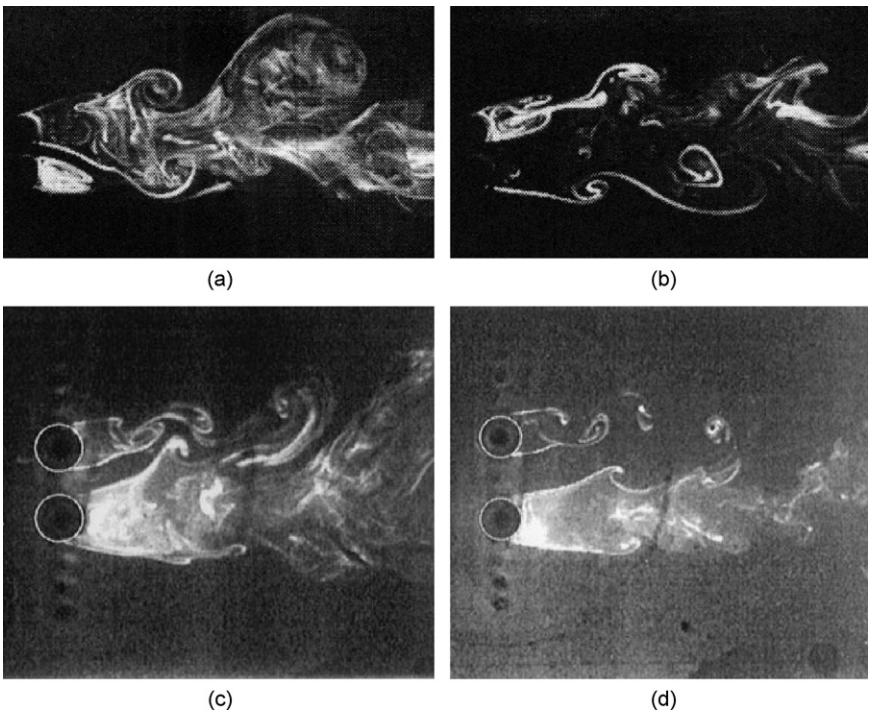

Fig. 18. Flow past two side-by-side circular cylinders at intermediate pitch ratios, showing examples of the biased flow pattern, flow from left to right: (a) $T/D = 1.4$, $Re = 150$, single vortex street (figure taken from Xu et al. (2003)); (b) $T/D = 1.4$, $Re = 300$, two vortex streets at $Re = 300$ (figure taken from Xu et al. (2003)); (c) $T/D = 1.5$, $Re = 1000$–3000 (figure taken from Sumner et al. (1999b)); and (d) $T/D = 2$, $Re = 1000$–3000.
(Figure taken from Sumner et al. (1999b)).

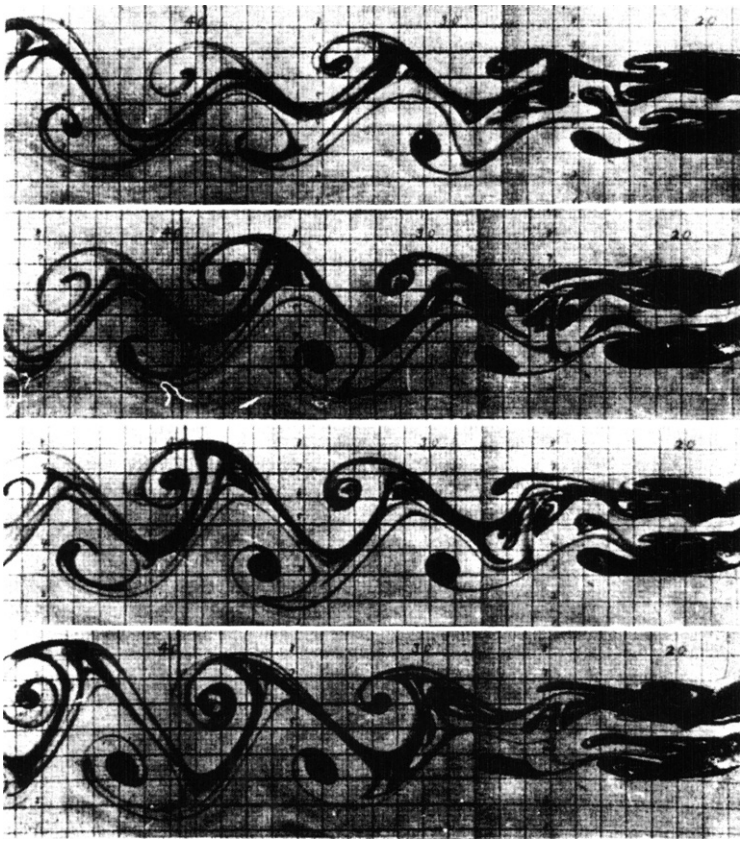

Fig. 19. Fundamental mode of vortex shedding for two side-by-side circular cylinders in the biased flow regime, $T/D = 1.85$, $\mathrm{Re} = 200$, flow from right to left.

(Figure taken from Williamson (1985)).

wake, resulting in an amalgamation of three vortices on the narrow-wake side of the flow. The schematic in Fig. 22 also shows symmetric formation of vortices on either side of the gap between the cylinders; this type of synchronization within the immediate near-wake of the cylinders was also observed by Sumner et al. (1999b). Such behaviour, under biased flow conditions, would seem to broadly correspond to the "quasiperiodic regime" noted by Peschard and Le Gal (1996).

In some cases, the biased flow pattern switches intermittently from being directed towards one cylinder to the other, and the flow pattern is termed "bistable" (Bearman and Wadcock, 1973; Kim and Durbin, 1988). This "flip-flopping" of the gap flow direction and wake sizes occurs spontaneously and irregularly, but between switchovers the flow remains stably biased to one of the cylinders for long durations (perhaps a few orders of magnitude larger than the vortex shedding period (Zhou et al., 2002)). The gap flow switching phenomenon has also been reproduced in numerical simulations (e.g., Chen et al. (2003)). The flow visualization experiments of Wang et al. (2002b) at $T/D = 1.7$ showed that the switchover of the biased flow pattern from one cylinder to the other was linked to the brief appearance and breakdown of larger gap vortex behind the cylinder with the wider wake. In the experiments of Alam et al. (2003a) at $\mathrm{Re} = 5.5 \times 10^4$, an intermediate flow pattern was observed at the time of switchover, in which the gap flow was unbiased and remained parallel to the wake centreline.

The bistable characteristic is not caused by misalignment of the cylinders or other extraneous influences, but is an intrinsic property of the flow; the transverse configuration may be considered to be the transitional arrangement between two staggered configurations of greater and lesser incidence to the incoming flow (Bearman and Wadcock, 1973; Kim and Durbin, 1988). It should be noted that in some experimental studies (e.g., Peschard and Le Gal (1996), Sumner et al. (1999b)) there was no evidence of bistable behaviour, and the flow was consistently biased towards one of the cylinders.

4.1.3. Parallel vortex streets

At higher pitch ratios, $T/D > 2$–2.2, the flow field regains its symmetry and both cylinders undergo Kármán vortex shedding at the same frequency. The two side-by-side circular cylinders now behave more as independent, isolated

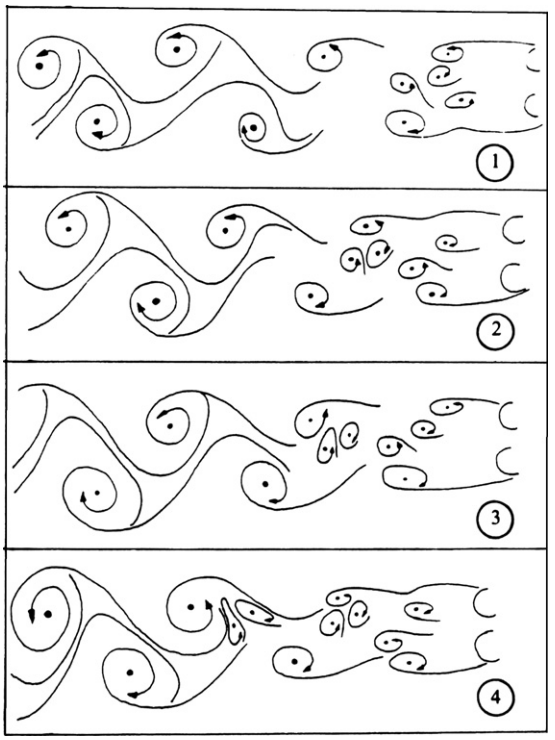

Fig. 20. Schematic of the fundamental mode of vortex shedding (shown in Fig. 19) for two side-by-side circular cylinders in the biased flow regime, flow from right to left.
(Figure taken from Williamson (1985)).

bluff-bodies. Proximity interference effects, however, lead to various modes of synchronization, anti-phase and in-phase (Fig. 23), in the vortex formation and shedding processes and the resulting parallel vortex streets. Some flow visualization examples are shown in Figs. 24 and 25.

The existence of two simultaneous, side-by-side vortex shedding processes and vortex streets for this arrangement of cylinders leads to complex vortex street interaction in the combined wake of the bodies (Williamson, 1985; Le Gal et al., 1990; Peschard and Le Gal, 1996). At these larger values of T/D, the two vortex streets predominantly synchronize in an anti-phase fashion (Figs. 23(a), 24, and 25(a)). Here, vortices are shed simultaneously on both sides of the gap between the cylinders, and the resulting pattern of vortices in the combined wake of the two cylinders is stable. The predominance of the anti-phase shedding broadly corresponds to the ''locking and phase opposition'' regime noted by Peschard and Le Gal (1996). An anti-phase pattern can persist for at least 20 diameters downstream of the cylinder pair (Zhou et al., 2002).

In some cases, the flow pattern may intermittently switch to in-phase synchronization of the vortex streets (Figs. 23(b) and 25(b)), and then revert back to anti-phase synchronization (Williamson, 1985). The in-phase synchronization leads to an unstable configuration of vortices and leads to the formation of what is essentially a single wake behind the cylinder pair containing a binary vortex street (Williamson, 1985) (Fig. 25(b)).

Alam et al. (2003a) and other researchers have shown that the predominance of the anti-phase shedding synchronization decreases with increasing T/D. Irregular shedding behaviour may also appear intermittently (Sumner et al., 1999b; Alam et al., 2003a).

The pitch ratio where transition occurs from the biased flow regime to one of parallel vortex streets, with a gap flow aligned with the mean flow direction, varies among the studies in the literature and is sensitive to Reynolds number (Zhou et al., 2009). From $T/D = 2.2$–2.5, Alam et al. (2003a) continued to notice a small deflection angle to the gap flow (see also Fig. 24(a)) and the bistable nature, but the vortex shedding processes exhibited anti-phase synchronization characteristic of higher pitch ratios. They characterized this range of T/D as an intermediate flow regime between the traditional biased flow and parallel vortex street behaviours.

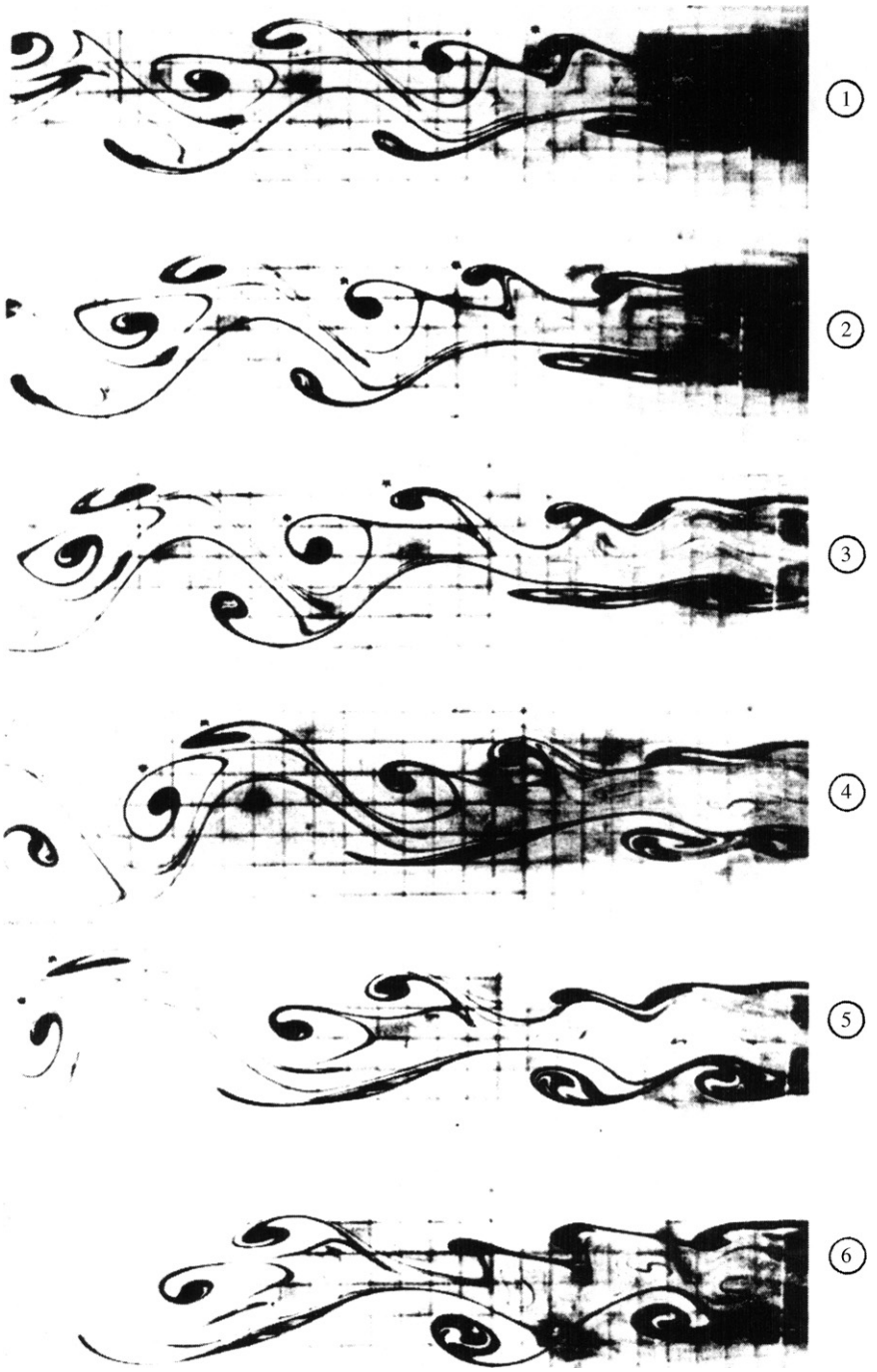

Fig. 21. Second harmonic mode of vortex shedding for two side-by-side circular cylinders in the biased flow regime, $T/D = 1.7$, $\mathrm{Re} = 200$, flow from right to left.

(Figure taken from Williamson (1985)).

4.2. Reynolds number effects

The Strouhal number measurements and flow visualization experiments of Xu et al. (2003) for a wide range of Reynolds numbers within the biased flow regime showed that at lower Reynolds numbers and smaller T/D, one cylinder

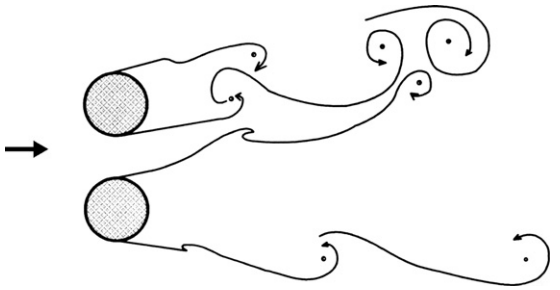

Fig. 22. Near-wake vortex formation, shedding, and interactions for two side-by-side circular cylinders at intermediate pitch ratios (shown here for $T/D = 1.7$).

(Figure taken from Wang et al. (2002b)).

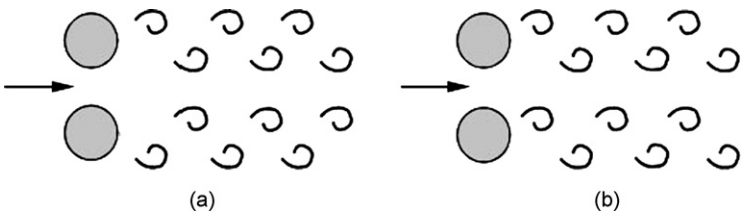

Fig. 23. Vortex street synchronization for two side-by-side circular cylinders: (a) anti-phase and (b) in-phase.

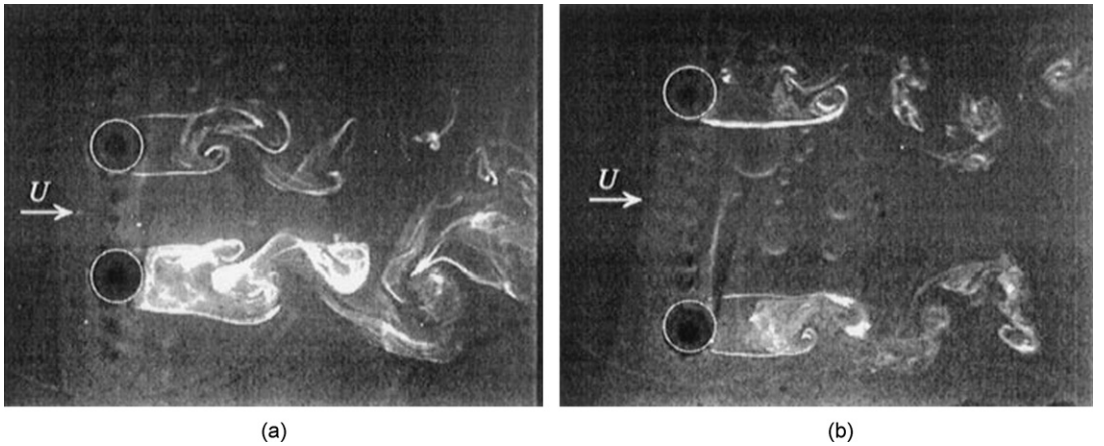

Fig. 24. Flow past two side-by-side circular cylinders at high pitch ratios showing anti-phase vortex shedding synchronization, Re = 1000–3000: (a) $T/D = 2.5$ and (b) $T/D = 4.5$.

(Figures taken from Sumner et al. (1999b)).

has a small closed wake and the combined wake of the cylinders is marked by a single vortex street of low Strouhal number. At higher Reynolds numbers and larger T/D, once the gap flow Reynolds number is sufficiently high, the small closed wake no longer forms; a twin vortex street wake is formed instead and two distinct Strouhal numbers are measured. The flow pattern boundaries for the single and twin vortex street combined wakes, as functions of Re and T/D. are shown in Fig. 26. Flow visualization examples for the two cases are shown in Fig. 27.

The Reynolds number sensitivity of the wake switching phenomenon in the biased flow regime was investigated by Brun et al. (2004). They determined that below a critical Reynolds number, which ranged between Re = 1000–1700, the biased flow tended to be stably biased towards one of the cylinders (as noticed in many of the studies at lower Reynolds numbers, such as Sumner et al. (1999b)), whereas above the critical Reynolds number, the wake switching phenomenon

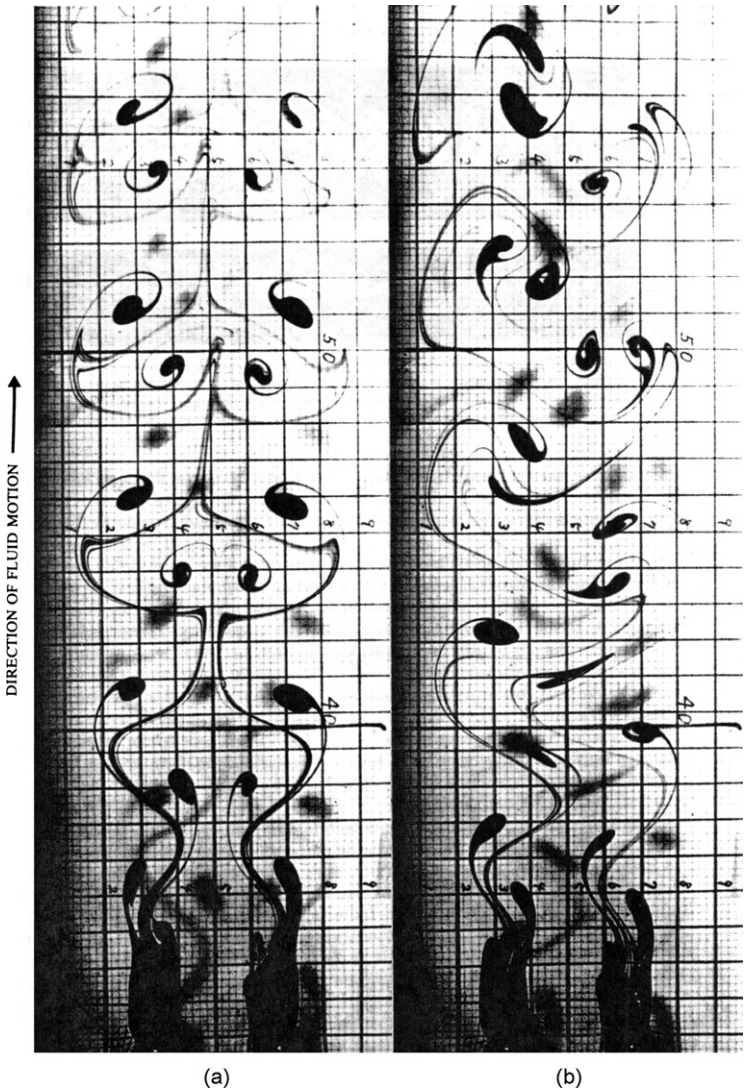

Fig. 25. Flow visualization examples for two side-by-side circular cylinders with $T/D = 3.4$, $\mathrm{Re} = 200$: (a) anti-phase synchronization and (b) in-phase synchronization leading to eventual formation of a binary vortex street.
(Figure taken from Williamson (1985)).

occurs. This onset of the wake switching phenomenon was related to the appearance of Kelvin–Helmholtz instability vortices in the separated shear layers (Brun et al., 2004). With increasing Reynolds number, the average time between switchovers in the biased flow pattern decreases (Brun et al., 2004).

4.3. Wake structure and vortex dynamics

Wake mean velocity and turbulence profiles have been provided by several researchers (e.g., Zhou et al. (2000), Brun et al. (2004)); see the summary of experimental studies in Table 2 for additional studies.

Greater details of the wake structure and the behaviour of the shed vortices were studied by Zhou et al. (2002) at $\mathrm{Re} = 5800$; an example is shown in Fig. 28. Their measurements were made between 10 and 40 diameters downstream from the cylinders, or the "intermediate wake", i.e., beyond the region where complex vortex street interactions occur (as shown in the flow visualization images presented earlier). For $T/D = 1.5$, within the biased flow pattern (Fig. 28(d, e, f)),

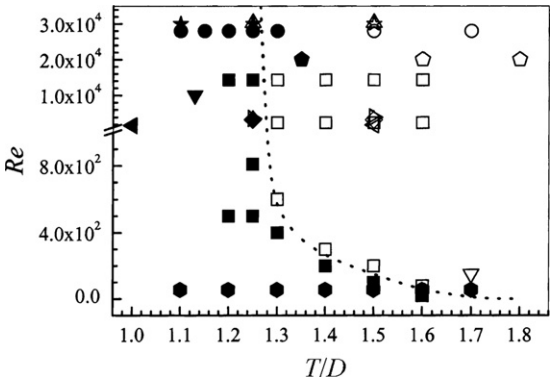

Fig. 26. Reynolds number dependence of the Strouhal numbers within the biased flow regime for two side-by-side circular cylinders. The solid symbols represent the detection of a single Strouhal number; the open symbols represent the detection of two Strouhal numbers. The dotted line is used to illustrate the approximate boundary between the single-St and dual-St regimes: ● and ○, Spivack (1946); ▷, Ishigai et al. (1972); ★ and ☆, Kamemoto (1976); △, Quadflieg (1977); ⬟ and OPEN ⬟, Kiya et al. (1980); ⬣ and OPEN ⬣, Williamson (1985); ♦ and ◇, Kim and Durbin (1988); ◀ and ◁, Sumner et al. (1999b); ▼ and ▽, Zhou et al. (2001); ■ and □, Xu et al. (2003). (Figure from Xu et al. (2003)).

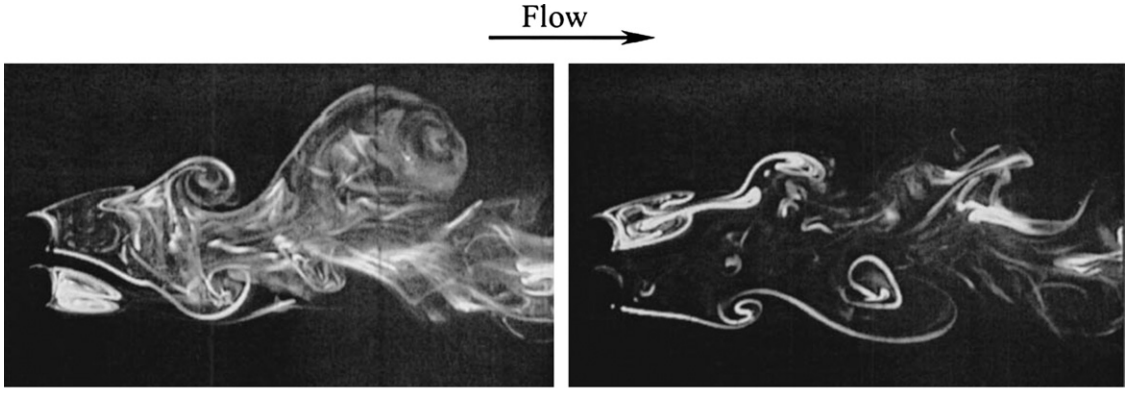

Fig. 27. Single and twin vortex street combined wakes within the biased flow regime for two side-by-side circular cylinders: (a) single vortex street structure, Re = 150 and (b) twin vortex street structure, Re = 300.
(Figure from Xu et al. (2003)).

a single vortex street is present at this distance downstream of the cylinders, but the street is asymmetric in terms of vortex strength and convection velocity, and clearly reflects the initial conditions and near-wake pattern. For $T/D = 3$ (Fig. 28(g, h, i)), where there are initially two vortex shedding processes synchronized in an anti-phase fashion, by 40 diameters these streets have evolved to a single street with the disappearance of the inner rows of vortices (Zhou et al., 2002).

4.4. Measurements

For the side-by-side configuration, there is an abundance of data for the Strouhal numbers, but relatively few studies have examined the aerodynamic forces compared to the tandem configuration; see Table 2 for a list of experimental studies and the types of measurements available (additional experimental data for both the tandem and side-by-side configurations can also be obtained from many of the studies on staggered cylinders; see Table 3). In addition to measurements of forces and shedding frequencies, some studies have measured the mean and fluctuating pressure coefficients (e.g., Bearman and Wadcock (1973), Sun et al. (1992), Alam et al. (2003a), Alam and Zhou (2007a). Some additional comments on the force coefficients and Strouhal number are presented in the following sub-sections.

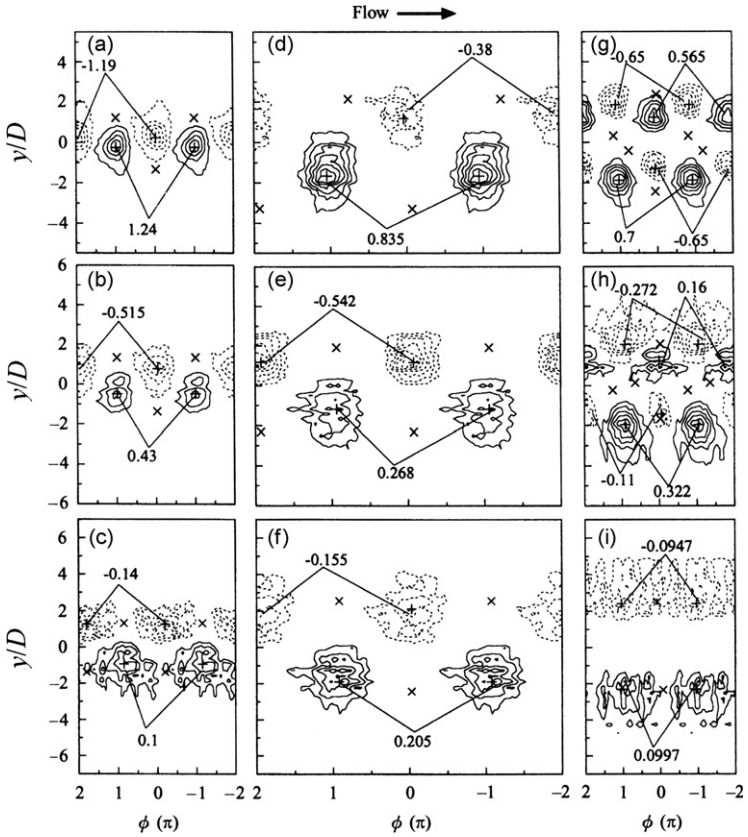

Fig. 28. Phase-averaged dimensionless vorticity contours in the intermediate wake of two side-by-side circular cylinders, Re = 5800, for phase, φ. Single circular cylinder: (a) $x/D = 10$, contour interval = 0.27; (b) $x/D = 20$, contour interval = 0.135; (c) $x/D = 40$, contour interval = 0.03. Side-by-side circular cylinders with $T/D = 1.5$: (d) $x/D = 10$, contour interval = 0.135; (e) $x/D = 20$, contour interval = 0.081; (f) $x/D = 40$, contour interval = 0.045. Side-by-side circular cylinders with $T/D = 3$: (g) $x/D = 10$, contour interval = 0.135; (h) $x/D = 20$, contour interval = 0.054; and (i) $x/D = 40$, contour interval = 0.0243. Solid lines represent positive (CCW) vorticity; dashed lines represent negative (CW) vorticity.

(Figure taken from Zhou et al. (2002)).

4.4.1. Force coefficients

Examples of the mean drag and lift coefficient data for two side-by-side circular cylinders are shown in Fig. 29. Beyond the biased flow regime, the mean drag coefficients approach the value for a single circular cylinder and the mean lift coefficients tend to zero. Within the biased flow regime, the cylinder with the narrow wake has a lower base pressure, higher mean drag coefficient, and lower mean lift coefficient (Bearman and Wadcock, 1973; Alam et al., 2003a). Except for very small pitch ratios, the mean lift coefficients for both cylinders are positive (outward-directed, repulsive) (Alam et al., 2003a). At very small pitch ratios, however, where the cylinders behave as if a single bluff body, highly deflected gap flow may lead the formation of a small separation bubble on the rear of the cylinder towards which the gap flow is deflected. The presence of this separation bubble leads to this cylinder experiencing a negative (inward-directed, attractive) lift force (Alam and Zhou, 2007a). Discontinuous changes in the near-wake flow structures at small pitch ratios can have pronounced effects on the mean lift coefficient (Alam and Zhou, 2007a). Marked differences in the fluctuating lift and drag coefficients are also noticed in the biased flow regime (Alam et al., 2003a).

4.4.2. Strouhal numbers

A collection of Strouhal number data from a wide range of experiments spanning a wide range of Reynolds numbers is shown in Fig. 30. At small pitch ratios, where the cylinders behave as if a single bluff body, the Strouhal number is lower than (approximately one half of) the single-cylinder value. Within the biased flow regime, one or two Strouhal numbers may be measured, depending on the Reynolds number and measurement location, with an approximate 3:1

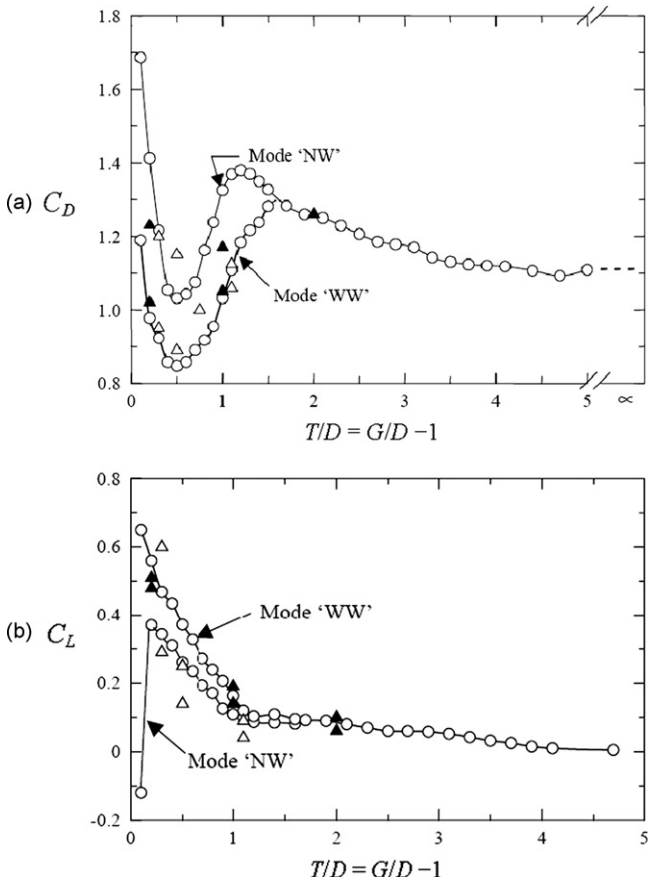

Fig. 29. Mean aerodynamic force coefficients for two side-by-side circular cylinders as a function of the dimensionless gap ratio: (a) mean drag force coefficient and (b) mean lift force coefficient: ▲, Hori (1959), Re = 8000; △, Zdravkovich and Pridden (1977), Re = 6×10^4; ○, Alam et al. (2003a), Re = 5.5×10^4. Mode 'NW' = cylinder with the narrow wake; Mode 'WW' = cylinder with the wide wake. (Figures taken from Alam et al. (2003a)).

ratio. As the pitch ratio increases beyond the biased flow regime, the Strouhal number approaches the value for a single cylinder.

Further illustration of the Reynolds number effects is shown in Fig. 31. Within the biased flow regime, the ratio of the two Strouhal numbers changes with increasing Reynolds number, as shown in Fig. 31(a, b). The upper limit of the biased flow regime also appears to be sensitive to Reynolds number, as shown by the St behaviour in Fig. 31(b). A critical Reynolds number of Re = 1×10^4 is noted in these data, where changes occur in the flow patterns at intermediate T/D (Zhou et al., 2009).

Additional Strouhal number data from Alam et al. (2003a) are shown in Fig. 32, which show some intermediate Strouhal numbers within the biased flow regime at approximately twice the lowest measured Strouhal number. This "intermediate frequency mode" was associated with the intermittent appearance of a symmetric flow pattern, similar to the anti-phase vortex street synchronization at higher T/D. Intermediate frequencies were also identified by Spivack (1946) and Bearman and Wadcock (1973), which led to Williamson's (1985) suggestions of harmonic modes of vortex shedding (Section 4.1.2).

5. Staggered configuration

The staggered configuration (Fig. 1(c)) is the most general arrangement of two circular cylinders. The geometry of the staggered pair of cylinders is set by the dimensionless centre-to-centre pitch ratio, P/D, and the angle of incidence, α; alternatively, the arrangement of the cylinders has been defined by some authors using the longitudinal and transverse

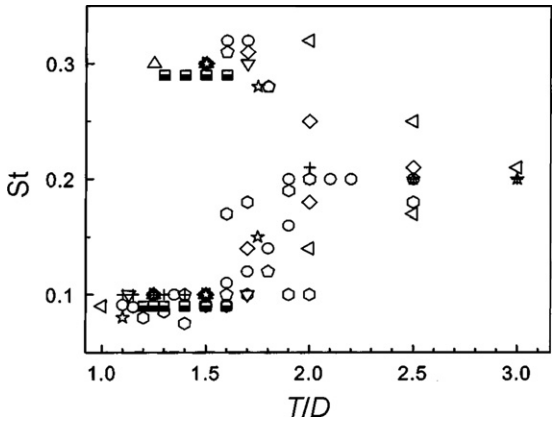

Fig. 30. Strouhal number data for two side-by-side circular cylinders as a function of transverse pitch ratio and Reynolds number: ○, Spivack (1946), $Re = 2.8 \times 10^4$; ▷, Ishigai et al. (1972), $Re = 1500$; +, Bearman and Wadcock (1973), $Re = 2.5 \times 10^4$; ☆, Kamemoto (1976), $Re = 3 \times 10^4$; △, Quadflieg (1977), $Re = 3 \times 10^4$; OPEN ⬟, Kiya et al. (1980), $Re = 2 \times 10^4$; OPEN ⬣, Williamson (1985), $Re = 55$, 100, 200; ◇, Kim and Durbin (1988), $Re = 3300$; ◁, Sumner et al. (1999b), $Re = 1200$–2200; ▽, Zhou et al. (2001), $Re = 120$ and 3500; □, Xu et al. (2003), $Re = 300$–1.43×10^4.

(Figure taken from Xu et al. (2003)).

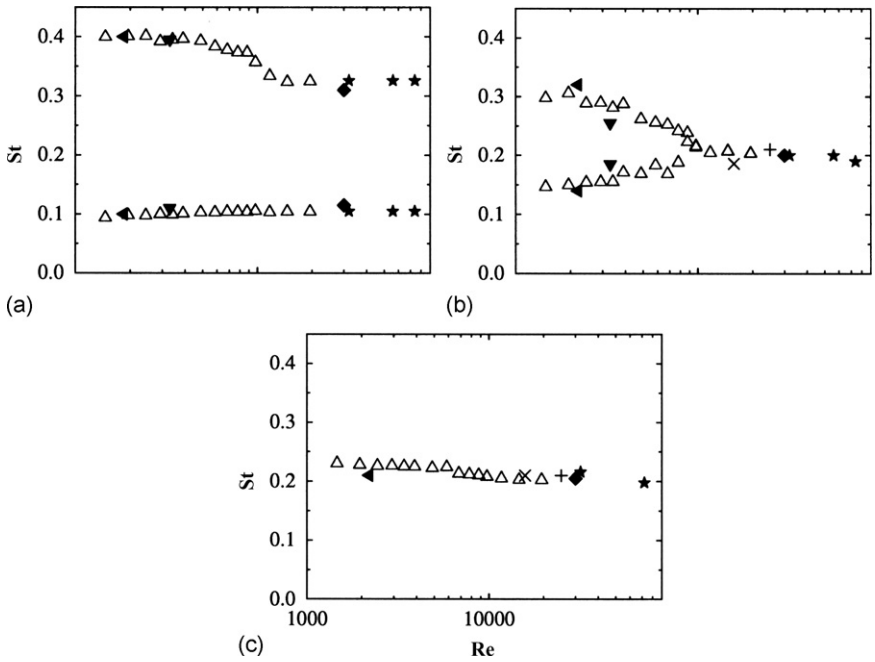

Fig. 31. Strouhal number data for two side-by-side circular cylinders and the effect of Reynolds number: (a) $T/D = 1.5$; (b) $T/D = 2$; and (c) $T/D = 3$: +, Bearman and Wadcock (1973); ◆, Kamemoto (1976); ×, Kiya et al. (1980); ▼, Kim and Durbin (1988); ◀, Sumner et al. (1999b); ★, Sumner et al. (2005); △, Zhou et al. (2009).

(Figure taken from Zhou et al. (2009)).

pitch ratios, L/D and T/D, respectively. Depending on the geometry, the cylinders may experience wake interference and/or proximity interference effects, including those effects noticed in the tandem and side-by-side configurations. The complexity of the flow arises from the interaction of four separated free shear layers, two Kármán vortex formation and shedding processes, and interactions between the two Kármán vortex streets (Fig. 33). The result is a large number of

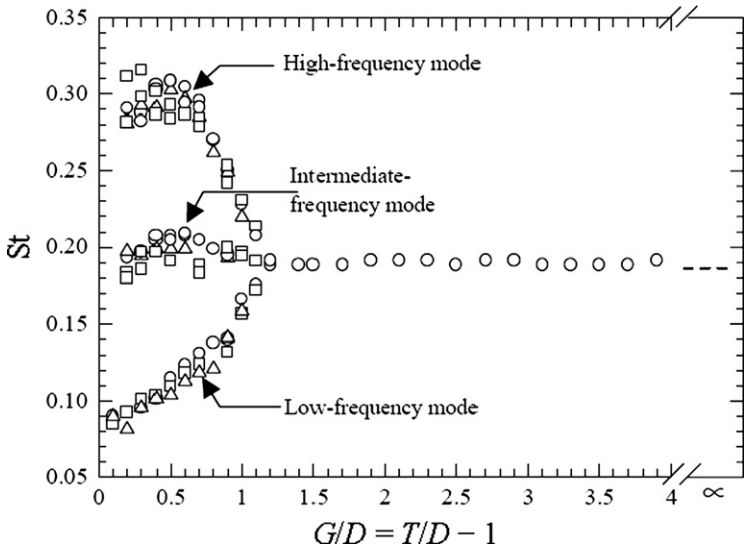

Fig. 32. Strouhal number data for two side-by-side circular cylinders, $Re = 5.5 \times 10^4$, as a function of dimensionless gap ratio, showing high-frequency, intermediate frequency, and low-frequency modes: ○, from fluctuating lift measurements; △, from fluctuating pressure measurements; □, from hot-wire measurements.

(Figure taken from Alam et al. (2003a)).

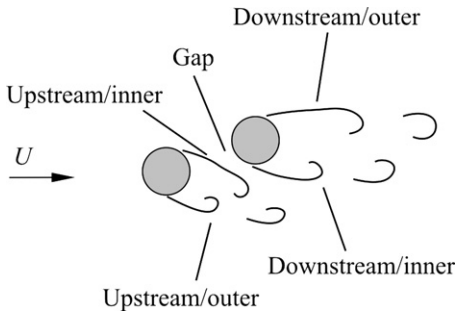

Fig. 33. Shear layer and vortex designations (for the upstream and downstream cylinders) for two staggered circular cylinders in cross-flow.

flow patterns for the staggered configuration, with an overview of the patterns identified by Sumner et al. (2000) shown in Fig. 34.

The staggered configuration has been studied primarily using experiments (as opposed to numerical simulations) and mostly at high subcritical Reynolds numbers (defined for a single circular cylinder), since these are more commonly found in industrial applications; a summary of selected experimental studies is given in Table 3. Measurements have focused mainly on the aerodynamic force coefficients and Strouhal numbers. Some insights into the effects of Reynolds number on the Strouhal numbers and flow patterns have recently been published (e.g., Zhou et al. (2009)). Because of the complexity of the flow, there have been relatively few numerical studies of the staggered configuration. Mittal et al. (1997) modelled the flow at $Re = 100$ and 1000 for a single widely spaced staggered configuration of $P/D = 5.54$ and $\alpha = 7.25°$. Jester and Kallinderis (2003) modelled the staggered cylinders at $Re = 80$–1000 and had some success at reproducing the experimentally observed flow patterns. Akbari and Price (2005) used the vortex method at $Re = 800$ to reproduce the wide range of flow patterns discovered by Sumner et al. (2000). Lee et al. (2009) modelled the flow at $Re = 100$ with a focus on the fluid forces.

Related studies in the literature that are not reviewed here include the effect of planar shear flow on two closely spaced staggered circular cylinders (Akosile and Sumner, 2003) and the flow around two staggered surface-mounted finite-height circular cylinders (e.g., Taniguchi et al. (1982), Li and Sumner (2009)).

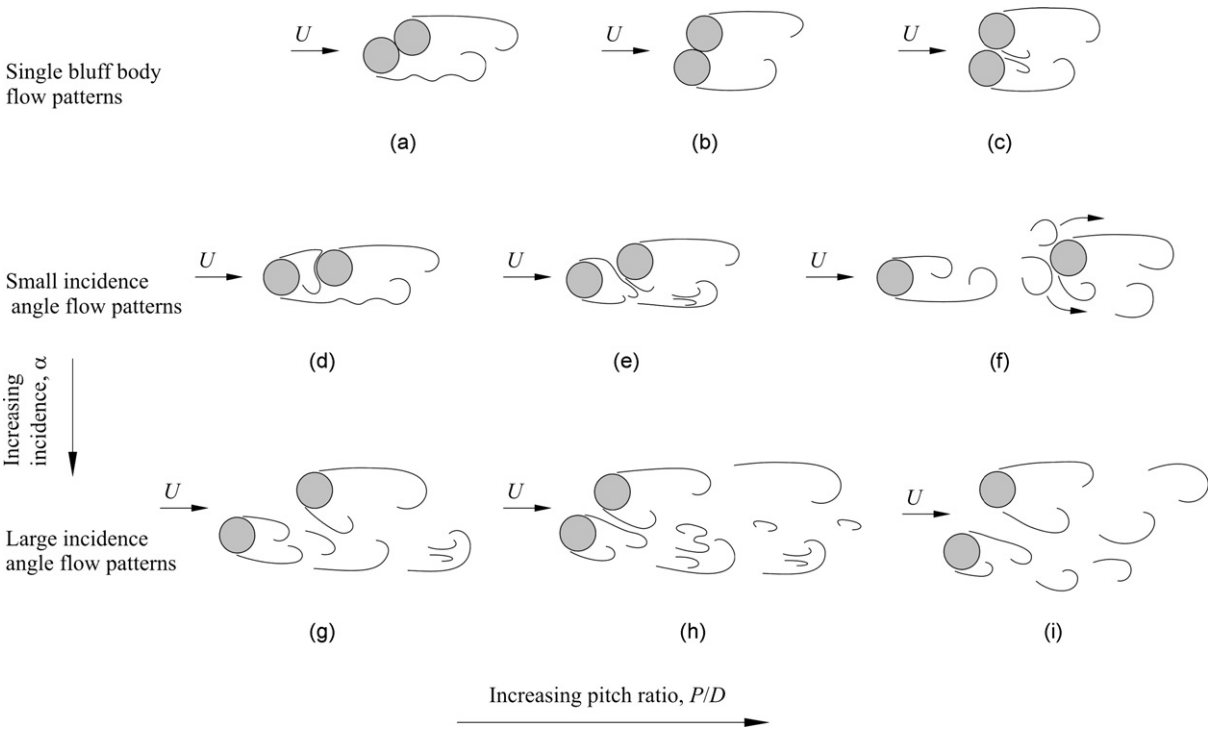

Fig. 34. Low subcritical regime flow patterns for two staggered circular cylinders in cross-flow, Re = 850–1900, identified by Sumner et al. (2000). Single bluff-body flow patterns: (a) type 1, SBB1; (b) type 2, SBB2; (c) base bleed, BB. Small incidence angle flow patterns: (d) shear layer reattachment, SLR; (e) induced separation, IS; (f) vortex impingement, VI. Large incidence angle flow patterns: (g) gap vortex pairing and enveloping, VPE; (h) gap vortex pairing, splitting and enveloping, VPSE; and (i) synchronized gap vortex shedding, SVS.

5.1. *Flow patterns*

One of the first studies to consider the flow patterns for the staggered configuration was conducted by Gu and Sun (1999), who extended Zdravkovich's (1987) classification to three different types, namely wake interference, shear layer interference, and neighbourhood interference. However, their study was limited to staggered configurations with small and intermediate pitch ratios in the high subcritical regime ($Re = 2.2 \times 10^5$–3.3×10^5). Their I_B, II_B, and III_B flow patterns are shown schematically in Fig. 35.

More extensive flow visualization and PIV experiments by Sumner et al. (2000) were conducted within the low subcritical regime (Re = 850–1900) and revealed a much wider range of flow patterns for the staggered configuration (Fig. 34). Nine distinct patterns were identified which incorporated various aspects of shear layer reattachment, alternate vortex shedding from one or both cylinders, vortex splitting, pairing and enveloping, synchronized vortex shedding, and vortex impingement. Approximate flow pattern boundaries are shown in Fig. 36. Some flow visualization examples of these flow patterns are shown in Fig. 37. The nine flow patterns can be more broadly grouped into single-bluff-body flow patterns, small-incidence-angle flow patterns, and large-incidence-angle flow patterns (Fig. 34).

5.1.1. *Single-bluff-body flow patterns*

At small pitch ratios (approx. $P/D = 1$–1.25), the two staggered cylinders behave as if a single bluff body, and three main flow patterns were identified by Sumner et al. (2000). A single vortex street occurs behind the cylinder pair, with vortices forming and shedding from the outer shear layers. The single bluff body type 1 (SBB1, Figs. 34(a) and 37(a)) flow pattern (approx. $P/D = 1$–1.125, $\alpha = 0$–45°) is characterized by instabilities in the elongated shear layer from the upstream cylinder. For the single bluff body type 2 (SBB1, Figs. 34(b) and 37(b)) flow pattern (approx. $P/D = 1$–1.125, $\alpha = 45$–90°), the outer shear layers are of similar length. At high incidence angles, the base-bleed (BB, Fig. 34(c)) flow pattern (approx. $P/D = 1.125$–1.25, $\alpha = 45$–90°) is observed, where the weak gap flow enters the base region. This gap

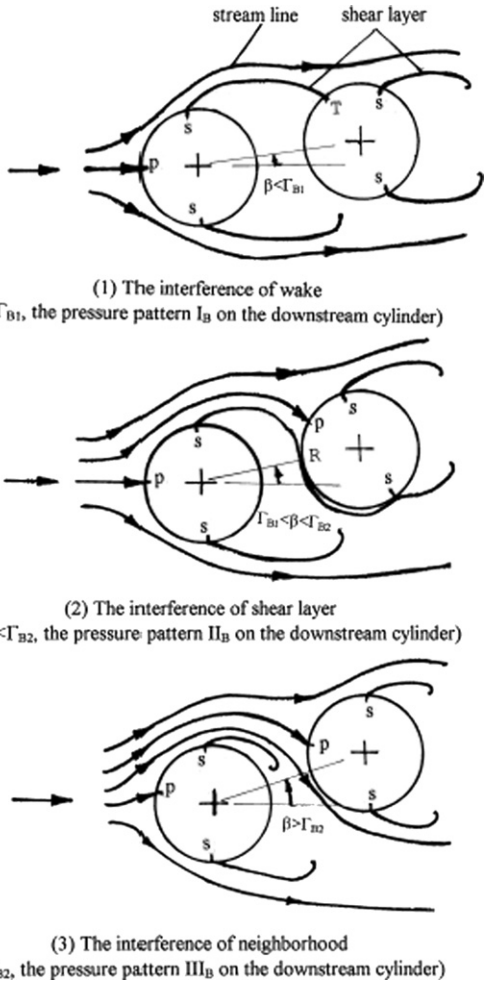

Fig. 35. Flow patterns for two staggered circular cylinders in cross-flow identified by Gu and Sun (1999). S = separation point; P = stagnation point; R = reattachment point; T = shear layer touch point; β = incidence angle; Γ = upper and lower limits on incidence angle: (1) the interference of wake ($\beta < \Gamma_{B1}$, the pressure pattern I_B on the downstream cylinder); (2) the interference of shear layer ($\Gamma_{B1} < \beta < \Gamma_{B2}$, the pressure pattern II_B on the downstream cylinder) and (3) the interference of neighbourhood ($\beta > \Gamma_{B2}$, the pressure pattern III_B on the downstream cylinder).

(Figure taken from Gu and Sun, 1999).

flow may be deflected towards either of the cylinders, similar to what is observed for two side-by-side circular cylinders (Section 4.1.1).

5.1.2. *Small-incidence-angle flow patterns*

At small incidence angles (approx. $\alpha = 0$–30°) for a wide range of pitch ratios (approx. $P/D = 1.125$–4), a larger gap between the cylinders leads to additional complexity to the flow patterns (Sumner et al., 2000). The shear layer reattachment (SLR, Figs. 34(d) and 37(c)) flow pattern (approx. $P/D = 1.125$–4 and $\alpha = 0$–20°) is marked by reattachment of the inner shear layer of the upstream cylinder onto the outer surface of the downstream cylinder. The wake of the cylinder is characterized by a single vortex street. The SLR flow pattern is similar to Pattern I_B of Gu and Sun (1999) (Fig. 35(a)). For the induced separation (IS, Figs. 34(e) and 37(d)) flow pattern (approx. $P/D = 1.125$–3 and $\alpha = 10$–30°), the inner shear layer from the upstream cylinder is deflected through the gap between the cylinders, and separated flow and vorticity generation is induced on the inner surface of the downstream cylinder. The IS flow pattern is similar to Pattern II_B of Gu and Sun (1999) (Fig. 35(b)). In the vortex impingement (VI, Figs. 34(f) and 37(h))

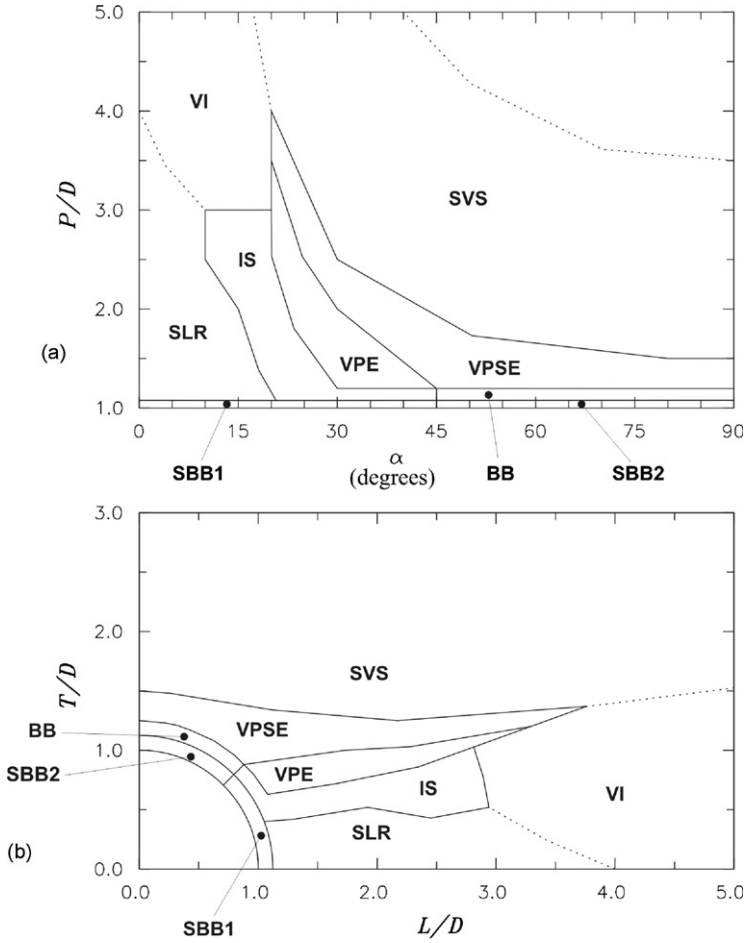

Fig. 36. Flow pattern boundaries for two staggered circular cylinders in cross-flow, Re = 850–1900, from Sumner et al. (2000): (a) P/D–α notation; (b) L/D–T/D notation. BB, base-bleed; IS, induced separation; SBB1, single bluff-body type 1; SBB2, single bluff-body type 2; SLR, shear layer reattachment; SVS, synchronized vortex shedding; VI, vortex impingement; VPE, gap vortex pairing and enveloping; VPSE, gap vortex pairing, splitting and enveloping. Dotted lines represent proposed boundaries.

flow pattern (approx. $P/D = 3$–5 and $\alpha = 0$–20°), the cylinders are spaced sufficiently far apart in the longitudinal direction that vortex shedding occurs from the upstream cylinder, but have a relatively small transverse spacing such that the shed vortices impinge upon the downstream cylinder (Sumner et al., 2000).

From the experiments of Alam et al. (2005) at $\mathrm{Re} = 5.5 \times 10^4$, two bistable flow regions were observed at $\alpha = 10^\circ$. For $P/D = 1.1$–2.3, the bistable flow was associated with the development and disappearance of a separation bubble on the downstream cylinder's inner surface. For $P/D = 3.1$–3.4, the bistable behaviour was related to the transition between the SLR and VI flow patterns, specifically the reattachment or detachment onto the downstream cylinder of the upstream cylinder's inner shear layer.

5.1.3. Large-incidence-angle flow patterns

At large incidence angles (approx. $\alpha = 15$–90°) and for a wide range of pitch ratios (approx. $P/D = 1.25$–5), vortex shedding occurs from both cylinders (Sumner et al., 2000). The vortex pairing and enveloping (VPE, Figs. 34(g) and 37(e)) flow pattern (approx. $P/D = 1.25$–3.5, $\alpha = 20$–45°) is denoted by pairing of gap vortices and enveloping of the vortex pair by a shed vortex from the outer shear layer of the upstream cylinder. This enveloping process is incomplete in the vortex pairing, splitting and enveloping (VPSE, Figs. 34(h) and 37(f)) flow pattern (approx. $P/D = 1.25$–4, $\alpha = 20$–90°). The VPE and VPSE flow patterns are similar to Pattern $\mathrm{III_B}$ of Gu and Sun (1999) (Fig. 35(c)). For a wide

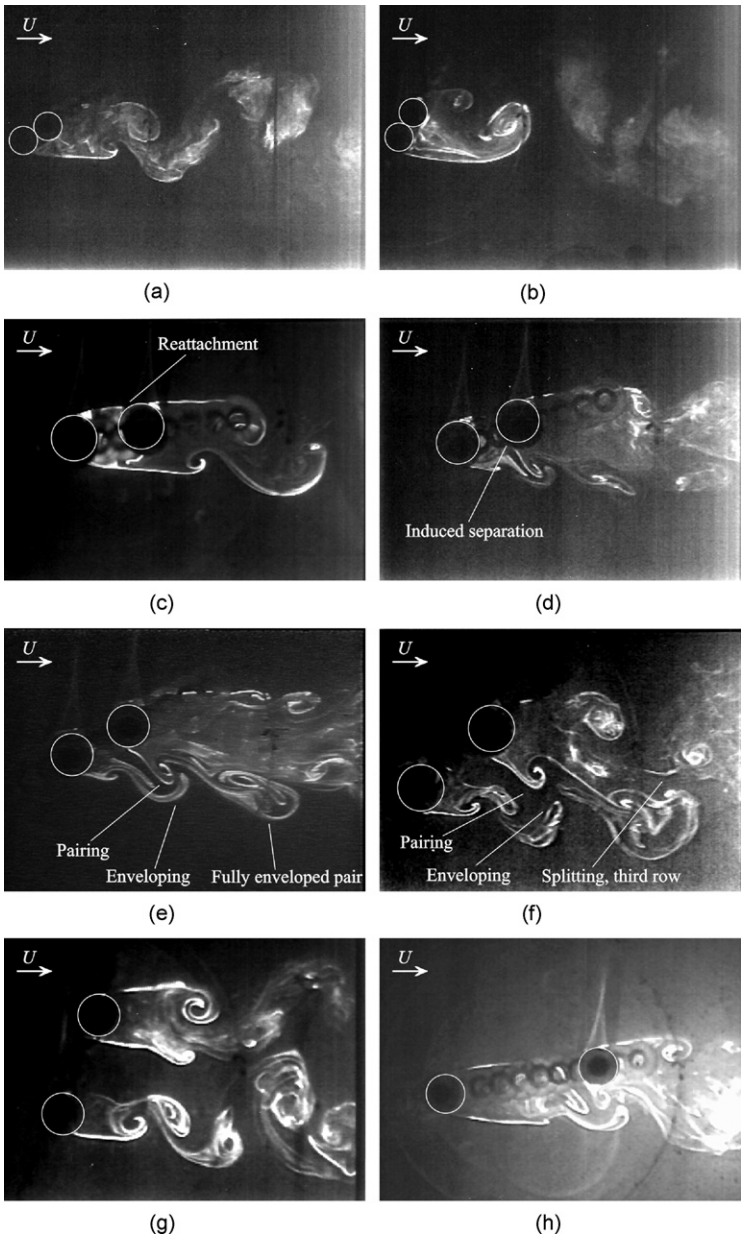

Fig. 37. Flow visualization examples for two staggered circular cylinders in cross-flow: (a) SBB1 flow pattern, $P/D = 1$, $\alpha = 30^\circ$, $\mathrm{Re} = 1320$; (b) SBB2 flow pattern, $P/D = 1$, $\alpha = 60^\circ$, $\mathrm{Re} = 1320$; (c) SLR flow pattern, $P/D = 1.5$, $\alpha = 10^\circ$, $\mathrm{Re} = 1300$; (d) IS flow pattern, $P/D = 1.5$, $\alpha = 20^\circ$, $\mathrm{Re} = 1320$; (e) VPE flow pattern, $P/D = 1.5$, $\alpha = 30^\circ$, $\mathrm{Re} = 850$; (f) VPSE flow pattern, $P/D = 2$, $\alpha = 40^\circ$, $\mathrm{Re} = 880$; (g) SVS flow pattern, $P/D = 2.5$, $\alpha = 70^\circ$, $\mathrm{Re} = 900$; and (h) VI flow pattern, $P/D = 4$, $\alpha = 10^\circ$, $\mathrm{Re} = 860$.

range of geometries, a synchronized vortex shedding (SVS, Figs. 34(i) and 37(g)) flow pattern (approx. $P/D = 1.5$–5, $\alpha = 15$–90°) is observed, where both cylinders undergo vortex shedding and anti-phase synchronization is observed (similar to two side-by-side circular cylinders, Section 4.1.3) (Sumner et al., 2000).

From the experiments of Alam et al. (2005) at $\mathrm{Re} = 5.5 \times 10^4$, two types of bistable flow were found at higher incidence angles. At $\alpha = 25^\circ$ for $P/D = 2.9$–3.1, bistable behaviour could basically be related to transition between a VPE/VPSE-type flow pattern and a SVS-type flow pattern. The other type of bistable flow occurred for small pitch ratios, from $P/D = 1.1$–1.5 and $\alpha = 25$–75°, and was related to changes in the gap flow patterns, specifically the

development or disappearance of a separation bubble on the inner surface of the upstream cylinder, or changes in shear layer reattachment behaviour.

5.2. Reynolds number effects

The most comprehensive study of Reynolds number effects for the staggered configuration was completed by Zhou et al. (2009), which was focused on the behaviour of the Strouhal numbers. Their classification of the Reynolds number effects included four types of behaviour (Figs. 38–41).

The Type 1 behaviour (Fig. 38) occurs mainly for single bluff body and base-bleed (SBB1, SBB2, BB) flow patterns, which are found at small pitch ratios (approx. $P/D = 1$–1.2). A single Strouhal number is found in the wake of the cylinder pair, which has only a weak dependence on Reynolds number (Zhou et al., 2009).

The Type 2 behaviour (Fig. 39) occurs for a wide range of pitch ratios (approx. $P/D > 1.1$–1.2) and small incidence angles (approx. $\alpha < 10^\circ$). A single Strouhal number is found in the wake of the cylinders, which has a discontinuous jump to a higher value of Strouhal number once a critical value of Reynolds number is attained (pitch-ratio dependent, but lies between Re = 6500–9500). In the Type 2A sub-classification, a single bluff body flow pattern (SBB1) transitions to a shear layer reattachment (SLR) flow pattern once the critical Reynolds number is exceeded. In the Type 2B sub-classification, the shear layer reattachment (SLR) flow pattern transitions to a vortex impingement (VI) flow pattern above the critical value of Reynolds number (Zhou et al., 2009).

Two distinct Strouhal numbers are found for Type 3 behaviour (Fig. 40), where the higher value of Strouhal number is strongly dependent on Reynolds number and the lower value is only weakly dependent. As the Reynolds number is increased, the higher Strouhal number suddenly drops to the lower value. The Type 3 behaviour occurs for low to intermediate pitch ratios (approx. 1.1–$1.2 < P/D < 1.5$–2.2) and a wide range of incidence angles (approx. $\alpha = 10$–75°). As a critical value of the Reynolds number is exceeded, a vortex pairing and enveloping (VPE) or vortex pairing, splitting and enveloping (VPSE) flow pattern switches to an induced separation (IS) or shear layer reattachment (SLR) flow pattern (Zhou et al., 2009).

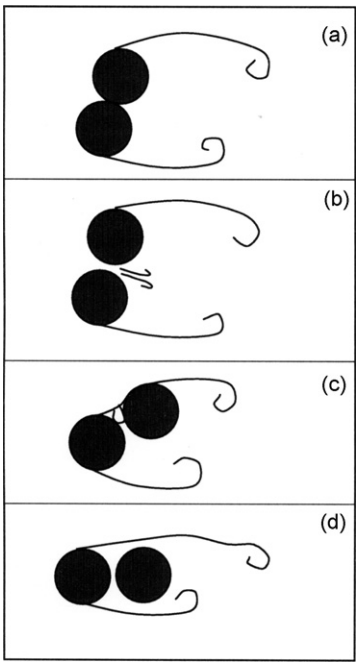

Fig. 38. Flow patterns for two staggered circular cylinders in cross-flow associated with Type 1 Strouhal–Reynolds number behaviour. Flow is from left to right: (a) single bluff-body type 2 (SBB2) flow pattern; (b) base-bleed (BB) flow pattern; and (c, d) single bluff-body type 1 (SBB1) flow pattern.

(Figure taken from Zhou et al. (2009)).

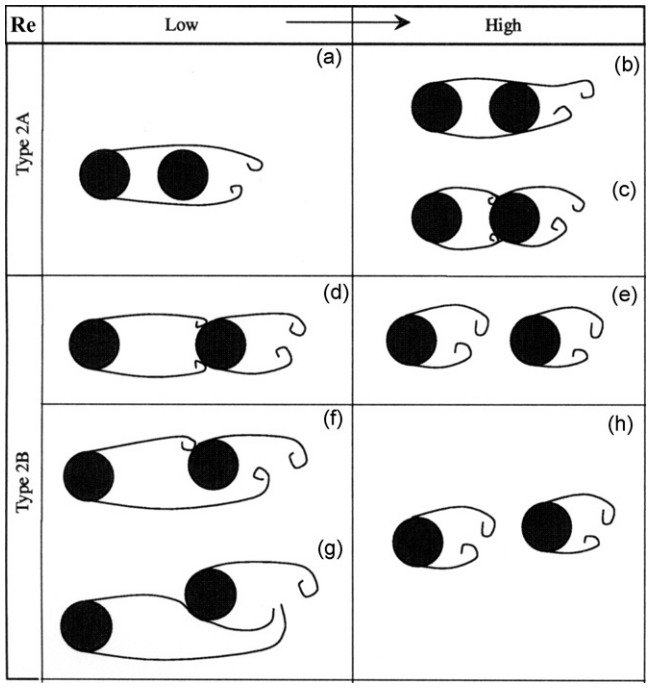

Fig. 39. Flow patterns for two staggered circular cylinders in cross-flow associated with Type 2 Strouhal–Reynolds number behaviour Flow is from left to right. As the Reynolds number is increased, the flow patterns in the left-hand column change to the flow patterns in the right-hand column: (a) single bluff-body type 1 (SBB1) or "overshooting" flow pattern; (b, c, d, f, g) shear layer reattachment (SLR) flow pattern; and (e, h) vortex impingement (VI) or "co-shedding" flow pattern.

(Figure taken from Zhou et al. (2009)).

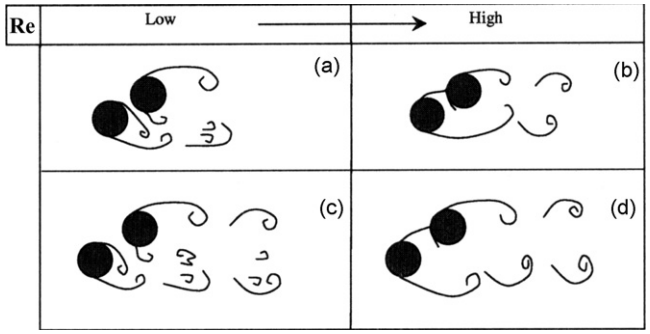

Fig. 40. Flow patterns for two staggered circular cylinders in cross-flow associated with Type 3 Strouhal–Reynolds number behaviour. Flow is from left to right. As the Reynolds number is increased, the flow patterns in the left-hand column change to the flow patterns in the right-hand column: (a) vortex pairing and enveloping (VPE) flow pattern; (b,d) shear layer reattachment (SLR) flow pattern; and (c) vortex pairing, splitting, and enveloping (VPSE) flow pattern.

(Figure taken from Zhou et al. (2009)).

The Type 4 behaviour (Fig. 41) is also associated with two distinct values of Strouhal number. As the Reynolds number is increased, a single Strouhal number is obtained that is close to the value for a single circular cylinder. In the Type 4A sub-classification (for approx. $P/D > 2.2$ and $\alpha = 10$–20°), an induced separation (IS) flow pattern transitions to a vortex impingement (VI) flow pattern with increasing Reynolds number. In the Type 4B sub-classification (for approx. $P/D > 2.2$ and $\alpha = 20$–88°) there is a change from a VPSE flow pattern to an SVS flow pattern, and both the high and low St values approach the single-cylinder St value. In the Type 4C sub-classification (for approx.

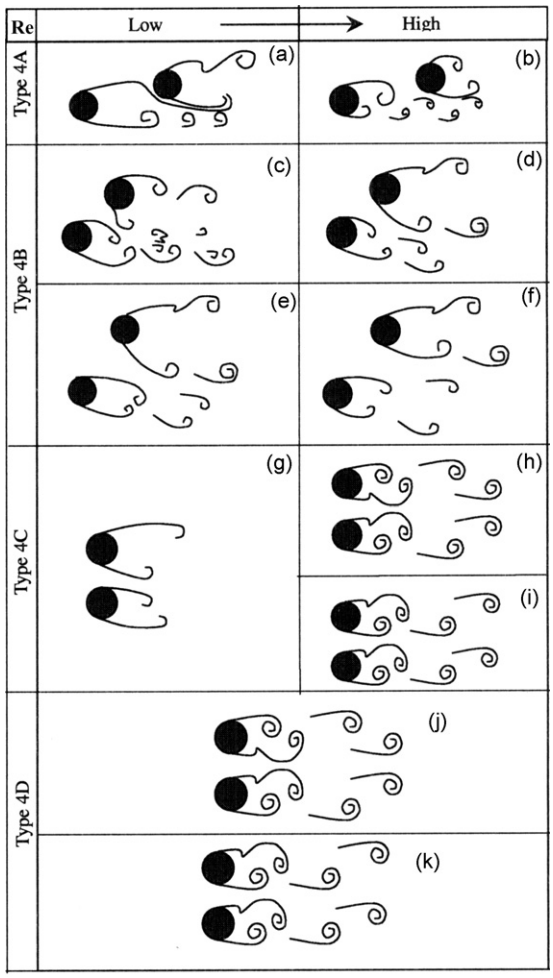

Fig. 41. Flow patterns for two staggered circular cylinders in cross-flow associated with Type 4 Strouhal–Reynolds number behaviour. Flow is from left to right. As the Reynolds number is increased, the flow patterns in the left-hand column change to the flow patterns in the right-hand column: (a) induced separation (IS) flow pattern; (b) vortex impingement (VI) or "co-shedding" flow pattern; (c) vortex pairing, splitting and enveloping (VPSE) flow pattern; (d, e, f, g) "no-enveloping" flow pattern (grouped into the synchronized vortex shedding (SVS) flow pattern of Sumner et al. (2000)); (h, i, j, k) synchronized vortex shedding (SVS) flow pattern, where (h, j) are anti-phased and (i, k) are in-phase.

(Figure taken from Zhou et al. (2009)).

$P/D = 1.7$–2.5 and $\alpha = 88$–90°), changes occur within the SVS flow pattern that are associated with the bias angle of the gap flow, similar to what is observed for two side-by-side circular cylinders in the biased flow regime (Section 4.1.2). In the Type 4D sub-classification (for approx. $P/D > 2.5$ and $\alpha = 88$–90°), the Strouhal number changes are similar to what are observed for two side-by-side circular cylinders in the parallel vortex street regime (Section 4.1.3) (Zhou et al., 2009).

The effects experienced by two staggered cylinders in the supercritical Reynolds number regime have been examined by Suzuki et al. (1971) and Sun et al. (1992).

5.3. Wake structure and vortex dynamics

Detailed studies of the intermediate wake, i.e., beyond the near-wake region which is the typical focus of the flow visualization studies), of two staggered circular cylinders were performed by Hu and Zhou (2008a) for $x/D \geq 10$. They identified three single-street modes (S-Ia, S-Ib, and S-II), shown in Fig. 42, and two twin-street modes (T-I and T-II),

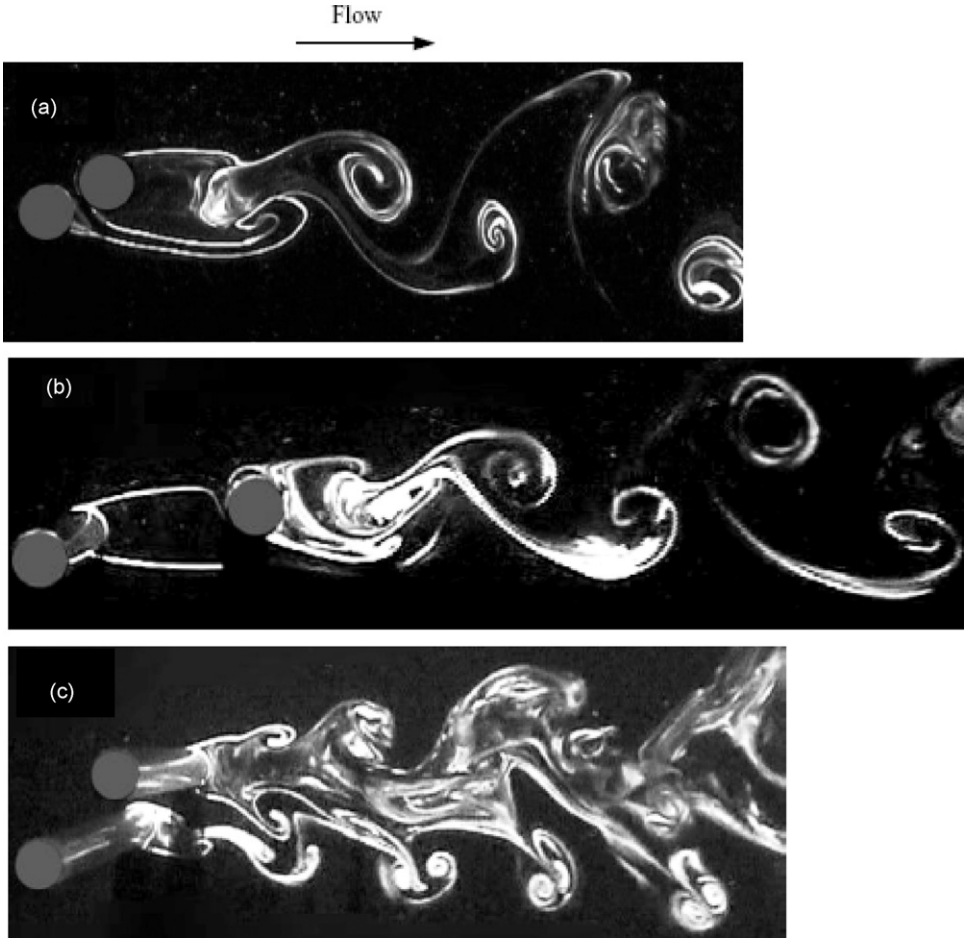

Fig. 42. Single-street wake modes identified by Hu and Zhou (2008a) for two staggered circular cylinders in cross-flow, Re = 300: (a) mode S-Ia, $P/D = 1.2$, $\alpha = 30^\circ$; (b) mode S-Ib, $P/D = 4$, $\alpha = 10^\circ$; and (c) S-II, $P/D = 2$, $\alpha = 40^\circ$.
(Figures taken from Hu and Zhou (2008a)).

shown in Fig. 43. The approximate pitch ratio and incidence angle boundaries for these modes are shown in Fig. 44. A follow-on study by Hu and Zhou (2008b) was focused on the temperature field in the wake of the staggered cylinders.

For the single-street modes, mode S-Ia (Fig. 42(a)) is observed for small pitch ratios (approx. $P/D \leq 1.2$ and $\alpha = 0$–90°, or $P/D \leq 1.5$ and $\alpha \leq 20^\circ$). The vortex street is similar to what is formed behind a single circular cylinder, with the rows of vortices having similar strengths. Mode S-Ib (Fig. 42(b)) occurs for intermediate and large pitch ratios at small incidence angles (approx. $P/D > 1.5$ and $\alpha \leq 10^\circ$), and the main characteristics of the single vortex street are weaker and smaller vortices compared to mode S-Ia. For mode S-II (Fig. 42(c)), which occurs for intermediate and large pitch ratios for various ranges of incidence angle (approx. $1.2 < P/D < 2.5$ and $\alpha > 20^\circ$, or $1.5 \leq P/D \leq 4$ and $10^\circ < \alpha \leq 20^\circ$), the single street is asymmetric about the wake centreline and the two rows of vortices are of different strength (Hu and Zhou, 2008a).

For the twin-street modes, mode T-I (Fig. 43(a)) is found for intermediate and large pitch ratios over a wide range of incidence angles (approx. $P/D \geq 2.5$ and $20^\circ < \alpha < 80^\circ$). Here, the two vortex streets are distinct in terms of vortex strengths and the overall pattern is asymmetric about the wake centreline. The second twin-street mode, T-II (Fig. 43(b)), occurs for large pitch ratios when the cylinders are nearly side-by-side (approx. $P/D \geq 2.5$ and $\alpha \geq 88^\circ$), and is characterized by predominantly anti-phase synchronization between the two parallel vortex streets, where both streets are similar in frequency and strength (Hu and Zhou, 2008a).

The occurrence of single and parallel vortex streets for staggered configurations has also been considered in the context of the universal wake number, by Sumner (2004) and Sumner and Schenstead (2006). For two closely spaced

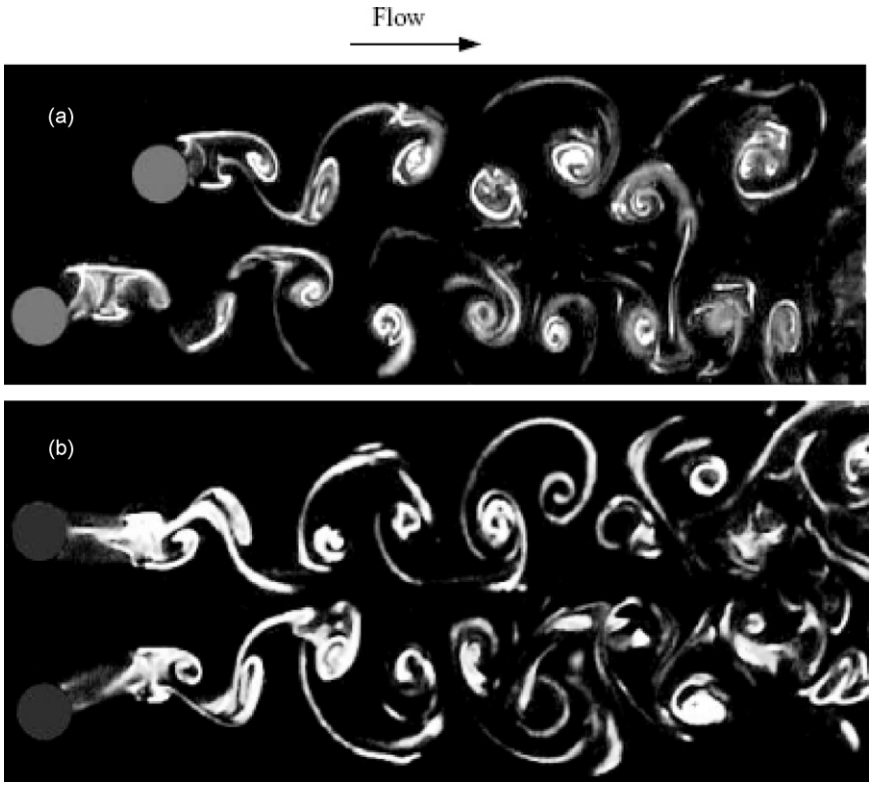

Fig. 43. Twin-street wake modes identified by Hu and Zhou (2008a) for two staggered circular cylinders in cross-flow, Re = 300: (a) mode T-I, $P/D = 4$, $\alpha = 50^\circ$ and (b) mode T-II, $P/D = 3$, $\alpha = 90^\circ$.
(Figures taken from Hu and Zhou (2008a)).

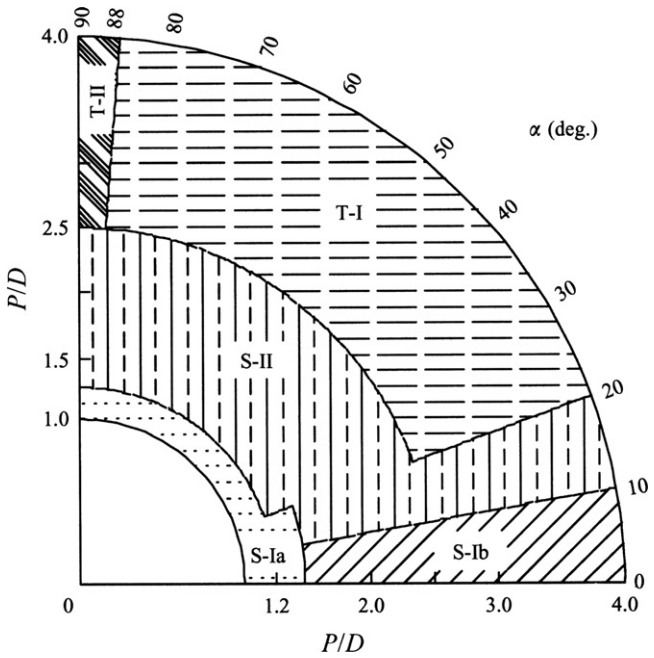

Fig. 44. Wake mode boundaries identified by Hu and Zhou (2008a) for two staggered circular cylinders in cross-flow, Re = 7000.
(Figure taken from Hu and Zhou (2008a)).

staggered cylinders, the flow pattern and single vortex street resemble that of a single bluff body. Using the total drag force acting on the cylinders and the average base pressure coefficient of the two closely spaced cylinders, the Griffin number ($G = St C_D(1-C_{PB})^{-3/2}$) was found to be an effective universal wake number. Its value was within 25% of the single-body value of G, implying that the vortex wake is, to some extent, similar to that of a single bluff body (Sumner, 2004). For moderately spaced staggered cylinders, from $P/D = 1.5$–2.5, vortex shedding occurs from both cylinders at most α, but there are complex interactions between the two individual vortex wakes. The universal wake number concept was most suitable for vortex shedding from the downstream cylinder when $\alpha \geq 30^\circ$, with the Griffin number being within 8% of the single-body value of G at $P/D = 2.5$. For widely spaced staggered cylinders, $P/D = 3$ and 4, both the upstream and downstream cylinders undergo vortex shedding at nearly all α, and the cylinders behave very similar to individual bluff bodies, particularly when $\alpha \geq 30^\circ$. The universal wake number was suitable for the vortex wakes of both the upstream and downstream cylinders, with Griffin numbers within 9% of the single-body value for the upstream cylinder at all α, and within 4% of the single-body value for the downstream cylinder provided $\alpha \geq 30^\circ$ (Sumner and Schenstead, 2006).

5.4. Measurements

For the staggered configuration, there is considerable data available in the literature for the mean aerodynamic force coefficients and Strouhal numbers; see Table 3 for a list of experimental studies and the types of measurements available. In addition to the mean force coefficients and Strouhal numbers, some studies have measured the mean surface static pressure coefficient distributions (e.g., Suzuki et al. (1971), Gu and Sun (1999), Alam et al. (2005)) and fluctuating pressure coefficients (e.g., Moriya and Sakamoto (1985), Sun et al. (1992), Alam et al. (2005)). Some additional comments on the force coefficients and Strouhal number are presented in the following sub-sections.

5.4.1. Force coefficients

Many studies of the staggered configuration have measured the mean aerodynamic forces on the cylinders, with most of the emphasis being on the downstream cylinder. Only a few studies have reported force measurements for the upstream cylinder (e.g., Wardlaw and Cooper (1973), Gu and Sun (1999), Alam et al. (2005), Sumner et al. (2005)). The lift forces on the cylinders follow the sign convention where a repulsive (outward-directed) lift force is associated with a positive sign, and an attractive (inward-directed) lift force is associated with a negative sign. Of particular concern have been specific staggered geometries that give rise to extreme values of C_L and C_D on the downstream cylinder (Price, 1976). Some noteworthy features of the aerodynamic force data include (i) an "inner" lift peak at small L/D and T/D, where the cylinders are nearly in-line, for which the inward-directed lift force on the downstream cylinder reaches a maximum and is highly sensitive to changes in P/D and α; (ii) an "outer" inward-directed lift peak, at larger L/D and T/D, that is less sensitive to changes in the geometry; and (iii) a minimum drag region, that coincides with the "inner" lift peak (Zdravkovich and Pridden, 1977). A number of different explanations for the origin of the inner and outer lift peaks have been provided in the literature, which were summarized by Ting et al. (1998). Recent experiments by Alam et al. (2005), involving mean and fluctuating force measurements, pressure measurements, surface oil flow visualization, and conventional flow visualization, have provided more physical insight into the subtle and complex changes in the behaviour of the force coefficients on both cylinders.

One of the more comprehensive sets of force data was obtained by Sumner et al. (2005) for $Re = 3.2 \times 10^4$–7×10^4, $P/D = 1$–4, $\alpha = 0$–90°, using very small increments in incidence angle; some sample data are shown in Fig. 45. The behaviour of the mean aerodynamic force coefficients was broadly grouped by pitch ratio according to whether the cylinders were closely spaced (approx. $P/D = 1.125$–1.25, Fig. 45(a)), moderately spaced (approx. $P/D = 1.5$–2.5, Fig. 45(b)), or widely spaced (approx. $P/D = 3$–4, Fig. 45(c)).

For closely spaced staggered configurations (Fig. 45(a)), the mean aerodynamic forces on both the upstream and downstream cylinders vary significantly with the incidence angle. Although the flow pattern for closely spaced cylinders is similar to a single bluff body, shear layer reattachment at small incidence angles, and base-bleed gap flow at large incidence angles, have profound effects on the forces experienced by each cylinder (similar to what was reported for two closely spaced side-by-side cylinders, Section 4.4.1). In addition to the inner lift peak for the downstream cylinder, several other critical incidence angles were identified, for both cylinders, which corresponded to local minimum or maximum values of the lift or drag forces, or a discontinuity (Sumner et al., 2005). Some physical explanations for these local maximum and minimum values of mean lift coefficient, involving the movement of stagnation points, the formation of regions of recirculating flow, and bistable behaviour, were provided by Alam et al. (2005).

For moderately spaced staggered configurations (Fig. 45(b)), the flow pattern undergoes a number of changes with α. Notable features are the inner lift peak, a corresponding minimum drag and high value of the Strouhal number, and a

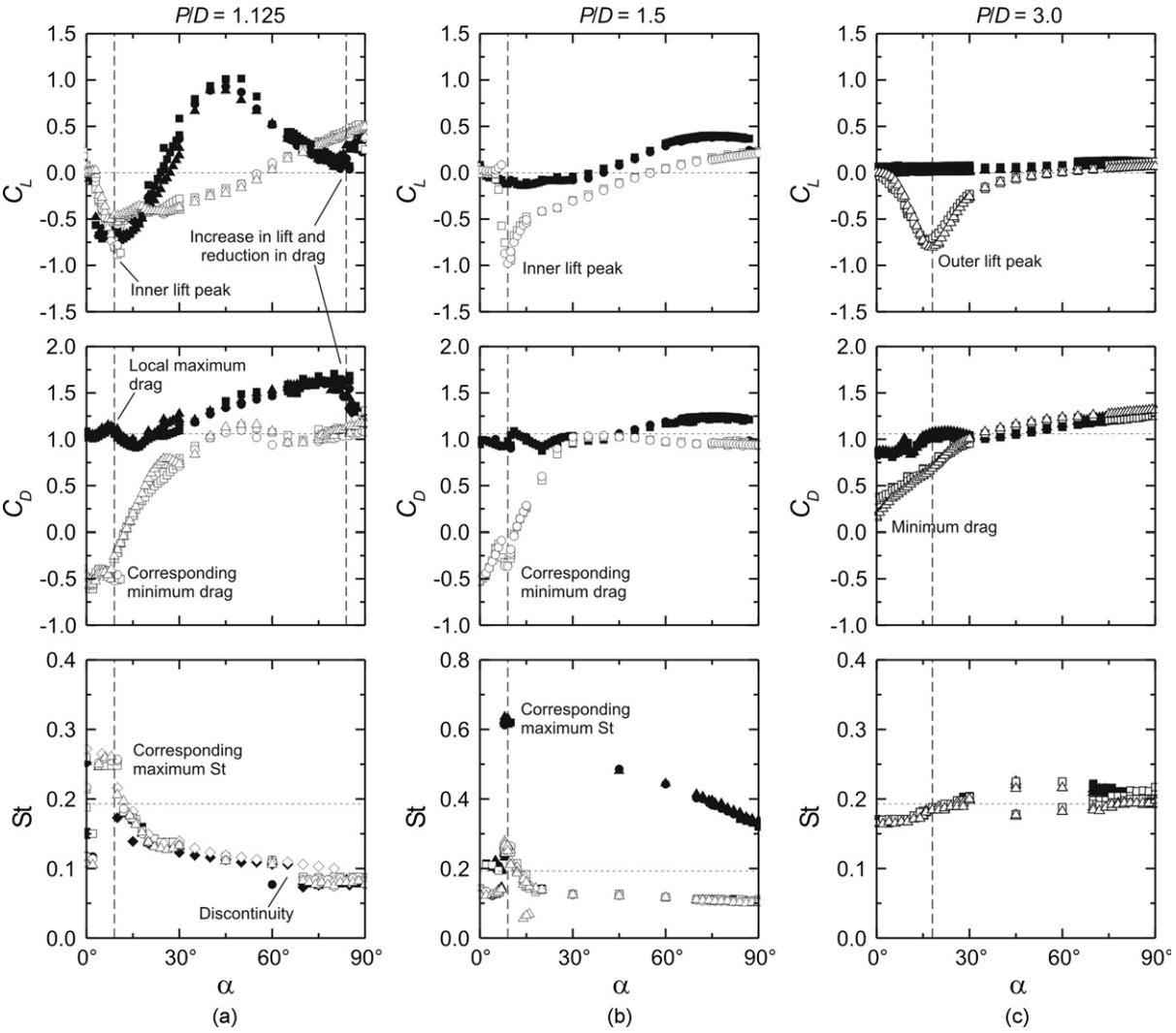

Fig. 45. Mean aerodynamic force coefficient and Strouhal number data for two staggered circular cylinders in cross-flow, from Sumner et al. (2005): (a) closely spaced staggered configurations, $P/D = 1.125$; (b) moderately spaced staggered configurations, $P/D = 1.5$; and (c) widely spaced staggered configurations, $P/D = 3$. ■ or □, $Re = 3.2 \times 10^4$; ◆ or ◇, $Re = 5 \times 10^4$; ● or ○, $Re = 5.6 \times 10^4$; ▲ or △, $Re = 7.2 \times 10^4$. Solid symbols: upstream cylinder. Open symbols: downstream cylinder. - - -, Single cylinder.

loss of lift with increasing α that becomes progressively more abrupt with increasing P/D. The power spectra of the velocity fluctuations at incidence angles near the inner lift peak are characterized by broad-banded peaks or an absence of sharply defined peaks. The sudden appearance or disappearance of periodic vortex shedding activity at small incidence angles, which may occur if the mean flow direction varies, is problematic for the reliable prediction of vortex-induced vibrations in staggered cylinder configurations. At higher α, when there is vortex shedding from the two cylinders, both experience outward-directed lift forces (Sumner et al., 2005).

For widely spaced staggered configurations (Fig. 45(c)), the two cylinders behave more independently, as single, isolated circular cylinders. Both cylinders undergo Kármán vortex shedding for the entire range of α, although vortex impingement on the downstream cylinder occurs at small α. The forces on the upstream cylinder are mostly unchanged from a single cylinder, except in the tandem and side-by-side configurations, where some interference from the downstream cylinder remains. For the downstream cylinder at small α, the outer lift peak replaces the inner lift peak and there is no corresponding minimum drag (Sumner et al., 2005).

5.4.2. Strouhal numbers

For many staggered configurations, two Strouhal numbers are measured (e.g., Kiya et al. (1980), Sumner et al. (2000), Sumner et al. (2005)). In some cases, an absence of reliable Strouhal number has been reported for specific combinations of P/D and α, indicating a weakened or absent vortex shedding activity (Sumner and Richards, 2003). There is some evidence from the study of the flow patterns by Sumner et al. (2000) that the Strouhal numbers may be more appropriately associated with individual shear layers rather than the individual cylinders. A complicating factor in the Strouhal number measurements (for all configurations of two cylinders) is that, when obtaining the vortex shedding frequencies from measurements of the velocity fluctuations, the number of frequencies are sensitive to the measurement location (e.g., Kiya et al. (1980), Sumner et al. (2000), Alam and Sakamoto (2005)).

The first comprehensive set of Strouhal number data for the staggered configuration was obtained by Kiya et al. (1980). Sumner et al. (2005) also obtained a comprehensive set of Strouhal number data simultaneously with their mean aerodynamic force coefficient data, using small increments in incidence angle. Similar to the mean aerodynamic force coefficients (Section 5.4.1), the behaviour of the St data can be broadly grouped by pitch ratio according to whether the cylinders are closely spaced (approx. $P/D = 1.125$–1.25, Fig. 45(a)), moderately spaced (approx. $P/D = 1.5$–2.5, Fig. 45(b)), or widely spaced (approx. $P/D = 3$–4, Fig. 45(c)).

At small pitch ratios (Fig. 45(a)), the same vortex shedding frequency is measured behind both the upstream and downstream cylinders, indicating that the cylinders behave as a single bluff body with a single vortex street. When the cylinders are nearly tandem and the incidence is less than the critical incidence angle of $\alpha \approx 9^\circ$, the Strouhal number is higher than the single-cylinder value. The peak value of St occurs at the critical incidence angle and coincides with the inner lift peak and its corresponding minimum drag. When α is greater than the critical incidence angle, the Strouhal number is lower than that of a single circular cylinder. The Strouhal number decreases with α to a value of $St \approx 0.1$ (one-half the vortex shedding frequency for an isolated circular cylinder). The lowering of the Strouhal number occurs as the near-wake region lengthens and widens with increasing α. The small discontinuous lowering of the Strouhal number between $\alpha = 60^\circ$ and 80° may be related to changes in the base bleed flow pattern within the combined wake of the cylinders (as discussed for two closely spaced side-by-side circular cylinders, Section 4.1.1).

At intermediate pitch ratios (Fig. 45(b)), for a wide range of incidence angles two distinct Strouhal numbers are measured, where the higher one broadly corresponds to the upstream cylinder and the other, lower, Strouhal number broadly corresponds to the downstream cylinder. A very high Strouhal number is found at the critical incidence angle, $\alpha \approx 7$–11°, corresponding to the inner lift peak and its associated minimum drag coefficient.

At large pitch ratios, the same Strouhal number is measured behind both cylinders for most incidence angles (Fig. 45(c)), and both cylinders therefore undergo vortex shedding at the same frequency. This Strouhal number remains close to that of a single circular cylinder indicating the reduced effects of interference between the cylinders.

The Reynolds number sensitivity of the Strouhal number data was investigated by Zhou et al. (2009), and led to the four types of behaviour described previously, under Reynolds number effects, in Section 5.2. From the Strouhal number measurements of Alam and Sakamoto (2005), several "multi-stable" flow patterns were identified. For instance, "tri-stable" flow patterns were found for $P/D = 2.2$–2.8 at $\alpha = 25^\circ$, where two distinct high and low Strouhal numbers could be measured, or the wakes of the two cylinders would intermittently "lock-in" to either the high Strouhal number or low Strouhal number.

6. Conclusions

This review article is an attempt to summarize the literature on the flow around two "infinite" circular cylinders of equal diameter, with an emphasis on the large number of key papers that have appeared in the last 10–20 years, since the most recent comprehensive review by Ohya et al. (1989). From the literature, it is clear that the three main configurations of two circular cylinders, namely the tandem, side-by-side, and staggered configurations, have been extensively studied in terms of identification and classification of flow patterns, identification of Reynolds number effects, experimental measurements of fluid forces, vortex shedding frequencies, velocity fields, and other parameters, and numerical modelling. Improved physical understanding of the flow fields has benefited greatly from advanced measurement and analysis techniques, such as particle image velocimetry, wavelet analysis, and phase-averaging, and improved and more powerful computational fluid dynamics techniques, using a variety of models. The staggered cylinder configuration, which is the most commonly encountered in engineering applications, has received considerable attention in the last 10 years, and the complexity of the flow field and the behaviour of the measured data are now much better understood and appreciated.

Despite the large number of studies in the literature, the complexity of the flow around two circular cylinders will continue to motivate further research. Some possible areas for future attention are given here, although this is not an exhaustive list. For tandem cylinders, additional study of the gap fluid dynamics is needed to better characterize the

shear layer reattachment and gap vortex shedding processes within the reattachment regime. An extensive study of the Reynolds number effects for the aerodynamic forces would also be beneficial, similar to what has been conducted for the Strouhal numbers. For side-by-side cylinders, there is a general lack of aerodynamic force measurements, in particular the mean lift force, over a range of Reynolds numbers, compared to the other two basic configurations. More extensive study, using PIV or other techniques, of the transition or evolution between the near-wake flow patterns and intermediate-wake vortex street modes, is needed. For the staggered configuration, similar to the tandem and side-by-side arrangements, the Reynolds number sensitivity of the aerodynamic force coefficients needs further exploration, similar to what has been done for the Strouhal numbers. For all configurations, the effects of high subcritical, supercritical, and transcritical Reynolds numbers, elevated freestream turbulence, surface roughness, free-end, ground-plane, and plane-wall proximity, and body cross-section, need more attention, especially since these conditions are often encountered in engineering applications. Deeper insight into the flow physics will also arise from more accurate numerical simulations at higher Reynolds numbers; presently, however, there is a general lack of experimental data at low Reynolds number to assist with the validation of current numerical simulations.

Acknowledgements

The support of the Natural Sciences and Engineering Research Council of Canada (NSERC) is gratefully acknowledged.

References

Agrawal, A., Djenidi, L., Antonia, R.A., 2006. Investigation of flow around a pair of side-by-side square cylinders using the lattice Boltzman method. Computers & Fluids 25, 1093–1107.

Aiba, S., Ota, T., Tsuchida, H., 1980a. Heat transfer of tubes closely-spaced in an in-line bank. International Journal of Heat and Mass Transfer 23, 311–319.

Aiba, S., Tsuchida, H., Ota, T., 1980b. Heat transfer around a tube in a bank. Bulletin of the JSME 23, 1163–1170.

Aiba, S., Tsuchida, H., Ota, T., 1981. Heat transfer around a tube in a bank. Bulletin of the JSME 24, 380–387.

Aiba, S., Yamazaki, Y., 1976. An experimental investigation of heat transfer around a tube in a bank. ASME Journal of Heat Transfer 98, 503–508.

Akbari, M.H., Price, S.J., 2005. Numerical investigation of flow patterns for staggered cylinder pairs in cross-flow. Journal of Fluids and Structures 20, 533–554.

Akosile, O.O., Sumner, D., 2003. Staggered circular cylinders in a uniform planar shear flow. Journal of Fluids and Structures 18, 613–633.

Alam, M.M., Moriya, M., Sakamoto, H., 2003a. Aerodynamic characteristics of two side-by-side circular cylinders and application of wavelet analysis on the switching phenomenon. Journal of Fluids and Structures 18, 325–346.

Alam, M.M., Moriya, M., Takai, K., Sakamoto, H., 2003b. Fluctuating fluid forces acting on two circular cylinders in a tandem arrangement at a subcritical Reynolds number. Journal of Wind Engineering and Industrial Aerodynamics 91, 139–154.

Alam, M.M., Sakamoto, H., 2005. Investigation of Strouhal frequencies of two staggered bluff bodies and detection of multistable flow by wavelets. Journal of Fluids and Structures 20, 425–449.

Alam, M.M., Sakamoto, H., Zhou, Y., 2005. Determination of flow configurations and fluid forces acting on two staggered circular cylinders of equal diameter in cross-flow. Journal of Fluids and Structures 21, 363–394.

Alam, M.M., Zhou, Y., 2007a. Flow around two side-by-side closely spaced circular cylinders. Journal of Fluids and Structures 23, 799–805.

Alam, M.M., Zhou, Y., 2007b. Phase lag between vortex shedding from two tandem bluff bodies. Journal of Fluids and Structures 23, 339–347.

Alam, M.M., Zhou, Y., 2008. Strouhal numbers, forces and flow structures around two tandem cylinders of different diameters. Journal of Fluids and Structures 24, 505–526.

Arie, M., Kiya, M., Moriya, M., Mori, H., 1983. Pressure fluctuations on the surface of two circular cylinders in tandem arrangement. ASME Journal of Fluids Engineering 105, 161–167.

Auger, J.L., Coutanceau, J., 1979. Ecoulement transversal de l'air à travers une grille de tubes: Phénomènes associés de vibrations mécaniques et acoustiques. Entropie 86, 13–27 (in French).

Auger, J.L., Coutanceau, J., 1978. On the complex structure of the downstream flow of cylindrical tube rows at various spacings. Mechanics Research Communications 5, 297–302.

Batham, J.P., 1973. Pressure distributions on circular cylinders at critical Reynolds numbers. Journal of Fluid Mechanics 57, 209–228.

Baxendale, A.J., Grant, I., Barnes, F.H., 1985. The flow past two cylinders having different diameters. Aeronautical Journal, 125–134.

Bearman, P.W., 1967. The effect of base bleed on the flow behind a two-dimensional model with a blunt trailing edge. The Aeronautical Quarterly 18, 207–224.
Bearman, P.W., Wadcock, A.J., 1973. The interaction between a pair of circular cylinders normal to a stream. Journal of Fluid Mechanics 61, 499–511.
Bhattacharyya, S., Dhinakaran, S., 2008. Vortex shedding in shear flow past tandem square cylinders in the vicinity of a plane wall. Journal of Fluids and Structures 24, 400–417.
Biermann, D., Herrnstein, W.H., 1934. The interference between struts in various combinations. NACA Report No. 468.
Bokaian, A., Geoola, F., 1984. Wake displacement as cause of lift force on cylinder pair. ASCE Journal of Engineering Mechanics 111, 92–99.
Brun, C., Tenchine, D., Hopfinger, E.J., 2004. Role of the shear layer instability in the near wake behaviour of two side-by-side circular cylinders. Experiments in Fluids 36, 334–343.
Carmo, B.S., Meneghini, J.R., 2006. Numerical investigation of the flow around two circular cylinders in tandem. Journal of Fluids and Structures 22, 979–988.
Carmo, B.S., Meneghini, J.R., Sherwin, S.J., 2010a. Possible states in the flow around two circular cylinders in tandem with separations in the vicinity of the drag inversion spacing. Physics of Fluids 22, 054101.
Carmo, B.S., Meneghini, J.R., Sherwin, S.J., 2010b. Secondary instabilities in the flow around two circular cylinders in tandem. Journal of Fluid Mechanics 644, 395–431.
Chang, K.S., Song, C.J., 1990. Interactive vortex shedding from a pair of circular cylinders in a transverse arrangement. International Journal of Numerical Methods in Fluids 11, 317–329.
Chatterjee, D., Biswas, G., Amiroudine, S., 2010. Numerical simulation of the flow past row of square cylinders for various separation ratios. Computers & Fluids 39, 49–59.
Chen, L., Tu, J.Y., Yeoh, G.H., 2003. Numerical simulation of turbulent wake flows behind two side-by-side cylinders. Journal of Fluids and Structures 18, 387–403.
Chen, S.S., 1987. In: Flow-Induced Vibration of Circular Cylindrical Structures. Hemisphere Publishing Corporation, Washington, DC, USA.
Cheng, M., Moretti, P.M., 1988. Experimental study of the flow field downstream of a single tube row. Experimental Thermal and Fluid Science 1, 69–74.
Chern, M.J., Kanna, P.R., Lu, Y.J., Cheng, I.C., Chang, S.C., 2010. A CFD study of the interaction of oscillatory flows with a pair of side-by-side cylinders. Journal of Fluids and Structures 26, 626–643.
Cokgor, S., Avci, I., 2003. Forces on partly buried, tandem twin cylinders in waves at low Keulegan–Carpenter numbers. Ocean Engineering 30, 1453–1466.
Cokgor, S., Avci, I., 2001. Hydrodynamic forces on partly buried tandem, twin pipelines in current. Ocean Engineering 28, 1349–1360.
Cooper, K.R., 1974. Wind tunnel measurements of the steady aerodynamics forces on a smooth circular cylinder immersed in the wake of an identical cylinder. National Research Council of Canada, LTR-LA-119.
Coutanceau, M., Defaye, J., 1991. Circular cylinder wake configurations: a flow visualization survey. Applied Mechanics Reviews 44, 255–305.
Deng, J., Ren, A.L., Zou, J.F., Shao, X.M., 2006. Three-dimensional flow around two circular cylinders in tandem arrangement. Fluid Dynamics Research 38, 386–404.
Eastop, T.D., Turner, J.R., 1982. Air flow around three cylinders at various pitch-to-diameter ratios for both a longitudinal and transverse arrangement. Transactions of the Institution of Chemical Engineers 60, 359–363.
Edamoto, K., Kawahara, M., 1998. Finite element analysis of two- and three-dimensional flows around square columns in tandem arrangement. International Journal for Numerical Methods in Fluids 28, 95–112.
Farrant, T., Tan, M., Price, W.G., 2000. A cell boundary element method applied to laminar vortex-shedding from arrays of cylinders in various arrangements. Journal of Fluids and Structures 14, 375–402.
Gerrard, J.H., 1978. The wakes of cylindrical bluff bodies at low Reynolds number. Philosophical Transactions of the Royal Society of London A 288, 351–382.
Gu, Z.F., Sun, T.F., 1999. On interference between two circular cylinders in staggered arrangement at high subcritical Reynolds numbers. Journal of Wind Engineering and Industrial Aerodynamics 80, 287–309.
Gu, Z.F., Sun, T.F., He, D.X., Zhang, L.L., 1993. Two circular cylinders in high-turbulence flow at supercritical Reynolds number. Journal of Wind Engineering and Industrial Aerodynamics 49, 379–388.
Hanson, R., Mohany, A., Ziada, S., 2009. Flow-excited acoustic resonance of two side-by-side cylinders in cross-flow. Journal of Fluids and Structures 25, 80–94.
Hetz, A.A., Dhaubhadel, M.N., Telionis, D.P., 1991. Vortex shedding over five in-line cylinders. Journal of Fluids and Structures 5, 243–257.
Hiwada, M., Taguchi, T., Mabuchi, I., Kumada, M., 1979. Fluid flow and heat transfer around two circular cylinders of different diameters in cross-flow. Bulletin of the JSME 22, 715–723.
Hiwada, M., Mabuchi, I., Yanagihara, H., 1982. Fluid flow and heat transfer around two circular cylinders. Bulletin of the JSME 25, 1737–1745.
Hori, E., 1959. Experiments on flow around a pair of parallel circular cylinders. In: Proceedings of the Ninth Japan National Congress for Applied Mechanics, Paper III-11, pp. 231–234.
Hu, J.C., Zhou, Y., 2008a. Flow structure behind two staggered cylinders, Part I: downstream evolution and classification. Journal of Fluid Mechanics 607, 51–80.

Hu, J.C., Zhou, Y., 2008b. Flow structure behind two staggered cylinders, Part II: heat and momentum transport. Journal of Fluid Mechanics 607, 81–107.

Huhe-Aode, Tatsuno, M., Taneda, S., 1985. Visual studies of wake structure behind two cylinders in tandem arrangement. Reports of Research Institute for Applied Mechanics (Kyushu University, Japan) 32 (99), 1–20.

Igarashi, T., 1981. Characteristics of the flow around two circular cylinders arranged in tandem (1st report). Bulletin of the JSME 24, 323–331.

Igarashi, T., 1982. Characteristics of a flow around two circular cylinders of different diameters arranged in tandem. Bulletin of the JSME 25, 349–357.

Igarashi, T., 1984. Characteristics of the flow around two circular cylinders arranged in tandem (second report, unique flow phenomenon at small spacing). Bulletin of the JSME 27, 2380–2387.

Igarashi, T., 1986. Characteristics of the flow around four circular cylinders arranged in-line. Bulletin of the JSME 29 (249), 751–757.

Igarashi, T., Suzuki, K., 1984. Characteristics of the flow around three circular cylinders arranged in-line. Bulletin of the JSME 27, 2397–2404.

Ishigai, S., Nishikawa, E., 1975. Experimental study of structure of gas flow in tube banks with tube axes normal to flow (Part II, On the structure of gas flow in single-column, single-row, and double-row tube banks). Bulletin of the JSME 18, 528–535.

Ishigai, S., Nishikawa, E., Nishimura, K, Cho, K., 1972. Experimental study of structure of gas flow in tube banks with tube axes normal to flow (Part I, Kármán vortex flow from two tubes at various spacings). Bulletin of the JSME 15, 949–956.

Ishigai, S., Nishikawa, E., Yagi, E., 1973. Structure of gas flow and vibration in tube banks with tube axes normal to flow. In: Proceedings of the International Symposium on Marine Engineering, Tokyo, Japan, pp. 1-5-2–1-15-33.

Jendrzejcyk, J.A, Chen, S.S., 1986. Fluid forces on two circular cylinders in crossflow. In: Proceedings of the Flow-Induced Vibration 1986, PVP-vol. 104, ASME, New York, pp. 1–13.

Jester, W., Kallinderis, Y., 2003. Numerical study of incompressible flow about fixed cylinder pairs. Journal of Fluids and Structures 17, 561–577.

Kamemoto, K., 1976. Formation and interaction of two parallel vortex streets. Bulletin of the JSME 19, 283–290.

Kim, H.J., Durbin, P.A., 1988. Investigation of the flow between a pair of circular cylinders in the flopping regime. Journal of Fluid Mechanics 196, 431–448.

Kitagawa, T., Ohta, H., 2008. Numerical investigation on flow around circular cylinders in tandem arrangement at a subcritical Reynolds number. Journal of Fluids and Structures 24, 680–699.

Kiya, M., Arie, M, Tamura, H., Mori, H., 1980. Vortex shedding from two circular cylinders in staggered arrangement. ASME Journal of Fluids Engineering 102, 166–173.

Kiya, M., Mochizuki, O., Ido, Y., Suzuki, T., Arai, T., 1992. Flip-flopping flow around two bluff bodies in tandem arrangement. In: Eckelmann, H., Graham, J.M.R., Huerre, P., Monkewitz, P.A. (Eds.), Proceedings of IUTAM Symposium, September 7–11, 1992 Göttingen, Germany. Springer-Verlag, Berlin, pp. 15–18.

Ko, N.W.M., Wong, P.T.Y., Leung, R.C.K., 1996. Interaction of flow structures within bistable flow behind two circular cylinders of different diameters. Experimental Thermal and Fluid Science 12, 33–44.

Kolář, V., Lyn, D.A., Rodi, W., 1997. Ensemble-averaged measurements in the turbulent near wake of two side-by-side square cylinders. Journal of Fluid Mechanics 346, 201–237.

Kondo, N., 2004. Numerical simulation of aerodynamic characteristics of two rectangular cylinders in side-by-side arrangement. International Journal of Computational Fluid Dynamics 18, 367–379.

Kostic, G., Oka, S.N., 1972. Fluid flow and heat transfer with two cylinders in cross-flow. International Journal of Heat and Mass Transfer 15, 279–299.

Kumada, M., Hiwada, M., Ito, M., Mabuchi, I., 1984. Wake interference between three circular cylinders arranged side-by-side normal to a flow. Transactions of the JSME 50, 1699–1707 (in Japanese).

Kumar, S.R., Sharma, A., Agrawal, A., 2008. Simulation of flow around a row of square cylinders. Journal of Fluid Mechanics 606, 369–397.

Kwon, S.H., Park, J., Ha, D.D., Lee, Y.H., 1996. Experimental study of flow fields around cylinder arrays using PIV. In: Proceedings of the Sixth International Offshore and Polar Engineering Conference, vol. III, Los Angeles, USA, May 26–31, 1996, pp. 145–150.

Lam, K.M., Wong, P.T.Y., Ko, N.W.M., 1993. Interaction of flows behind two circular cylinders of different diameters in side-by-side arrangement. Experimental Thermal and Fluid Science 7, 189–201.

Lee, D.S., Ha, M.Y., Yoon, H.S., Balachandar, S., 2009. A numerical study on the flow patterns of two oscillating cylinders. Journal of Fluids and Structures 25, 263–283.

Lee, K., Yang, K.S., Yoon, D.H., 2009. Flow-induced forces on two circular cylinders in proximity. Computers & Fluids 38, 111–120.

Lee, T., Basu, S., 1997. Nonintrusive measurements of the boundary layer developing on a single and two circular cylinders. Experiments in Fluids 23, 187–192.

Lee, T., Panagakos, A., 1997. Investigation of boundary layer behaviour on single and tandem cylinders. In: Proceedings of the Fourth International Symposium on Fluid–Structure Interactions, Aeroelasticity, Flow-Induced Vibration & Noise, Dallas, USA, vol. 1, ASME, New York, pp. 103–112.

Le Gal, P., Chauve, M.P., Lima, R., Rezende, J., 1990. Coupled wakes behind two circular cylinders. Physical Review A 41, 4566–4569.

Le Gal, P., Peschard, I., Chauve, M.P., Takeda, Y., 1996. Collective behaviour of wakes downstream a row of cylinders. Physics of Fluids 8, 2097–2106.

Li, H., Sumner, D., 2009. Vortex shedding from two finite circular cylinders in a staggered configuration. Journal of Fluids and Structures 25, 479–505.

Li, J., Chambarel, A., Donneaud, M., Martin, R., 1991. Numerical study of laminar flow past one and two circular cylinders. Computers & Fluids 19, 155–170.

Lin, J.C., Yang, Y., Rockwell, D., 2002. Flow past two cylinders in tandem: instantaneous and averaged flow structure. Journal of Fluids and Structures 16, 1059–1071.

Liu, C.H., Chen, J.M., 2002. Observations of hysteresis in flow around two square cylinders in a tandem arrangement. Journal of Wind Engineering and Industrial Aerodynamics 90, 1019–1050.

Liu, Y., Cui, Z.X., 2006. Two side-by-side cantilevered cylinders in a cross flow. In: Proceedings of PVP2006-ICPVT-11, 2006 ASME Pressure Vessels and Piping Division Conference, July 23–27, 2006, Vancouver, Canada, Paper No. PVP2006-ICPVT-11-93894, 9 pp.

Ljungkrona, L., 1992. Characteristics of mean and fluctuating surface pressure distributions on tubes in tandem arrangement and in-line tube bundles. Ph.D. Thesis, Department of Thermodynamics and Fluid Dynamics, Chalmers University of Technology, Göteborg, Sweden.

Ljungkrona, L., Norberg, C., Sundén, B., 1991. Free-stream turbulence and tube spacing effects on surface pressure fluctuations for two tubes in an in-line arrangement. Journal of Fluids and Structures 5, 701–727.

Ljungkrona, L., Sundén, B., 1993. Flow visualization and surface pressure measurement on two tubes in an inline arrangement. Experimental Thermal and Fluid Science 6, 15–27.

Luo, S.C., Gan, T.L., Chew, Y.T., 1996. Uniform flow past one (or two in tandem) finite length circular cylinders. Journal of Wind Engineering and Industrial Aerodynamics 59, 69–93.

Mahir, N., Rockwell, D., 1996a. Vortex formation from a forced system of two cylinders, Part I: tandem arrangement. Journal of Fluids and Structures 10, 473–489.

Mahir, N., Rockwell, D., 1996b. Vortex formation from a forced system of two cylinders, Part II: side-by-side arrangement. Journal of Fluids and Structures 10, 491–500.

Meneghini, J.R., Saltara, F., Siqueira, C.L.R., Ferrari Jr., J.A., 2001. Numerical simulation of flow interference between two circular cylinders in tandem and side-by-side arrangements. Journal of Fluids and Structures 15, 327–350.

Miau, J.J., Wang, H.B., Chou, J.H., 1996. Flopping phenomenon of flow behind two plates placed side-by-side normal to the flow direction. Fluid Dynamics Research 17, 311–328.

Mittal, S., Kumar, V., Raghuvanshi, A., 1997. Unsteady incompressible flows past two cylinders in tandem and staggered arrangements. International Journal for Numerical Methods in Fluids 25, 1315–1344.

Mohany, A., Ziada, S., 2009. Effect of acoustic resonance on the dynamic lift forces acting on two tandem cylinders in cross-flow. Journal of Fluids and Structures 25, 461–478.

Mohany, A., Ziada, S., 2005. Flow-excited acoustic resonance of two tandem cylinders in cross-flow. Journal of Fluids and Structures 21, 103–119.

Moriya, M., Sakamoto, H., 1985. Fluctuating fluid forces acting on a downstream circular cylinder in the staggered arrangement. Transactions of the JSME 51, 2098–2104 (in Japanese).

Moriya, M., Sakamoto, H., 1986. Effect of a vibrating upstream cylinder on a stationary downstream cylinder. ASME Journal of Fluids Engineering 108, 180–184.

Morkovin, M.V., 1964. Flow around circular cylinder—a kaleidoscope of challenging fluid phenomena. In: Hansen, A.G. (Ed.), Proceedings of the Symposium on Fully Separated Flows, ASME Fluids Engineering Division Conference, Philadelphia, USA, May 18−20, 1964, pp. 102−118.

Moretti, P.M., Cheng, M., 1987. Instability of flow through tube rows. ASME Journal of Fluids Engineering 109, 197–198.

Ng, C.W., Ko, N.W.M., 1995. Flow interaction behind two circular cylinders of equal diameter—a numerical study. Journal of Wind Engineering and Industrial Aerodynamics 54–55, 277–287.

Nishimura, T., 1986. Flow across tube banks. In: Cheremisinoff, N.P. (Ed.), Encyclopedia of Fluid Mechanics—Flow Phenomena and Measurement, vol. 1. Gulf Publishing Company, Houston, USA, pp. 763–785.

Nishimura, T., Ohori, Y., Kawamura, Y., 1986. Flow pattern and rate of mass transfer around two cylinders in tandem. International Chemical Engineering 26, 123–129.

Nishiyama, H., Ota, T., Matsuno, T., 1988. Heat transfer and flow around elliptic cylinders in tandem arrangement. JSME International Journal Series II 31, 410–419.

Norberg, C., 1994. An experimental investigation of the flow around a circular cylinder: influence of aspect ratio. Journal of Fluid Mechanics 258, 287–316.

Ohya, Y.O., Okajima, A., Hayashi, M., 1989. Wake interference and vortex shedding. In: Cheremisinoff, N.P. (Ed.), Encyclopedia of Fluid Mechanics—Aerodynamics and Compressible Flow, vol. 8. Gulf Publishing Company, Houston, USA, pp. 322–389.

Okajima, A., 1979. Flows around two tandem circular cylinders at very high Reynolds numbers. Bulletin of the JSME 22, 504–511.

Ota, T., Nishiyama, H., 1986. Flow around two elliptic cylinders in tandem arrangement. ASME Journal of Fluids Engineering 108, 98–103.

Ota, T., Nishiyama, H., Kominami, J., Sato, K., 1986. Heat transfer from two elliptic cylinders in tandem arrangement. ASME Journal of Heat Transfer 108, 525–531.

Ozono, S., Oda, J., Yoshida, Y., Wakasugi, Y., 2001. Critical nature of the base pressure of the upstream circular cylinder in two staggered ones in cross-flow. In: Theoretical and Applied Mechanics, vol. 50, Proceedings of the 50th Japan National Congress on Theoretical and Applied Mechanics, January 23–25, 2001, Tokyo, pp. 335–340.

Palau-Salvador, G., Stoesser, T., Rodi, W., 2008. LES of the flow around two cylinders in tandem. Journal of Fluids and Structures 24, 1304–1312.

Papaioannou, G.V., Yue, D.K.P., Triantafyllou, M.S., Karniadakis, G.E., 2008. On the effect of spacing on the vortex-induced vibrations of two tandem cylinders. Journal of Fluids and Structures 24, 833–854.

Papaioannou, G.V., Yue, D.K.P., Triantafyllou, M.S., Karniadakis, G.E., 2006. Three-dimensionality effects in flow around two tandem cylinders. Journal of Fluid Mechanics 558, 387–413.

Park, C.W., Lee, S.J., 2003. Flow structure around two finite circular cylinders located in an atmospheric boundary layer: side-by-side arrangement. Journal of Fluids and Structures 17, 1043–1058.

Peschard, I., Le Gal, P., 1996. Coupled wakes of cylinders. Physical Review Letters 77, 3122–3125.

Prasanth, T.K., Mittal, S., 2009a. Flow-induced oscillation of two circular cylinders in tandem arrangement at low Re. Journal of Fluids and Structures 25, 1029–1048.

Prasanth, T.K., Mittal, S., 2009b. Vortex-induced vibration of two circular cylinders at low Reynolds number. Journal of Fluids and Structures 25, 731–741.

Price, S.J., 1976. The origin and nature of the lift force on the leeward of two bluff bodies. The Aeronautical Quarterly 27, 154–168.

Price, S.J., Païdoussis, M.P., 1984. The aerodynamic forces acting on groups of two and three circular cylinders when subject to a cross-flow. Journal of Wind Engineering and Industrial Aerodynamics 17, 329–347.

Price, S.J., Païdoussis, M.P., Krishnamoorthy, S., 2007. Cross-flow past a pair of nearly in-line cylinders with the upstream cylinder subjected to a transverse harmonic oscillation. Journal of Fluids and Structures 23, 39–57.

Quadflieg, H., 1977. Vortex-induced loads on a pair of cylinders in incompressible flow at high Reynolds numbers. Forschung im Ingenieurwesen 43, 9–18 (in German).

Sarode, R.S., Gai, S.L., Ramesh, C.K., 1981. Flow around circular- and square-section models of finite height in a turbulent shear flow. Journal of Wind Engineering and Industrial Aerodynamics 8, 223–230.

Sharman, B., Lien, F.S., Davidson, L., Norberg, C., 2005. Numerical prediction of low Reynolds number flows over two tandem circular cylinders. International Journal for Numerical Methods in Fluids 47, 423–447.

Singha, S., Sinhamahapatra, K.P., 2010. High-resolution numerical simulation of low Reynolds number incompressible flow about two cylinders in tandem. ASME Journal of Fluids Engineering 132, 011101 (10 pp).

Spivack, H.M., 1946. Vortex frequency and flow pattern in the wake of two parallel cylinders at varied spacing normal to an air stream. Journal of the Aeronautical Sciences 13, 289–297.

Sumer, B.M., Fredsøe, J., 1997. In: Hydrodynamics around Cylindrical Structures. World Scientific, London.

Sumner, D., 2004. Closely spaced circular cylinders in cross-flow and a universal wake number. ASME Journal of Fluids Engineering 126, 245–249.

Sumner, D., Price, S.J., Païdoussis, M.P., 2000. Flow-pattern identification for two staggered circular cylinders in cross-flow. Journal of Fluid Mechanics 411, 263–303.

Sumner, D., Price, S.J., Païdoussis, M.P., 1999a. Tandem cylinders in impulsively started flow. Journal of Fluids and Structures 13, 955–965.

Sumner, D., Price, S.J., Païdoussis, M.P., 1997. Investigation of impulsively started flow around side-by-side circular cylinders: application of particle image velocimetry. Journal of Fluids and Structures 11, 597–615.

Sumner, D., Richards, M.D., 2003. Some vortex-shedding characteristics of the staggered configuration of circular cylinders. Journal of Fluids and Structures 17, 345–350.

Sumner, D., Richards, M.D., Akosile, O.O., 2005. Two staggered circular cylinders of equal diameter in cross-flow. Journal of Fluids and Structures 20, 255–276.

Sumner, D., Schenstead, A.J., 2006. Moderately and widely spaced circular cylinders in cross-flow and a universal wake number. ASME Journal of Fluids Engineering 128, 1122–1125.

Sumner, D., Wong, S.S.T., Price, S.J., Païdoussis, M.P., 1999b. Fluid behaviour of side-by-side circular cylinders in steady cross-flow. Journal of Fluids and Structures 13, 309–338.

Sun, T.F., Gu, Z.F., He, D.X., Zhang, L.L., 1992. Fluctuating pressure on two circular cylinders at high Reynolds numbers. Journal of Wind Engineering and Industrial Aerodynamics 41–44, 577–588.

Suzuki, N., Sato, H., Iuchi, M., Yamamoto, S., 1971. Aerodynamic forces acting on circular cylinders arranged in a longitudinal row. In: Wind Effects on Buildings and Structures, International Wind Conference, Tokyo, Part II, pp. 20-1–20-10.

Taniguchi, S., Sakamoto, H., Arie, M., 1982. Interference between two circular cylinders of finite height vertically immersed in a turbulent boundary layer. ASME Journal of Fluids Engineering 104, 529–536.

Ting, D.S.K., Wang, D.J., Price, S.J., Païdoussis, M.P., 1998. An experimental study on the fluidelastic forces for two staggered circular cylinders in cross-flow. Journal of Fluids and Structures 12, 259–294.

Wang, X.W., Zhang, H.J., Zhou, Y., Tu, J.Y., 2002a. Flow visualization behind three cylinders of equal and unequal spacing. Journal of Flow Visualization & Image Processing 9, 139–151.

Wang, Z.J., Zhou, Y., Li, H., 2002b. Flow-visualization of a two side-by-side cylinder wake. Journal of Flow Visualization & Image Processing 9, 123–138.

Wardlaw, R.L., Cooper, K.R., 1973. A wind tunnel investigation of the steady aerodynamic forces on smooth and stranded twin bundled power conductors for the Aluminum Company of America. National Research Council of Canada, LTR-LA-117.

Williamson, C.H.K., 1996. Vortex dynamics in the cylinder wake. Annual Review of Fluid Mechanics 28, 477–539.

Williamson, C.H.K., 1985. Evolution of a single wake behind a pair of bluff bodies. Journal of Fluid Mechanics 159, 1–18.

Wood, C.J., 1967. Visualization of an incompressible wake with base bleed. Journal of Fluid Mechanics 29, 259–272.
Wu, J., Welch, L.W., Wels, M.C., Sheridan, J., Walker, G.J., 1994. Spanwise wake structures of a circular cylinder and two circular cylinders in tandem. Experimental Thermal and Fluid Science 9, 299–308.
Xu, G., Zhou, Y., 2004. Strouhal numbers in the wake of two inline cylinders. Experiments in Fluids 37, 248–256.
Xu, S.J., Zhou, Y., So, R.M.C., 2003. Reynolds number effects on the flow structure behind two side-by-side cylinders. Physics of Fluids 15, 1214–1219.
Yen, S.C., San, K.C., Chuang, T.H., 2008. Interactions of tandem square cylinders at low Reynolds numbers. Experimental Thermal and Fluid Science 32, 927–938.
Zdravkovich, M.M., 1997. Flow around Circular Cylinders, vol. 1: Fundamentals. Oxford University Press, Oxford, UK.
Zdravkovich, M.M., 2003. Flow Around Circular Cylinders, vol. 2: Applications. Oxford University Press, Oxford, UK.
Zdravkovich, M.M., 1993. Interstitial flow field and fluid forces. In: Au-Yang, M.K. (Ed.), Technology for the 90s: A Decade of Progress. ASME, New York, USA, pp. 594–658.
Zdravkovich, M.M., 1985. Flow induced oscillations of two interfering circular cylinders in cross flow. Journal of Sound and Vibration 101, 511–521.
Zdravkovich, M.M., 1987. The effects of interference between circular cylinders in cross flow. Journal of Fluids and Structures 1, 239–261.
Zdravkovich, M.M., 1977. Review of flow interference between two circular cylinders in various arrangements. ASME Journal of Fluids Engineering 99, 618–633.
Zdravkovich, M.M., Pridden, D.L., 1977. Interference between two circular cylinders; series of unexpected discontinuities. Journal of Industrial Aerodynamics 2, 255–270.
Zdravkovich, M.M., Stonebanks, K.L., 1990. Intrinsically nonuniform and metastable flow in and behind tube arrays. Journal of Fluids and Structures 4, 305–319.
Zhang, H., Melbourne, W.H., 1992. Interference between two circular cylinders in tandem in turbulent flow. Journal of Wind Engineering and Industrial Aerodynamics 41–44, 589–600.
Zhang, H.J., Zhou, Y., 2001. Effect of unequal cylinder spacing on vortex streets behind three side-by-side cylinders. Physics of Fluids 13, 3675–3686.
Zhou, Y., 2003. Vortical structures behind three side-by-side cylinders. Experiments in Fluids 34, 68–76.
Zhou, Y., Feng, S.X., Alam, M.M., Bai, H.L., 2009. Reynolds number effect on the wake of two staggered cylinders. Physics of Fluids 21, 125105.
Zhou, Y., So, R.M.C., Liu, M.H., Zhang, H.J., 2000. Complex turbulent wakes generated by two and three side-by-side cylinders. International Journal of Heat and Fluid Flow 21, 125–133.
Zhou, Y., Wang, Z.J., So, R.M.C., Xu, S.J., Jin, W., 2001. Free vibrations of two side-by-side cylinders in a cross flow. Journal of Fluid Mechanics 443, 197–229.
Zhou, Y., Yiu, M.W., 2006. Flow structure, momentum and heat transport in a two-tandem-cylinder wake. Journal of Fluid Mechanics 548, 17–48.
Zhou, Y., Zhang, H.J., Yiu, M.W., 2002. The turbulent wake of two side-by-side circular cylinders. Journal of Fluid Mechanics 458, 303–332.